

Partial oxidation of methane to synthesis gas : reaction kinetics and reactor modelling

Citation for published version (APA):

Smet, de, C. R. H. (2000). *Partial oxidation of methane to synthesis gas : reaction kinetics and reactor modelling*. [Phd Thesis 1 (Research TU/e / Graduation TU/e), Chemical Engineering and Chemistry]. Technische Universiteit Eindhoven. <https://doi.org/10.6100/IR535178>

DOI:

[10.6100/IR535178](https://doi.org/10.6100/IR535178)

Document status and date:

Published: 01/01/2000

Document Version:

Publisher's PDF, also known as Version of Record (includes final page, issue and volume numbers)

Please check the document version of this publication:

- A submitted manuscript is the version of the article upon submission and before peer-review. There can be important differences between the submitted version and the official published version of record. People interested in the research are advised to contact the author for the final version of the publication, or visit the DOI to the publisher's website.
- The final author version and the galley proof are versions of the publication after peer review.
- The final published version features the final layout of the paper including the volume, issue and page numbers.

[Link to publication](#)

General rights

Copyright and moral rights for the publications made accessible in the public portal are retained by the authors and/or other copyright owners and it is a condition of accessing publications that users recognise and abide by the legal requirements associated with these rights.

- Users may download and print one copy of any publication from the public portal for the purpose of private study or research.
- You may not further distribute the material or use it for any profit-making activity or commercial gain
- You may freely distribute the URL identifying the publication in the public portal.

If the publication is distributed under the terms of Article 25fa of the Dutch Copyright Act, indicated by the "Taverne" license above, please follow below link for the End User Agreement:

www.tue.nl/taverne

Take down policy

If you believe that this document breaches copyright please contact us at:

openaccess@tue.nl

providing details and we will investigate your claim.

Partial Oxidation of Methane to Synthesis Gas: Reaction Kinetics and Reactor Modelling

Proefschrift

ter verkrijging van de graad van doctor aan de Technische Universiteit Eindhoven, op gezag van de Rector Magnificus, prof.dr. M. Rem, voor een commissie aangewezen door het College voor Promoties in het openbaar te verdedigen op maandag 29 mei 2000 om 16.00 uur

door

Carlo Rudy Harold de Smet

geboren te Terneuzen

Dit proefschrift is goedgekeurd door de promotoren:

prof.dr.ir. J.C. Schouten

prof.dr.ir. G.B. Marin

copromotor:

dr. M.H.J.M. de Croon

The work described in this thesis was in part financially supported by the Commission of the European Union in the framework of the JOULE Program, Contract No. JOU2-CT92-0073 and No. JOU3-CT95-0026, and the Copernicus Project, Contract No. 41GO4597.

CIP-DATA LIBRARY TECHNISCHE UNIVERSITEIT EINDHOVEN

Smet, Carlo R.H. de

Partial oxidation of methane to synthesis gas : reaction kinetics

and reactor modelling / by Carlo R.H. de Smet. - Eindhoven :

Technische Universiteit Eindhoven, 2000. - Proefschrift. -

ISBN 90-386-2921-4

NUGI 813

Trefwoorden: partiële oxidatie / methaan / synthese gas / reactormodellering / reaktiekinetiek

Subject headings: partial oxidation / methane / synthesis gas / reactor modelling / kinetics

© Copyright 2000 by C.R.H. de Smet, Terneuzen, The Netherlands.

All rights reserved. No part of this publication may be reproduced, stored in a retrieval system, or transmitted, in any form or by any means, electronic, mechanical, photocopying, recording or otherwise, without prior permission of the author.

Summary

Natural gas will become increasingly important as feedstock for the chemical industry in the near future, as a result of tightening supplies of liquid hydrocarbons and more stringent environmental demands. Natural gas utilization accordingly has developed into a major research area in the past decades. Global research efforts have also been unfolded by industry and academia to develop gas-to-liquids (GTL) technology for the conversion of methane, the major constituent of natural gas, into high-added-value liquid products. In addition, natural gas conversion into hydrogen, which can be converted to electricity in fuel cells, is attracting widespread attention. All of the above processes require the initial conversion of methane towards synthesis gas, a mixture of CO and H₂. Recent advances in synthesis gas production, in particular the progress in catalytic partial oxidation (CPO) towards syngas, have been a key driving force.

This thesis aims at the investigation of the reaction kinetics of the catalytic partial oxidation reaction and at reactor modeling of synthesis gas production via CPO at industrially relevant conditions. The kinetic studies are performed at low conversions to obtain insight into the primary reaction products. A fixed-bed reactor is used to investigate the kinetics in case of a 0.3 wt% Rh/ α -Al₂O₃ catalyst. Special emphasis is placed on the relative importance of homogeneous gas-phase reactions and heterogeneous catalytic reactions. Partial oxidation of methane is also investigated in a laboratory reactor containing a single Pt metal gauze catalyst, at conditions where heat and mass-transport limitations cannot be neglected. Reactor modeling is carried out to design adiabatic fixed-bed reactors for methanol and hydrogen-for-fuel-cells production.

Partial oxidation reactions and reactors - Literature review

Both Ni and Rh are presently considered to be the most promising CPO catalysts. Ni catalysts show high conversions and selectivities, but suffer from catalyst deactivation due to coke formation. Both high activity and stability was observed in case of Rh catalyst: the high cost and limited availability will probably determine whether commercial application is viable. Application of fixed-bed reactors appears to be limited to low pressures, due to the possible occurrence of hot spots in the catalyst bed. Monolith reactors, however, were identified in the

literature to be particularly suitable for the production of large amounts of synthesis gas in compact reactors. Fluidized bed and membrane reactors also appeared as promising reactor configurations. The kinetics of the CPO reaction were found to depend primarily on the applied reaction conditions. Both direct synthesis gas production, yielding CO and H₂ in a single step, as well as indirect formation, via total oxidation and steam reforming in series, were proposed in the literature. A clear distinction between direct and indirect mechanisms requires experimental data at low conversions. Kinetic studies reported in the literature, however, were generally performed at high conversions. This justifies the experimental approach applied in this thesis, i.e. to study the kinetics at low conversions.

Partial oxidation of methane over Rh/ α -Al₂O₃

The catalytic partial oxidation of methane to synthesis gas was studied in a fixed-bed reactor using a 0.3 wt% Rh/ α -Al₂O₃ catalyst. Homogeneous gas-phase reactions and heterogeneous catalytic reactions were investigated at temperatures between 1273 and 1345 K, pressures between 400 and 800 kPa, using 6.7/3.3/90 CH₄/O₂/He mixtures. Both total and partial oxidation products as well as significant amounts of C₂-hydrocarbons were observed at these conditions. The homogeneous gas-phase experiments were accurately described with a kinetic model consisting of 40 reversible gas-phase reactions. Reactor simulations with this model showed that gas-phase reactions were very important at the applied conditions: homogeneous reactions contributed at least 50 % to the conversions obtained with the α -Al₂O₃ support alone. A comparison of measured conversions obtained with the support and with the Rh/ α -Al₂O₃ catalyst revealed that both homogeneous gas-phase reactions and heterogeneous catalytic reactions were important in case of the Rh catalyst. The product yields measured on the support and the catalyst showed that Rh/ α -Al₂O₃ primarily catalysed methane total oxidation at 1345 K. However, at 1273 K there are strong indications that Rh also promoted the direct partial oxidation of methane to synthesis gas.

Partial oxidation of methane in a structured Pt gauze reactor

During the catalytic partial oxidation of methane strong heat-transport limitations can occur as a result of the high reaction rates. An experimental reactor, containing a single Pt gauze catalyst, was developed to study the intrinsic kinetics of the CPO reaction in the presence of heat-transport limitations. The catalyst temperature was measured directly by means of a spotwelded thermocouple. At catalyst temperatures between 1030 and 1200 K, residence times of 0.02 to 0.2 milliseconds, CH₄/O₂ ratios between 1.8 and 5.0, and O₂ conversions between 9 and 46%, CO, CO₂, and H₂O were the main products. CO was found to be the primary product. Hydrogen was observed only at temperatures above 1273 K. At these conditions, however, the catalyst did not exhibit stable performance with time-on-stream. The methane and oxygen conversions were

independent of the catalyst temperature, and thus were completely determined by mass-transport. The CO formation rate, however, was influenced significantly by the reaction kinetics. A reactor model was developed to determine the intrinsic kinetics of the CO formation rate. This flat-plate reactor model, consisting of two rows of flat plates in series, was validated by comparing the calculated conversions and gas-phase temperatures to FLUENT simulations of the 3D geometry of the gauze catalyst. A kinetic model consisting of six reaction steps was developed to account for the conversions and selectivities measured with the Pt gauze catalyst. Analysis of analytical expressions for the intrinsic CO selectivity indicated that methane adsorption had to be considered as oxygen-assisted to describe primary CO formation. The intrinsic kinetic parameters were obtained from literature and from single-response regression applied to the observed CO selectivity. Statistically significant and physically consistent estimates of the intrinsic kinetic parameters of methane adsorption were acquired. The model adequately reproduced the effects of the catalyst temperature, reactant space-time, and inlet methane-to-oxygen ratio on conversions and selectivity. Initial CO selectivities between 86 and 96 % were calculated. The role of surface kinetics and mass-transfer in CO formation was illustrated quantitatively.

Partial oxidation reactors for methanol and hydrogen-for-fuel-cells production

Adiabatic fixed-bed CPO reactors for methanol and hydrogen-for-fuel-cells production were investigated using a steady-state, one-dimensional heterogeneous reactor model. The reactor model explicitly accounted for intraparticle concentration gradients: pellet scale continuity equations were solved at each point along the reactor coordinate. Simulations were carried out using supported Ni catalysts, which catalyse indirect synthesis gas formation. Rate equations for methane oxidation, steam reforming, and water-gas shift were thus combined in the calculations. Adiabatic fixed-bed reactors for operation of a 10 kW fuel cell are feasible due to low catalyst temperatures, typically below 1000 K. At high pressure conditions suitable for the production of 1000 metric tons per day of methanol, however, high catalyst temperatures (> 1450 K) were calculated. Hence, catalyst deactivation will be very important in this case. The influence of the reforming kinetics was studied by performing simulations with two different reforming models from the literature. In case of the low-pressure fuel-cell case, these reforming models resulted in significantly different catalyst temperature profiles. At methanol conditions, a temperature maximum was always observed near the reactor inlet, independent of the applied reforming model. Reduced oxidation activity resulted in lower catalyst temperatures in the fuel-cell case, whereas only minor influences were observed at methanol conditions. Fixed-bed reactors for hydrogen production can be operated safely as gas-phase reactions are not likely to ignite. At methanol conditions, however, gas-phase reactions will be very important.

Samenvatting

Aardgas zal in de nabije toekomst steeds belangrijker worden als grondstof voor de chemische industrie als gevolg van het teruglopende aanbod van vloeibare koolwaterstoffen en de steeds strengere milieuwetgeving. Aardgasconversie heeft zich daarom ontwikkeld tot een belangrijk onderzoeksgebied in de afgelopen decennia. Globale onderzoeksprogramma's zijn geïnitieerd door de industrie en universiteiten voor het ontwikkelen van gas-naar-vloeistof (GTL) technologie voor de omzetting van methaan, de belangrijkste component van aardgas, naar hoogwaardige vloeibare producten. Tevens wordt op dit moment veel aandacht besteed aan de omzetting van aardgas naar waterstof, dat met lucht in een brandstofcel kan worden geconverteerd naar elektriciteit. De initiële omzetting van methaan naar synthesegas, een mengsel van CO en H₂, is de eerste stap bij toepassing van bovenstaande processen. Recente ontwikkelingen in synthesegas productie, met name de vooruitgang in katalytische partiële oxidatie (CPO), zijn hierbij een belangrijke drijfveer geweest.

Dit proefschrift is gericht op het onderzoeken van de kinetiek van de CPO reactie en op het modelleren van reactoren voor synthesegasproductie via CPO bij industrieel relevante condities. De kinetische studies zijn uitgevoerd bij lage conversiegraden om inzicht te krijgen in de primaire producten van de reactie. Een vastbedreactor is toegepast om de kinetiek over een Rh/ α -Al₂O₃ katalysator te onderzoeken. In deze studie wordt voornamelijk aandacht besteed aan het relatieve belang van homogene gasfasereacties en heterogene katalytische reacties. De CPO reactie is tevens onderzocht in een laboratoriumreactor, waarin één enkel Pt gaasje is opgenomen, bij condities waar warmte- en stofoverdrachtslimiteringen niet kunnen worden verwaarloosd. Het modelleren van reactoren is gebaseerd op gedragen Ni-katalysatoren en is uitgevoerd om adiabatische vastbedreactoren te onderzoeken voor de productie van methanol en waterstof-voor-brandstofcellen.

Partiële oxidatiereacties en reactoren - Literatuuroverzicht

Zowel Ni als Rh worden op dit moment in de literatuur aangeduid als meest veelbelovende katalysatoren. Ni katalysatoren vertonen hoge conversies en selectiviteiten, maar leiden onder

katalysator-desactivering. In geval van Rh katalysatoren is zowel hoge activiteit als hoge stabiliteit waargenomen: de hoge prijs van dit edelmetaal zal waarschijnlijk bepalen of commerciële toepassing al dan niet mogelijk is. Toepassing van vastbedreactoren is beperkt tot lage drukken als gevolg van mogelijke vorming van hot-spots in het katalysatorbed. Monolietreactoren worden echter in de literatuur aangeduid als geschikt reactortype voor de productie van grote hoeveelheden synthegas in compacte reactoren. Fluidbed- en membraanreactoren zijn eveneens naar voren gekomen als veelbelovend reactorconcept. De kinetiek van de CPO reactie hangt voornamelijk af van de toegepaste reactiecondities. Zowel directe productie van synthegas, waarin CO en H₂ in één enkele stap worden gevormd, als indirecte productie, waarbij synthegas wordt gevormd via totale oxidatie, stoom reforming en water-gas-shift reacties, worden in de literatuur voorgesteld. De kinetische studies zijn meestal uitgevoerd bij hoge methaan- en zuurstofconversies. Voor het maken van een duidelijk onderscheid tussen directe en indirecte productie van synthegas zijn echter experimentele gegevens bij lage conversies nodig. Dit rechtvaardigt de aanpak toegepast in dit proefschrift, namelijk het bestuderen van de kinetiek bij lage conversies.

Partiële oxidatie van methaan over Rh/ α -Al₂O₃

De katalytische partiële oxidatie van methaan naar synthegas werd bestudeerd in een vastbedreactor in aanwezigheid van een Rh/ α -Al₂O₃ katalysator. Homogene gasfasereacties en heterogene katalytische reacties zijn onderzocht bij temperaturen tussen 1273 en 1345 K, drukken tussen 400 en 800 kPa, en met 6.7/3.3/90 CH₄/O₂/He mengsels. Totale en partiële verbrandingsproducten en aanzienlijke hoeveelheden C₂-koolwaterstoffen werden waargenomen bij deze condities. De homogene gasfasereacties werden bestudeerd in afwezigheid van de katalysator, en werden nauwkeurig beschreven met een kinetisch model dat bestaat uit 40 reversibele gasfasereacties. Reactorsimulaties met dit model gaven aan dat gasfasereacties zeer belangrijk zijn bij de toegepaste condities: homogene gasfasereacties droegen tenminste 50% bij tot de conversies verkregen met de α -Al₂O₃ drager. Een vergelijking tussen de gemeten conversies verkregen met de drager en met de Rh/ α -Al₂O₃ katalysator wees uit dat zowel homogene gasfasereacties als heterogene katalytische reacties belangrijk zijn bij de Rh katalysator. De productopbrengsten gemeten met de drager en met de katalysator toonden aan dat Rh/ α -Al₂O₃ voornamelijk de totale oxidatie van methaan katalyseert bij temperaturen van 1345 K. Echter, bij 1273 K zijn er tevens duidelijke aanwijzingen dat op Rh ook directe partiële oxidatie van methaan naar synthegas plaatsvindt.

Partiële oxidatie van methaan in een gestructureerde Pt gaasreactor

Tijdens de katalytische partiële oxidatie van methaan kunnen sterke warmteoverdrachts-limiteringen optreden ten gevolge van hoge reactiesnelheden. Een experimentele reactor, waarin

één enkel Pt gaasje is aangebracht, werd ontwikkeld om de intrinsieke kinetiek van de CPO reactie te onderzoeken in aanwezigheid van warmteoverdrachtslimiteringen. De temperatuur van de katalysator werd direct gemeten met behulp van een puntgelast oppervlaktethermokoppel. Bij de toegepaste condities, d.w.z. bij katalysatortemperaturen tussen 1030 en 1200 K, verblijftijden tussen 0.02 en 0.2 milliseconden, CH_4/O_2 verhoudingen tussen 1.8 en 5.0 en zuurstof conversies tussen 9 en 46 %, werden CO, CO_2 en H_2O als belangrijkste producten waargenomen. Bij korte verblijftijden was CO het primaire product. Waterstof werd alleen waargenomen bij temperaturen hoger dan 1273 K: bij deze condities vertoonde de katalysator echter geen constante activiteit in de tijd. De methaan en zuurstof conversies waren onafhankelijk van de katalysatortemperatuur en werden bijgevolg volledig bepaald door stofoverdracht. De CO vormingssnelheid werd echter in voldoende mate bepaald door de kinetiek van de reactie. Een reactormodel werd afgeleid om de intrinsieke kinetiek van de CO vormingssnelheid te bepalen. Dit vlakke platen model, dat bestaat uit twee rijen vlakke platen in serie, werd gevalideerd door berekende conversies en gasfasetemperaturen te vergelijken met FLUENT simulaties van de 3D geometrie van de gaaskatalysator. Een kinetisch model met zes reactiestappen werd ontwikkeld voor het beschrijven van de invloed van de reactiecondities op de conversies en selectiviteiten gemeten met de Pt gaaskatalysator. Analyse van wiskundige uitdrukkingen voor de intrinsieke CO selectiviteit gaf aan dat adsorptie van methaan zuurstof-geassisteerd moet worden verondersteld om de primaire vorming van CO te kunnen beschrijven. De bijbehorende kinetische parameters werden verkregen met het vlakke platen model, dat stofoverdrachtsverschijnselen op kwantitatieve wijze in rekening brengt. Regressieanalyse met één responsie, namelijk de waargenomen CO selectiviteit, resulteerde in statistisch significante en fysisch-chemisch consistente schattingen van de intrinsieke kinetische parameters van methaan adsorptie. Het model reproduceerde de effecten van katalysatortemperatuur, reactant ruimtetijd en inlaat methaan/zuurstof verhouding op de conversies en selectiviteiten op adequate wijze. Initiële CO selectiviteiten tussen 86 en 96 % werden berekend. De invloed van oppervlaktekinetiek en stofoverdracht op de vorming van CO werd op kwantitatieve wijze geïllustreerd.

Partiële oxidatiereactoren voor productie van methanol en waterstof-voor-brandstofcellen

Adiabatische vastbed CPO reactoren voor de productie van methanol en waterstof-voor-brandstofcellen werden onderzocht met een steady-state, 1-dimensionaal heterogeen reactormodel. In dit reactormodel werden concentratiegradiënten in de katalysatorkorrel expliciet in rekening gebracht: de continuïteitsvergelijkingen voor de korrelfase werden op elke positie in de vastbedreactor opgelost. Simulaties werden uitgevoerd voor gedragen Ni katalysatoren die de indirecte partiële oxidatie van methaan naar synthese gas katalyseren. Snelheidsvergelijkingen voor methaanoxidatie, stoom-reforming en water-gas-shift werden gecombineerd in de berekeningen. Toepassing van adiabatische vastbedreactoren voor het bedrijven van een 10 kW brandstofcel is mogelijk als gevolg van lage katalysatortemperaturen, typisch lager dan 1000 K. Bij de hoge druk condities geschikt voor de productie van 1000 ton methanol per dag werden

echter hoge katalysatortemperaturen berekend (> 1450 K). Katalysatordeactivering als gevolg van sinteren zal bij deze condities erg belangrijk zijn. De invloed van de reformingkinetiek op de simulatieresultaten werd onderzocht door berekeningen uit te voeren met twee verschillende reformingmodellen uit de literatuur. Deze reformingmodellen resulteerden in geval van de brandstofcel in significant verschillende katalysatortemperatuurprofielen. Bij de methanol condities werd altijd een temperatuurmaximum waargenomen aan de reactor inlaat, onafhankelijk van het toegepaste reformingmodel. De invloed van de kinetiek van de oxidatiereactie werd eveneens onderzocht. Reductie van de oxidatie activiteit gaf aanzienlijk lagere katalysatortemperaturen in geval van de brandstofcel, terwijl slechts kleine invloeden werden waargenomen bij methanolcondities. Vastbedreactoren voor waterstofproductie kunnen veilig worden bedreven aangezien gasfasereacties niet zullen ontsteken. Gasfasereacties zullen echter zeer belangrijk zijn in geval van vastbedreactoren voor methanolproductie.

Contents

Summary	3
Samenvatting	7
1 Introduction	15
1.1 Developments in industrial feedstock	15
1.2 Relevance of reaction kinetics and reactor modelling	17
1.3 Aim, scope, and outline of this thesis	19
References	20
2 Partial oxidation reactions and reactors – A literature review	23
2.1 Introduction	23
2.2 Partial oxidation reactions	24
2.3 Historic background	27
2.4 Fixed-bed reactors	29
2.5 Monolith reactors	35
2.6 Fluidized-bed reactors	38
2.7 Membrane reactors	40
2.8 CPO research in industry	43
2.9 Conclusions	45
2.10 Relation to present thesis	46
References	47
3 Partial oxidation of methane over Rh/α-Al₂O₃ – Relative importance of heterogeneous catalytic and homogeneous gas-phase reactions at low conversions	51
Abstract	51
3.1 Introduction	52
3.2 Experimental equipment, procedures, and conditions	53
3.3 Investigation of homogeneous gas-phase reactions at low reactant partial pressures	55

3.4	Investigation of heterogeneous catalytic reactions in the presence of supported catalyst	62
3.5	Conclusions	68
	Notation	69
	References	70
4	An experimental reactor to study the intrinsic kinetics of the catalytic partial oxidation of methane in the presence of heat- transport limitations	73
	Abstract	73
4.1	Introduction	74
4.2	Experimental equipment and procedures	75
4.3	Experimental results	79
4.4	Reactor model development	81
4.5	Application of the flat-plate reactor model using a series-parallel CPO reaction mechanism	91
4.6	Conclusions	93
	Notation	94
	References	96
	Appendix A : Derivation of Eq. (11) for calculation of λ_p	98
	Appendix B : Derivation of Eq. (17) for calculation of $D_{m,i} _p$	100
5	Intrinsic kinetics for the partial oxidation of methane on a Pt gauze at low conversions	103
	Abstract	103
5.1	Introduction	104
5.2	Experimental equipment, procedures, and conditions	105
5.3	Modelling procedures	107
5.4	Effects of reaction conditions	109
5.5	Kinetic model development	111
5.6	Simulation Results and Discussion	119
5.7	Conclusions	127
	Acknowledgement	127
	Notation	127
	References	129

6	Design of adiabatic fixed-bed reactors for the partial oxidation of methane to synthesis gas. Application to production of methanol and hydrogen-for-fuel-cells	131
	Abstract	131
	6.1 Introduction	132
	6.2 Model description and solution procedure	133
	6.3 Model simulations results	142
	6.4 Model sensitivity analysis	149
	6.5 Influence of gas-phase reactions	151
	6.6 Conclusions	152
	Acknowledgement	153
	Notation	153
	References	155
7	General conclusions & Outlook	157
	Dankwoord	159
	Curriculum vitae	161

1

Introduction

1.1 Developments in industrial feedstock

The rapid advances of the chemical industry in the 20th century have been driven to a large extent by a change in feedstock, resulting from a continuous search for cleaner and cheaper raw materials. Initially, coal was the main source of both energy and industrial feedstock, the so-called synthesis gas. Then, a transition took place to liquid hydrocarbon feedstocks from refineries and from crude oil wells. This structural change from solids to liquids particularly resulted in an extraordinary acceleration of economic growth. The increasing natural gas reserves and the high oil prices, peaking at about 35 US\$ per barrel at the beginning of the 1980's (BP Amoco, 1999), resulted in a clear focus on natural gas as a source of petrochemicals and transportation fuels. Efficient use of natural gas resources will be crucial in coping with the challenges currently facing industry, e.g. environmental mandates for the production of clean transportation fuels (Sie et al., 1991).

Global natural gas reserves have grown steadily in the past decades, see Figure 1. The proven reserves would be sufficient for nearly 70 years at current consumption rates. The largest volumes of natural gas are present in the former Soviet Union and in the Middle East. Europe and North America account for more than 50 % of the total natural gas consumption, indicating that a considerable unbalance exists in the geographical distribution of reserves and consumption. Indeed, most natural gas reserves are located in remote and inaccessible areas. Hence, industry is currently facing the challenge of reducing this geographical imbalance by developing technologies and processes to market remote natural gas reserves.

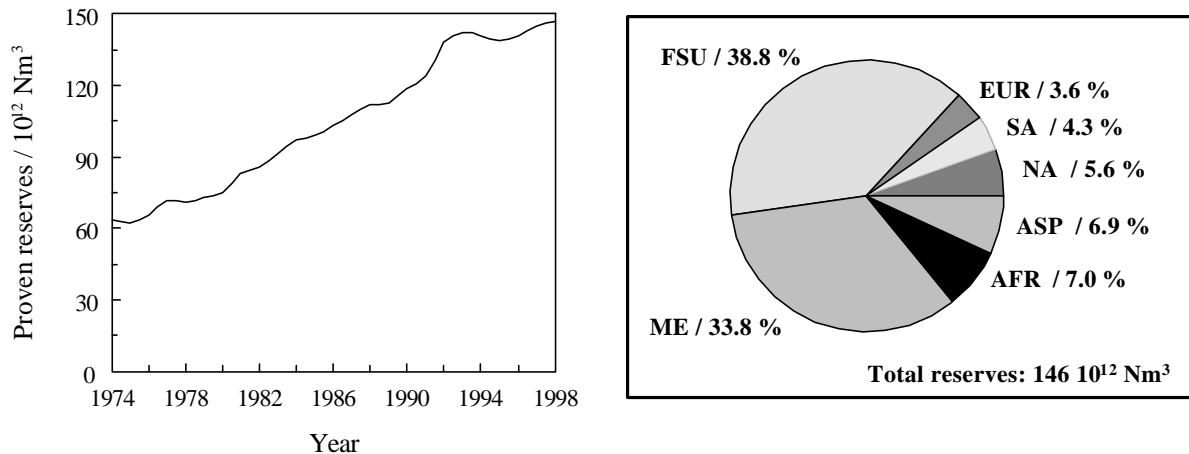


Figure 1. Proven natural gas reserves from 1974 to 1998 and geographic distribution of reserves in 1998 (BP Amoco, 1999). FSU = Former Soviet Union, EUR = Europe, SA = South America, NA = North America, ASP = Asia Pacific, AFR = Africa, ME = Middle east.

Extensive research efforts have been unfolded by industry and academia to develop gas-to-liquids (GTL) technology for the chemical conversion of remote natural gas reserves into high-added-value liquid products. These liquid products, e.g. methanol and synthetic fuels, can be more easily transported to markets, or can be used on-site as environmentally desirable transportation fuel. For instance, GTL conversion would be a viable solution for economic exploration of the large natural gas reserves on Alaska's North Slope (Venkatamaran et al., 1998). At present, crude oil from the giant Alaskan Prudhoe Bay field is transported via the Trans Alaska Pipeline system to Valdez for tanker shipment. Oil production of that field, however, is declining at a rate of about 10 to 12 percent per year. Future projections indicate that the minimum economic pipeline throughput rate will be reached by the year 2009. Natural gas conversion into liquid products, which can be transported via the pipeline system, would significantly increase the window of opportunity of the Trans Alaskan Pipeline. GTL technology would also ensure that the remaining North Slope oil will not be "shut-in" due to insufficient pipeline utilization.

Another incentive for natural gas utilization originates from the chemical conversion of natural gas into hydrogen, which can be converted to electricity in fuel cells. Fuel cells have much higher energy efficiency compared to current combustion-based electric power plants. Also, hydrogen is a much cleaner fuel than hydrocarbon feedstocks: emissions from hydrogen fuel cells are almost negligible. Fuel cells could be adapted for small-scale domestic energy supply and for use in cars and buses. Hydrogen-powered cars thus could be the solution to the stringent environmental demands on exhaust gas pollution. A number of organizations have initiated programs for the development of fuel-cell vehicles, e.g. Zevco (Zero Emission

Vehicle Company), DBB (Daimler Benz Ballard), and the CFCP (California Fuel Cell Partnership). The latter consortium of industrial companies and governmental organizations has planned to place about 50 fuel-cell passenger cars and electric buses on the road between 2000 and 2003. In addition to process development, considerable effort is devoted to the supply and distribution of hydrogen fuels. Natural gas represents the interim feedstock to establishing a global hydrogen economy, ultimately based on renewable resources.

Natural gas conversion processes involve the initial chemical conversion of natural gas into synthesis gas, a mixture of CO and H₂. Synthesis gas can be converted consecutively into liquid fuels or methanol, or can be used directly in conjunction with fuel cells after shift and CO removal. Recent advances in synthesis gas production, in particular the progress in catalytic partial oxidation (CPO), have been a key driving force for development of natural gas conversion processes. Despite the intensive research efforts, however, commercial application of CPO has not been realised yet. The cornerstones of catalytic process development, in particular reaction kinetics and reactor modelling, still require considerable attention.

1.2 Relevance of reaction kinetics and reactor modelling

The development of GTL conversion and the use of hydrogen fuel cells requires safe and economic conversion of natural gas towards synthesis gas. At present, synthesis gas is produced either by catalytic steam reforming or by non-catalytic gasification of methane, the major constituent of natural gas. The catalytic partial oxidation of methane to synthesis gas has been put forward in the past decade as a compact and low capital expenditure alternative to both processes. Extensive investigations have been initiated to study the oxidation reaction on a laboratory reactor scale. These studies primarily aimed at developing suitable catalysts and at the elucidation of the intrinsic kinetics of the oxidation reaction, i.e. the dependence of the reaction rates on the various process parameters. Laboratory experiments and derivation of the intrinsic reaction kinetics are generally the first steps towards the development of industrial reactors, see Figure 2. Catalyst optimization is usually carried out to identify proper catalyst additives and promoters. The intrinsic kinetics of the appropriate catalyst are then combined with reactor models, accounting for the relevant conservation laws and physical properties, to design industrial reactors. This approach allows to overcome costly and time-consuming step-by-step scale up via bench-scale reactors and pilot-plants. It has been argued, that the latter scale-up method is indeed quite ineffective for partial oxidation (Schmidt et al., 1994) because of the exothermic nature of the reaction and possible occurrence of non-selective homogeneous gas-phase reactions.

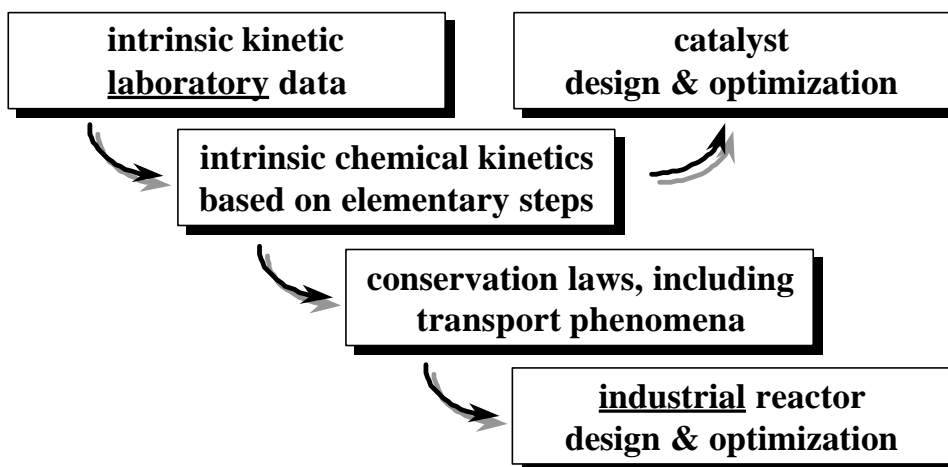


Figure 2. Catalytic process development from laboratory experiments to industrial reactor design (Marin et al., 2000).

The intrinsic kinetics and reaction mechanism of the partial oxidation reaction have been debated extensively in the literature. Both indirect synthesis gas production routes (Prettre et al., 1946, Vernon et al., 1990) and direct synthesis gas formation (Hickman and Schmidt, 1992, Mallens et al., 1995) have been proposed. Direct production of synthesis gas involves initial formation of CO and H₂, which preferentially desorb from the catalyst surface before being converted towards the total oxidation products CO₂ and H₂O, see Figure 3. In case of indirect synthesis gas production, part of the methane is converted to the total oxidation products, which are reformed consecutively with the remaining methane towards synthesis gas. A clear distinction between direct and indirect synthesis gas production routes requires experimental data at short residence times, i.e. at low oxygen conversions. At these conditions, the primary products of the reaction can be identified in a straightforward way. Most kinetic studies, however, have been conducted at conditions corresponding to high or complete oxygen conversion. Experimental studies reported in this thesis were always conducted at low oxygen conversions, to allow investigating the primary products of the CPO reaction in detail.

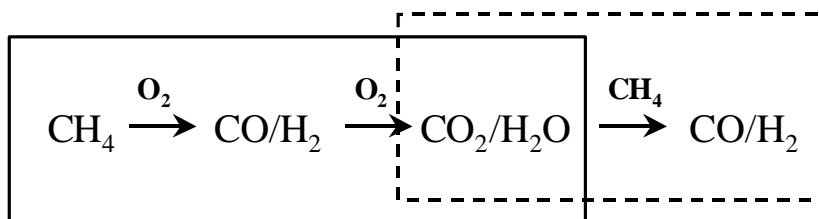


Figure 3. Production of synthesis gas from methane and oxygen: direct production (closed frame) vs indirect production (dotted frame).

Direct production of synthesis gas from methane is a mildly exothermic reaction. In case of the indirect route, however, the heat produced in the total combustion reactions can lead to very high catalyst temperatures. Furthermore, high pressures are required in downstream processes such as methanol and synthetic fuel production. At these conditions, non-selective homogeneous reactions can occur. Reactor modelling is a useful tool to investigate the influence of the latter effects on reactor operation and performance. Reactor simulations can be carried out at conditions which cannot be realised safely in the laboratory. Design and investigation of industrial CPO reactors using both intrinsic kinetic and reactor models will be addressed in detail in this thesis.

1.3 Aim, scope, and outline of this thesis

The main part of the work described in this thesis was performed within the framework of the “Methane-to-syngas” JOULE projects of the European Commission, no. JOU2-CT92-0073, and no. JOU3-CT95-0026. The main objective of these programs was to investigate the potential of partial oxidation technology in the areas of gas-to-liquids conversion and fuel cell operation. Within this context, the present thesis aims to contribute to fundamental insights into (1) the reaction kinetics of the partial oxidation reaction, using different catalysts and reactor configurations, and (2) the operation of industrial scale CPO reactors for production of methanol and hydrogen-for-fuel-cells by means of reactor modelling.

In **Chapter 2** a literature review is presented with respect to the developments of catalytic partial oxidation in the past decade. The reactions occurring during the partial oxidation of methane are discussed, emphasizing on selective and non-selective heterogeneous and homogeneous reactions. Pioneering work on the partial oxidation reaction is highlighted. Progress in CPO research in the past decade is discussed with special emphasis on different reactor configurations, catalysts, and reaction mechanisms. The relation of the work presented in this thesis to the research described in the literature is indicated.

At present, both Ni and Rh have been identified in the literature as the most active and selective catalysts for the CPO reaction. Ni catalysts will be preferred from industrial point of view due to low costs. Rh based catalysts display higher stability compared to Ni, but suffer from high cost and limited availability. In **Chapter 3** the intrinsic kinetics of the CPO reaction are studied in a fixed-bed reactor at low oxygen conversions using a 0.3 wt% Rh/ α -Al₂O₃ catalyst. Experiments are performed at conditions as close as possible to the industrially desired values, i.e. at high temperatures and pressures. At these conditions, non-selective homogeneous gas-phase reactions can become important. Hence, both heterogeneous catalytic and homogeneous gas-phase reactions were investigated. The relative importance of

homogeneous and heterogeneous reactions at low oxygen conversions will be discussed.

The partial oxidation of methane to synthesis gas is only mildly exothermic when carried out selectively. Due to the high reaction rates (Hickman and Schmidt, 1992), however, heat-transport limitations will be inevitable, even at high synthesis gas selectivities. Investigation of the intrinsic kinetics therefore requires dedicated reactors to account for the latter limitations. In **Chapters 4 and 5** an experimental reactor is described, containing a single Pt metal gauze, which allows to investigate the partial oxidation of methane at low oxygen conversions in the presence of heat-transport limitations. **Chapter 4** focuses on the experimental results and the derivation of a reactor model to estimate the intrinsic kinetic parameters of the CPO reaction from non-intrinsic laboratory data. An elementary step kinetic model was developed to describe the experimental results obtained with the Pt metal gauze. This kinetic model is described in **Chapter 5**, emphasizing primary formation of CO and the influence of mass-transport herein.

As indicated in this chapter, reactor modelling is a useful tool to investigate the CPO reaction at conditions which cannot be realised safely in a laboratory reactor. Hence, the design of adiabatic fixed-bed reactors for the catalytic partial oxidation of methane at conditions suitable for methanol and hydrogen-for-fuel-cells production is presented in **Chapter 6**. The proposed reactor designs are based on supported Ni catalysts. Intrinsic kinetics are taken from the literature. Special attention was paid in the simulations to hot-spot formation due to exothermic total oxidation reactions. Sensitivity analyses are presented with respect to the intrinsic reforming and oxidation kinetics. Also, the possible occurrence of homogeneous gas-phase reactions is considered.

In **Chapter 7** the main results of this thesis are discussed and a short overview of expected future developments is given.

References

- BP Amoco statistical review of world energy (1999). Available at internet address: <http://www.bpamoco.com/worldenergy>
- Hickman, D.A., & Schmidt L.D. (1992). Synthesis gas formation by direct oxidation of methane over Pt monoliths. *J. Catal.*, *13*, 267-282.
- Mallens, E.P.J., Hoebink, J.H.J.B. and Marin, G.B. (1995). An investigation on the reaction mechanism for the partial oxidation of methane to synthesis gas over platinum. *Catal. Lett.*, *33*, 291-304.
- Marin, G.B., Kapteijn, F., van Diepen, A.E., & Moulijn J.A. (2000). Catalytic reaction and reactor engineering, in Combinatorial catalysis and high throughput catalyst design and testing, Kluwer.
- Prettre, M., Eichner, Ch., & Perrin, M. (1946). The catalytic oxidation of methane to carbon monoxide and hydrogen. *Trans. Farad. Soc.*, *43*, 335-340.
- Schmidt, L.D., Huff, M., & Bharadwaj, S.S. (1994). Catalytic partial oxidation reactions and reactors. *Chem. Eng. Sci.*, *49*, 3981-3994.

- Sie, S.T., Senden, M.M.G., & van Weghem, H.M.H. (1991). Conversion of natural gas to transportation fuels via the Shell Middle Distillate Synthesis Process (SMDS). *Catal. Today*, 8, 371-394.
- Venkatamaran, V.K., Guthrie, H.D., Avellanet, R.A., & Driscoll, D.J. (1998). Overview of US DOE's natural gas-to-liquids RD&D program and commercialization strategy. *Stud. Surf. Sci. Catal.*, 119, 913-918.
- Vernon, P.D.F., Green, M.L.H. Cheetham, A.K., & Ashcroft, A.T. (1990). Partial oxidation of methane to synthesis gas. *Catal. Lett.*, 6, 181-186.

2

Partial oxidation reactions and reactors

A literature review

2.1 Introduction

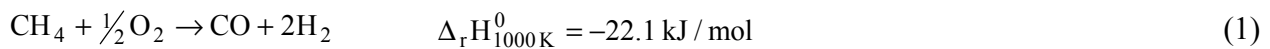
Natural gas utilization has become an important research area in the past decades. Both direct and indirect conversion routes for methane, the major constituent of natural gas, towards high-added-value chemicals have been investigated intensively. Direct conversion routes, e.g. the oxidative coupling of methane towards ethylene, received much attention in the second part of the 1980's and the early 1990's. The product yields obtained in this process, however, were insufficient to justify commercial application. Hence, indirect conversion routes, with synthesis gas as intermediate, attracted widespread attention in recent years. A rapid look at the proceedings of the Natural Gas Conversion Symposia (Holmen et al., 1990, Curry-Hyde and Howe, 1993, Parmaliana et al., 1998) held in the past years clearly shows the growing interest devoted to synthesis gas production via catalytic partial oxidation (CPO). In the present chapter, a literature review will be presented with respect to the developments of the catalytic partial oxidation of methane to synthesis gas. Partial oxidation reactions will be dealt with first, emphasizing on selective and possible non-selective heterogeneous and homogeneous reactions. Pioneering work on the CPO reaction will be presented next. In addition, the most important contributions to CPO research in industry and academia of the past decade will be discussed. In particular, different reactor concepts, catalysts, reaction mechanisms, as well as practical difficulties will be addressed. Finally, general conclusions and the relation to the work described in this thesis will be highlighted.

2.2 Partial oxidation reactions

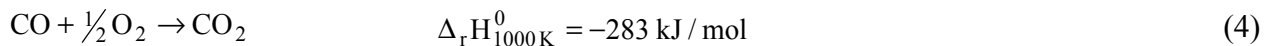
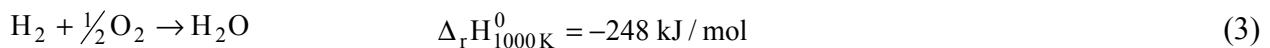
This section provides an introduction to selective and non-selective heterogeneous catalytic reactions as well as homogeneous gas-phase reactions that can occur during the partial oxidation of methane to synthesis gas. Special reference is made to the work performed within the Laboratory of Chemical Reactor Engineering at Eindhoven University of Technology.

2.2.1 Heterogeneous catalytic reactions

The direct catalytic partial oxidation of methane to synthesis gas ideally proceeds via:

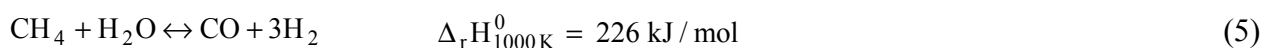


The 2:1 H₂/CO ratio of the reaction product is considered to be optimal for downstream production of methanol or liquid fuels via Fischer-Tropsch synthesis. The selectivities towards CO and H₂, however, can be influenced by the simultaneous occurrence of the total combustion of methane, and secondary oxidation reactions of CO and H₂:

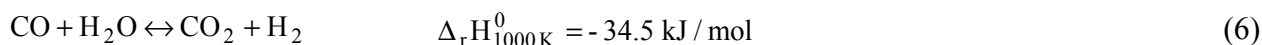


These exothermic, non-selective oxidation reactions can result in high catalyst temperatures, which are undesirable with respect to the catalyst stability and can cause severe heat-transport limitations. At low temperatures, atmospheric pressure, and 2:1 CH₄/O₂ ratio, thermodynamics indeed indicate that the equilibrium product composition consists of a mixture of total and partial oxidation products. At temperatures above 1200 K and 1 bar pressure, however, synthesis gas is produced with 100% selectivity at complete oxygen conversion (Mallens, 1996).

The main advantage of catalytic partial oxidation over conventional steam reforming is the slight exothermicity of the former reaction. Steam reforming of methane towards synthesis gas is highly endothermic, thus requiring external heat input to drive the reaction:

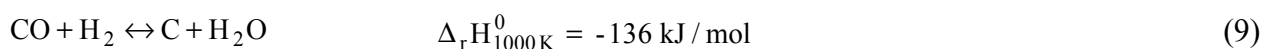
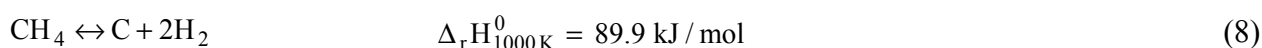


In addition, the 3:1 H₂/CO ratio is too high for downstream applications and is therefore modified in a second reactor by means of the water-gas shift reaction:



At the applied reaction conditions, i.e. temperatures above 1100 K, the equilibrium of the latter reaction will shift to the left, resulting in a lower H₂/CO ratio. Steam reformers require residence times in the order of 1 s to obtain equilibrium synthesis gas yields. Hence, the reforming reaction is carried out in large tubular reactors, whereas the CPO reaction can be carried out in significantly smaller reactors, due to high reaction rates (Hickman and Schmidt, 1992).

A significant drawback in catalytic partial oxidation and methane steam reforming is the possible occurrence of carbon deposition, via the Boudouard reaction (7), decomposition of methane (8), and the CO reduction reaction (9):



The exothermic Boudouard and CO reduction reactions are obviously favored at low temperatures and high pressures, whereas methane decomposition is favored at high temperatures and low pressures. Carbon deposition should always be minimized, since it can lead to catalyst deactivation and reactor plugging. Equilibrium calculations including elementary carbon as possible reaction product, indicate that carbon formation is not favored at temperatures higher than 1200 K at atmospheric pressure and 2:1 CH₄/O₂ ratio (Mallens, 1996). At a pressure of 100 bar, temperatures above 1250 K are required to avoid carbon formation (Mallens, 1996).

2.2.2 Homogeneous gas-phase reactions

Industrial application of methane partial oxidation requires high temperatures to obtain high synthesis gas yields, and high operating pressures to reduce downstream compression costs. At these conditions, however, homogeneous gas-phase reactions can become important and may lead to explosions, thermal runaway, and to the formation of undesired products. Gas-phase reactions can occur either in parallel to catalytic reactions, or can be initiated heterogeneously by the catalyst surface, cf. the oxidative coupling of methane to higher hydrocarbons. Several homogeneous gas-phase kinetic models can be found in the literature. Kinetic models have been proposed for the total combustion of hydrocarbons (Tsang and Hampson, 1986), and for the homogeneous oxidative coupling of methane (Chen et al., 1994). However, the latter kinetic models are optimized at conditions that bear little relation to methane partial oxidation.

Berger and Marin (1999) therefore developed a gas-phase kinetic model at conditions more typical for the partial oxidation of methane to synthesis gas, i.e. at temperatures of 1000-1300 K, pressures of 3-8 bar, and CH_4/O_2 ratios between 2 and 3. Kinetic experiments were conducted in an empty sintered-alumina reactor. At the applied conditions, both total and partial oxidation products were observed, as well as significant amounts of C_2H_6 and C_2H_4 . The experimental data were described using a kinetic model consisting of 40 reversible gas-phase reactions between 13 molecular (H_2 , H_2O , H_2O_2 , O_2 , CH_4 , C_2H_6 , C_2H_4 , C_2H_2 , C_3H_8 , C_3H_6 , CH_2O , CO , and CO_2) and 10 radical species ($\text{H}\bullet$, $\text{O}\bullet$, $\text{OH}\bullet$, $\text{HO}_2\bullet$, $\text{CH}_3\bullet$, $\text{C}_2\text{H}_5\bullet$, $\text{C}_2\text{H}_3\bullet$, $\text{C}_3\text{H}_7\bullet$, $\text{CH}_3\text{O}\bullet$, and $\text{CHO}\bullet$). The kinetic rate parameters were obtained from literature and from regression analysis. The most important initiation, propagation, and termination steps during the initial stage of the reaction are shown in Table 1. The authors suggested that the gas-phase kinetic model can be used as a tool to investigate the feasibility of CPO reactors operating at high temperatures and pressures.

Table 1. *Predominating radical reactions during the ignition stage (Berger and Marin, 1999). Conditions: $p = 5$ bar, $T = 1107$ K, $\text{CH}_4/\text{O}_2 = 2.6$*

Reaction
$\text{CH}_4 + \text{OH}\bullet \rightleftharpoons \text{CH}_3\bullet + \text{H}_2\text{O}$
$\text{CH}_4 + \text{HO}_2\bullet \rightleftharpoons \text{CH}_3\bullet + \text{H}_2\text{O}_2$
$\text{CH}_3\bullet + \text{O}_2 \rightleftharpoons \text{CH}_2\text{O} + \text{OH}\bullet$
$2 \text{CH}_3\bullet + \text{M} \rightleftharpoons \text{C}_2\text{H}_6 + \text{M}$
$\text{CH}_2\text{O} + \text{CH}_3\bullet \rightleftharpoons \text{CHO}\bullet + \text{CH}_4$
$\text{CHO}\bullet + \text{M} \rightleftharpoons \text{CO} + \text{H}\bullet + \text{M}$
$\text{O}_2 + \text{H}\bullet + \text{M} \rightleftharpoons \text{HO}_2\bullet + \text{M}$
$\text{H}_2\text{O}_2 + \text{M} \rightleftharpoons \text{OH}\bullet + \text{OH}\bullet + \text{M}$

Gas-phase reactions are generally suppressed during laboratory experiments by carrying out the CPO reaction at rather low temperatures and at pressures close to atmospheric conditions. Also, low reactant partial pressures are applied by diluting the feed mixtures. As indicated previously, industrial application requires high temperatures and pressures. Dietz III and Schmidt (1995) therefore investigated the partial oxidation of methane at different total pressures. The reaction was carried out using Rh coated monoliths at 1273 K, residence times of 10^{-3} s, pressures between 1 and 5 bar, CH_4/air and CH_4/O_2 feeds. The experimental results indicated that the selectivities to CO and H_2 remained high at increasing pressures. Formation of C_2 -hydrocarbons, indicative of gas-phase reactions, was not observed. The authors thus concluded that gas-phase reactions were not important at the applied reaction conditions. In contrast, Slaa et al. (1997) did

observe significant formation of C_2H_6 and C_2H_4 during the partial oxidation of methane over 0.3 wt% Rh/ Al_2O_3 at 1273 K and 4 bar, using 6.7/3.3/90 $CH_4/O_2/He$ mixtures. However, preliminary reactor simulations with the slightly modified gas-phase kinetic model of Chen et al. (1994), obtained at conditions typical for oxidative coupling of methane, indicated that gas-phase reactions were not important. The authors thus concluded that the products were produced entirely via heterogeneous reactions on the Rh catalyst. In the absence of helium, however, the gas-phase model showed that homogeneous reactions occurred to a significant extent.

2.3 Historic background

The work of Prettre et al. (1946) can be considered as a historic benchmark for research on the catalytic partial oxidation of methane to synthesis gas. The reaction was investigated in a fixed-bed reactor using a reduced 10 wt% refractory-supported Ni catalyst, at temperatures of 923-1323 K, CH_4/O_2 ratios between 1.7 and 2.0, and atmospheric pressure. The CH_4 conversion amounted to 96 % with synthesis gas selectivities as high as 97 % at an outlet catalyst bed temperature of 1173 K. At the investigated conditions, the gas-phase composition at the reactor outlet agreed well with thermodynamic calculations indicating that thermodynamic equilibrium was attained in all cases. Measured axial temperature profiles showed that a strongly exothermic reaction was followed by an endothermic stage, see Figure 1.

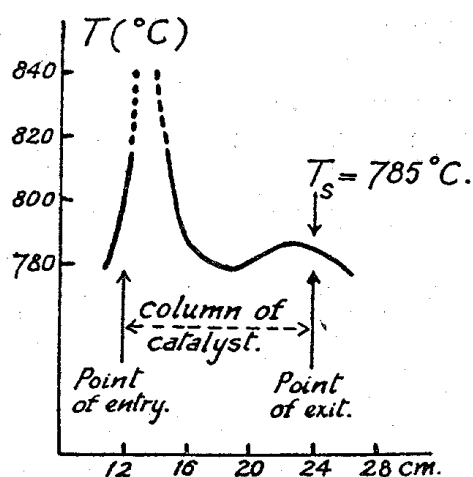


Figure 1. Measured axial temperature profile in a fixed-bed reactor over a 10 wt% refractory-supported Ni catalyst (Prettre et al., 1946).

The strong increase of the catalyst temperature near the reactor inlet was assigned to complete combustion of part of the methane. The subsequent endothermic stage was explained on the basis of reforming reactions of the remaining methane with H_2O and CO_2 , produced in the combustion reaction. This proposed reaction sequence of combustion and reforming in series is

generally referred to in the literature as the indirect syngas formation route.

Prettre et al. suggested that kinetic studies of methane partial oxidation are difficult to conduct as a result of the high reaction rates. Hence, Huszar et al. (1971) investigated the CPO reaction in a single-pellet reactor, which allowed measuring the corresponding reaction rates. Experiments were performed with 1-20 wt% Ni-mullite single-pellet catalysts at temperatures of 1033-1173 K using a 25% CH₄/air mixture. The principal products of the reaction were H₂, CO, and H₂O, even at low conversions. The experimental results indicated that the oxygen conversion rates were hardly influenced by the catalyst temperature. The authors thus concluded that the kinetics were determined by diffusion of oxygen across the boundary layer surrounding the catalyst grain. As a result of these mass-transport limitations, the concentration of oxygen was very low at the catalyst surface. Consequently, it was suggested that the Ni-catalyst was in the reduced state during reaction. At high oxygen concentrations, however, the catalyst was found to deactivate due to oxidation of the Ni metal.

Supported nickel catalysts were also studied by Gavalas et al. (1984). The activity of 6.6 wt% NiO on α -Al₂O₃ and ZrO₂ supports in the fuel-rich oxidation of methane was measured as a function of time-on-stream using a fixed-bed reactor. The catalyst bed temperature and the CH₄/O₂ ratio were varied in the range from 910 to 1030 K and 0.8 to 9.0, respectively. The reactor was operated in the differential mode, with methane conversions of 2% or less. Hence, it was assumed that the catalyst surface was oxidized at the applied reaction conditions. At a typical reaction temperature of 983 K and CH₄/O₂ ratios between 0.8 and 5.0, CO₂ was the only oxygenated carbon-containing product. At a CH₄/O₂ ratio of 9.0, however, selectivities to CO and CO₂ were comparable. The initial activity of the Ni catalyst increased significantly after reduction in H₂. The authors concluded that the activity increase was caused by reduction of NiO to Ni⁰. However, the methane consumption rates after reduction decreased with time-on-stream due to reoxidation of Ni⁰ to NiO.

The group of Green and co-workers initiated renewed interest in methane partial oxidation. Both rare-earth ruthenium oxides of the pyrochlore type (Ashcroft et al., 1990), and supported transition metals (Vernon et al., 1990) were studied. Ashcroft et al. (1990) showed that ruthenium analogues of rare-earth tin oxides, which were shown to be very active for the oxidative coupling of methane, were also very active and selective for the partial oxidation of methane to synthesis gas. Both rare-earth Ru oxides, of general formula Ln₂Ru₂O₇ (Ln = lanthanide element, e.g. Pr, Sm, Eu, Gd) and alumina-supported Ru catalysts were investigated. At a catalyst bed temperature of 1050 K, atmospheric pressure, and with diluted CH₄/O₂/N₂ mixtures, methane conversions above 90 % and synthesis gas selectivities in the range from 95 to 99 % were observed. XPS analysis of the used rare-earth oxides revealed that partial reduction of the pyrochlores had taken place. The authors thus concluded that the active component for partial oxidation is metallic Ru.

Vernon et al. (1990) investigated the activity of supported transition metals (Ni, Ru, Rh, Pd, Ir, and Pt) at temperatures of 650-1050 K, pressures between 1 and 20 bar, using 2:1:4 CH₄/O₂/N₂ mixtures. The experiments indicated high conversions and synthesis gas yields on most of the catalysts studied: equilibrium conditions were always established. The results corroborated the findings of Ashcroft et al. (1990), suggesting that the active phase of the catalyst is the reduced metal. A CH₄/O₂ ratio of 2.0 was found to give optimum CO and H₂ yields, as expected from stoichiometry. The experiments also indicated that synthesis gas production was favored at low pressure and high temperature, in accordance with thermodynamics. Both Ashcroft et al. (1990) and Vernon et al. (1990) suggested that the reaction mechanism might involve initial combustion of part of the methane, followed by a sequence of steam reforming and water-gas shift.

The work of Prettre et al. (1946), Huszar et al. (1971), and Gavalas et al. (1984) covers to a large extent the research on catalytic partial oxidation in the period up to the 1990's. The results of Ashcroft et al. (1990) and Vernon et al. (1990) in particular catalyzed the systematic investigation of CPO in the past decade. An overview of the corresponding literature will be presented in the next sections. First, the discussion is centered on fixed-bed reactors, which have been widely applied in academia. Experimental work on monolith and fluidized-bed reactors will be presented next. Finally, membrane reactor types for the catalytic partial oxidation of methane will be discussed.

2.4 Fixed-bed reactors

In the previous section, characteristic features of the catalytic partial oxidation of methane to synthesis gas were illustrated. The possible occurrence of high catalyst bed temperatures during indirect CPO over Ni catalysts was indicated. It was shown additionally that high reaction rates could lead to mass transport limitations, thus complicating kinetic studies. Also, the oxidation state of the catalyst was found to influence the observed activity and selectivity considerably. In the past decade, these issues were systematically investigated using fixed-bed reactors. Supported group VIII metal catalysts (Fe, Co, Ni, Ru, Rh, Pd, Ir, Pt) were analysed in particular. Comparative studies on the activity of various supported group VIII metals can be found in Boucouvalas et al. (1996) and Nakagawa et al. (1998). At present, both Ni and Rh-based catalysts have been identified to be the most promising CPO catalysts. Hence, an overview will be presented in this section on fixed-bed reactor studies in case of Ni and Rh catalysts.

2.4.1 Ni-based catalysts

In accordance with the work of Prettre et al. (1946), Vermeiren et al. (1992) also observed a steep temperature profile over the catalyst bed in case of 1 and 5 wt% Ni catalysts loaded on

Al_2O_3 , $\text{SiO}_2/\text{Al}_2\text{O}_3$, $\text{SiO}_2/\text{ZrO}_2$ and H-Y zeolite. Application of the 5 wt% $\text{Ni}/\text{Al}_2\text{O}_3$ catalyst, 2:1:7 $\text{CH}_4/\text{O}_2/\text{N}_2$ feed mixtures, $W/F_0 = 2.4 \text{ kg s mol}^{-1}$, and a fixed furnace temperature of 873 K, resulted in a temperature maximum near the inlet of the catalyst bed of approximately 1000 K. Support effects were found in case of the 1 wt% Ni catalyst loaded on acidic $\text{SiO}_2/\text{ZrO}_2$ and H-Y zeolite. In the latter cases, lower conversions were found compared to the Al_2O_3 supports. Thermodynamic calculations indicated that the CPO reaction could be described by the initial combustion of methane to carbon oxides and water, in combination with the steam reforming and water-gas shift reactions.

Similar conclusions with respect to the reaction mechanism were drawn by Dissanayake et al. (1991). The influence of the catalyst bed temperature and oxidation state of a 25 wt% $\text{Ni}/\text{Al}_2\text{O}_3$ catalyst were investigated. At atmospheric pressure, using a 1.8:1:25 $\text{CH}_4/\text{O}_2/\text{He}$ mixture, typical hysteresis phenomena were observed when the catalyst bed temperature was increased, see Figure 2.

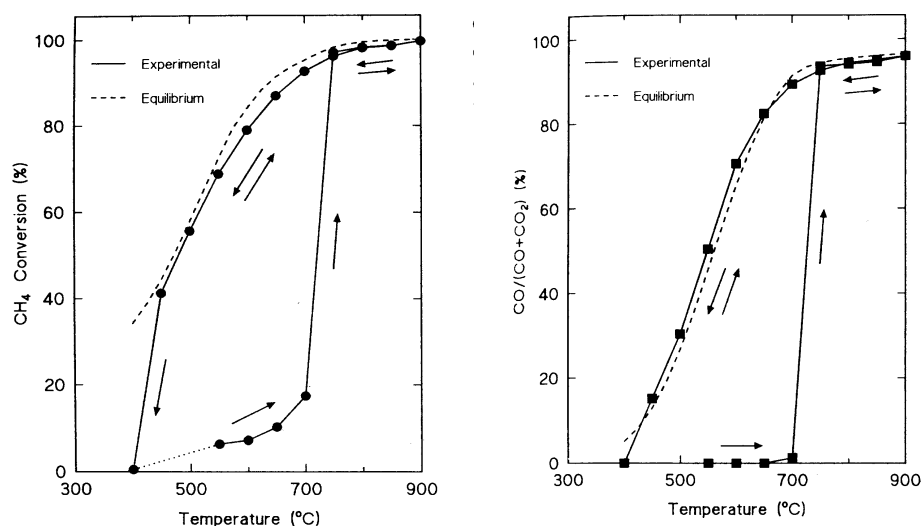


Figure 2. Effect of the catalyst bed temperature on CH_4 conversion and CO selectivity over precalcined $\text{Ni}/\text{Al}_2\text{O}_3$ (Dissanayake et al., 1991). Conditions: $\text{CH}_4/\text{O}_2 = 1.8$; Space velocity = 750 h^{-1} .

The observed conversions and selectivities were interpreted in terms of different oxidation states of the Ni catalyst, as determined by XRD and XPS analysis. At temperatures up to 973 K, low methane conversions were observed, with CO_2 and H_2O as the main products. At these conditions, the catalyst bed consisted of a NiAl_2O_4 phase with moderate total oxidation activity. A sudden transition occurred at 973 K to high conversions with equilibrium selectivities of CO and H_2 . At these conditions, a small part of the NiAl_2O_4 was decomposed near the reactor inlet to $\text{NiO}/\text{Al}_2\text{O}_3$, due to sufficiently low oxygen partial pressures. Part of the methane was oxidized to

CO₂ and H₂O on the NiO phase, resulting in a 50 K temperature increase at the reactor inlet. The remaining CH₄/CO₂/H₂O mixture consecutively reduced the catalyst bed to Ni⁰, which catalyzed the reforming reactions to equilibrium. At decreasing catalyst bed temperatures, the Ni⁰ and NiO zones were progressively reoxidized, causing the observed drop in conversion and selectivity. Below 723 K, the catalyst bed was reverted completely to the NiAl₂O₄ phase. In case of reduced Ni/Al₂O₃ catalysts, the conversions and selectivities were immediately determined by the high-activity state as shown in Figure 2.

Choudhary et al. (1992, 1993) reported H₂ and CO selectivities higher than the corresponding equilibrium values over NiO loaded on different supports (CaO, Al₂O₃, and rare earth oxides). Low catalyst bed temperatures (≤ 973 K) and short contact times (7 ms) were applied. Reduced Ni was identified as the active surface for the CPO reaction. The steam and carbon dioxide reforming rates were found to be small at the applied temperatures. Hence, it was suggested that synthesis gas was formed directly from methane without formation of CO₂ and H₂O as primary products. Dissanayake et al. (1993) tested a Ni/Yb₂O₃ catalyst similar to the one used by Choudhary et al. (1993). Experiments indicated, however, that hot spots could be formed with temperatures as much as 300 K higher than the measured catalyst bed temperature. It was thus concluded that the reported deviations from thermodynamic equilibrium probably resulted from a small hot zone in the reactor and incorrect measurement of the actual temperature.

Hot spot formation was eliminated in the work of Hu and Ruckenstein (1995) by using a pulse technique, involving very small amounts of reactants. A 20 wt% Ni/La₂O₃ catalyst was studied, using 2:1 CH₄/O₂ mixtures, and catalyst bed temperatures of 873 K. At the applied reaction conditions, conversions and selectivities were significantly lower than the corresponding equilibrium values. In case of reduced catalysts, the CO selectivity was found to increase at decreasing residence times. Consequently, it was concluded that CO was the primary product of the CPO reaction, whereas CO₂ was generated from CO. A pyrolysis mechanism for methane partial oxidation at low temperature was proposed, see Table 2.

Table 2. CPO reaction mechanism on Ni/La₂O₃ at 873 K according to Hu and Ruckenstein (1995).

site + CH ₄ → CH _{4(s)}	(1)	C _(s) + O _(s) → CO _(s) → CO _(g)	(7)
site + O ₂ → 2O _(s)	(2)	CO _(s) + O _(s) → CO _{2(s)} → CO _{2(g)}	(8)
CH _{4(s)} → CH _{3(s)} + H _(s)	(3)	H _(s) + H _(s) → H _{2(s)}	(9)
CH _{3(s)} → CH _{2(s)} + H _(s)	(4)	H _(s) + O _(s) → OH _(s)	(10)
CH _{2(s)} → CH _(s) + H _(s)	(5)	OH _(s) + H _(s) → H _{2O(s)}	(11)
CH _(s) → C _(s) + H _(s)	(6)	H _{2O(s)} → H _{2O(g)}	(12)

Direct formation of CO was also suggested by Lemonidou et al. (1997) and Drago et al. (1998), using 0.5 wt% Ni/CaO·2Al₂O₃ and 10 wt% NiO/SiO₂ catalysts, respectively.

The tendency for coke deposition is generally considered to be the main drawback in the application of supported Ni catalysts. Carbon deposition can lead to rapid catalyst deactivation, whereas whisker-carbon formation can result in reactor plugging. Claridge et al. (1993) indeed reported that Al₂O₃ supported Ni catalysts displayed considerably higher carbon deposition rates compared to supported noble metal catalysts. Hence, many studies have been conducted in the past decade to develop supported Ni catalysts with high resistance to coke formation. Tang et al. (1998) and Ruckenstein and Hu (1999) reported that NiO/MgO catalysts showed high activity and selectivity with very low carbon deposition rates. It was suggested that the formation of a NiO/MgO solid solution suppressed the agglomeration of small Ni particles to large crystallites, which are generally susceptible to carbon deposition. Nakagawa et al. (1999) investigated a bimetallic Ir-Ni/La₂O₃ catalyst with low metal loadings, 0.25 and 0.5 wt%, respectively. As a result of the low Ni content, carbon deposition could be suppressed effectively. Despite the low Ni content, the activity remained sufficiently high by addition of highly active Ir. Recently, Ito et al. (1999) proposed a carbon deposition/removal procedure for supported Ni catalysts, which resulted in very low carbon deposition rates with minor influences on the catalytic activity. The procedure was based on the hypothesis that Ni sites, active for whisker-carbon formation, are different from catalytically active Ni sites and can be effectively removed.

2.4.2 Rh-based catalysts

In contrast to supported Ni catalysts, Rh-based catalysts display both high activity and stability during the catalytic partial oxidation of methane to synthesis gas. Rh catalysts also showed the highest resistance to carbon formation (Claridge et al., 1993). As indicated in section 2.3, Vernon et al. (1990) studied synthesis gas formation over a 1 wt% Rh/Al₂O₃ catalyst. Equilibrium conversions and synthesis gas selectivities were generally established. It was suggested that the reaction mechanism involved total oxidation of part of the methane, followed by steam reforming and water-gas shift reactions. Boucouvalas et al. (1994) also proposed the indirect CPO reaction mechanism in case of 0.2 and 0.5 wt% Rh/ γ -Al₂O₃ catalysts at temperatures between 723 and 973 K. Both the CO and H₂ selectivities were found to increase at increasing space times, suggesting the sequence of total oxidation and reforming reactions.

Buyevskaya et al. (1994) and Walter et al. (1994) studied the reaction mechanism over a 1 wt% Rh/ γ -Al₂O₃ catalyst using the Temporal Analysis of Products (TAP) setup and diffuse reflectance infrared spectroscopy (DRIFTS). The TAP investigations at 1013 K revealed that the product distribution strongly depended on the degree of surface reduction: the CO production

Table 3. Mars-van Krevelen mechanism for synthesis gas formation over a Rh-sponge catalyst at 930-1073 K (Mallens et al., 1997).

	σ
$\text{CH}_{4(g)} + 5^* \rightarrow \text{C}^* + 4\text{H}^*$	2
$\text{C}^* + \text{Rh}_x\text{O} \rightarrow \text{Rh}_x^0 + \text{CO}_{(g)} + ^*$	2
$\text{O}_{2(g)} + 2\text{Rh}_x^0 \rightarrow 2\text{Rh}_x\text{O}$	1
$2\text{H}^* \rightarrow \text{H}_{2(g)} + 2^*$	4
$2\text{CH}_4 + \text{O}_2 \rightarrow 2\text{CO} + 4\text{H}_2$	

Slaa et al. (1997) studied mechanistic aspects of methane partial oxidation on a 0.3 wt% Rh/ α -Al₂O₃ catalyst at temperatures above 1273 K and pressures up to 8 bar. High temperatures were applied in order to avoid carbon formation and to obtain high equilibrium selectivities to CO and H₂. Intrinsic kinetic data were obtained when the feed was diluted with helium. The experimental results indicated that the observed product distribution depended strongly on the oxidation state of the Rh catalyst. At low oxygen conversions, i.e. in the oxidized state, CO₂, H₂O, and C₂H₆ were identified as the primary products. Significant amounts of CO, H₂, and C₂H₄ were found at increasing oxygen conversions. High selectivities to CO and H₂ were obtained at complete oxygen conversion, i.e. in the reduced state of the catalyst. The observed trends in conversions and selectivities at low oxygen conversions were also found in case of experiments with the α -Al₂O₃ support alone.

The work of Buyevskaya et al. (1994), Walter et al. (1994), and Slaa et al. (1997) clearly illustrated that the applied supports are not completely inert at the investigated reaction conditions. Wang et al. (1996) and Tian et al. (1999) showed that Al₂O₃ supports can act as additional oxygen source through the inverse spillover of water or hydroxyl species onto the Rh particles. Heitnes Hofstad et al. (1998) indicated that introduction of Al₂O₃ supports resulted in faster formation of oxygenated products over Rh. Also, the time required to obtain a completely reduced catalyst significantly increased with Al₂O₃ supports. Recently, Wang and Ruckenstein (1999) studied the activity and stability of 1 wt% Rh supported on MgO and SiO₂. At 1023 K and atmospheric pressure, the Rh/MgO catalyst displayed high and constant activity and selectivity during 100 h of operation. The Rh/SiO₂ catalyst, however, deactivated rapidly due to carbon deposition. It was suggested that the strong interactions between Rh and MgO, especially the formation of MgRh₂O₄, were responsible for the high stability of the MgO-supported catalysts.

2.5 Monolith reactors

Noble metal-coated monoliths are extensively used in the automotive catalytic converter for the removal of NO, CO, and hydrocarbons from exhaust gases. In the past decade, the monolith reactor has also been recognized as a suitable catalyst configuration for the catalytic partial oxidation of methane to synthesis gas. Monoliths have a large surface-to-volume ratio compared to catalyst particles, indicating that the required reactor volume can be significantly reduced. In addition, high flow rates can be realised without large pressure drop in extruded and structured monoliths. Hence, monoliths are particularly suitable to study fast and exothermic oxidation reactions, since high flow rates result in high mass and heat transfer rates.

Korchnak et al. (1990) proposed a pilot-scale catalytic partial oxidation reactor consisting of noble metals supported by an alumina washcoat on cordierite extruded monoliths. Residence times of ~40 ms were required to obtain essentially complete conversion of methane. Hochmut (1992) used the design proposed by Korchnak et al. (1990) to investigate synthesis gas formation on a laboratory scale at high temperatures, $1000 < T < 1200$ K, and pressures between 22 and 31 bar. Monoliths containing 300 pores per square inch (300 ppi) were coated with a 1:1 weight ratio of Pt/Pd on a ceria stabilized γ -Al₂O₃ washcoat. The measured product concentrations in case of CH₄/O₂/H₂O feed mixtures closely corresponded to the equilibrium values. Analysis of the axial concentration and temperature profiles revealed that methane initially reacted with oxygen towards CO, CO₂, and H₂O, resulting in a large temperature exotherm. Reforming and water-gas shift reactions occurred downstream of the hot spot, resulting in a continuous temperature decrease.

Schmidt and co-workers intensively investigated synthesis gas production in monolith reactors. Hickman and Schmidt (1992) first reported experimental results obtained with Pt and Pt-Rh coated foam and extruded monoliths, as well as with Pt-10%Rh gauzes. The reactors were operated autothermally, i.e. without external heat input, at space times between 10^{-4} and 10^{-2} s and atmospheric pressure. In case of CH₄/air mixtures, H₂ and CO selectivities of respectively 50 and 95 % were found with Pt-Rh coated monoliths, at 80 % CH₄ conversion and outlet temperature of 1373 K. The oxygen conversion was always complete. At flow rates high enough to minimize mass-transfer limitations, the gauze catalyst as well as the foam and extruded monoliths resulted in similar conversions and selectivities. The product gas compositions did not correspond to the thermodynamic equilibrium values: the approach to equilibrium, however, was significantly accelerated by preheating the feed and by operating with pure oxygen. The applied space times allowed to investigate the CPO reaction independent of the reforming and water-gas shift reactions. Hence, high synthesis gas selectivities at short space times indicated that CO and H₂ were the primary products of the CPO reaction. Primary formation of CO and H₂ was also confirmed during experiments with the Pt-10%Rh gauze at different space times: the selectivities

increased at decreasing space time. Methane pyrolysis, $\text{CH}_4 \rightarrow \text{C} + 4\text{H}$, from which H_2 desorbs and C is oxidized to CO, was considered to be the primary surface reaction.

Hickman et al. (1993) also compared 11.6 wt% Pt and 9.8 wt% Rh coated foam monoliths at identical space times. The experimental results showed that Rh was superior to Pt in producing H_2 . In case of room temperature feed, Pt monoliths resulted in $S(\text{H}_2) = 43\%$ and $S(\text{CO}) = 89\%$, whereas Rh gave $S(\text{H}_2) = 73\%$ and $S(\text{CO}) = 90\%$. Also, higher methane conversions were found with Rh monoliths compared to Pt. The large difference in H_2 selectivity was explained by a higher activation energy for OH formation on Rh compared to Pt, see Figure 4. As a result, hydrogen adatoms are more stable on the Rh surface and can recombine towards H_2 and desorb into the gas phase. Higher conversions on Rh were caused by a lower methane activation energy compared to Pt. With oxygen instead of air and feed temperatures of 733 K, optimum selectivities to CO and H_2 of 96 and 90% were found in case of Rh.

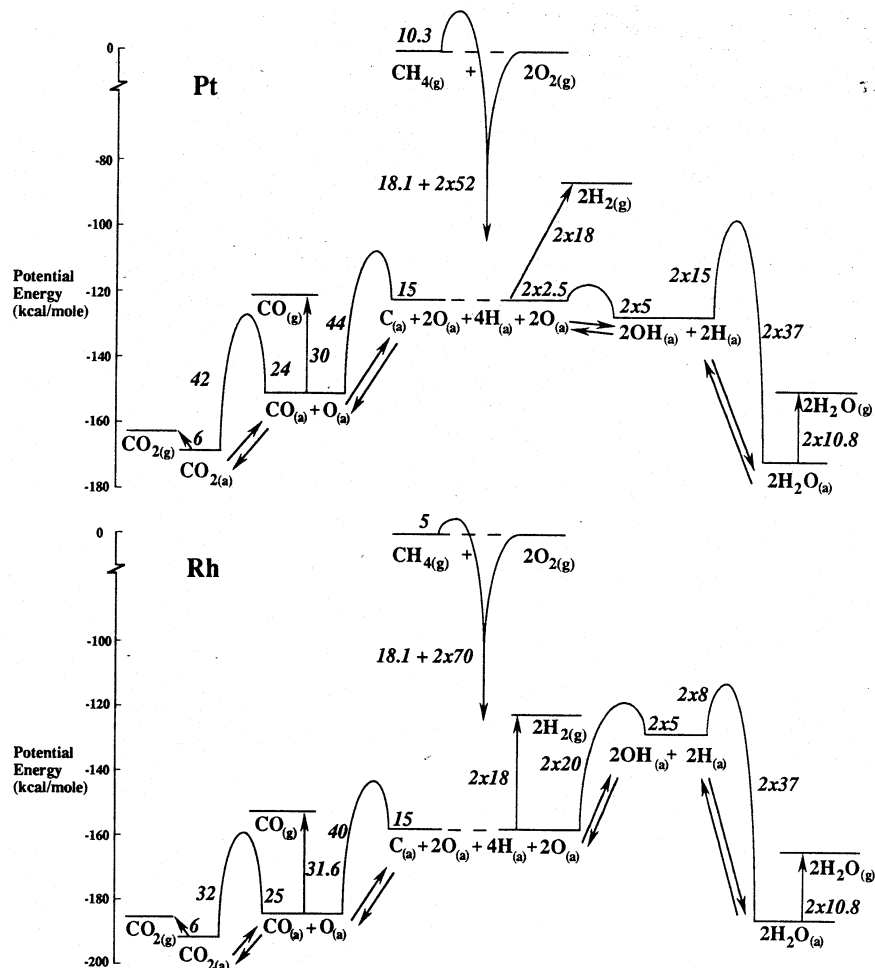


Figure 4. Potential energy diagrams for methane partial oxidation on Pt and Rh catalysts (Hickman and Schmidt, 1993). The activation energies were calculated relative to gaseous methane and oxygen.

Based upon previous work, Hickman and Schmidt (1993) proposed elementary step kinetic models for methane partial oxidation on Pt and Rh catalysts. Adsorption, desorption, and surface reactions were taken into account, with rate parameters obtained from literature and from fits to experiments. The model predictions were consistent with the experimental results, thereby confirming the direct oxidation mechanism in case of the monoliths. The difference between Pt and Rh catalysts, as illustrated above, could be explained by comparing individual surface reaction steps.

Different group VIII metal coated monoliths (Rh, Pt, Pd, Ir, Ni, Fe, Co, Re, and Ru) were investigated by Tornaiainen et al. (1994). The highest conversions and selectivities were found in case of Rh and Ni. The Rh coated monoliths showed stable performance for several hours, whereas the Ni coated monolith deactivated due to metal evaporation and formation of NiO and NiAl₂O₄. Pt and Ir also showed high stability, but significantly lower conversions and selectivities compared to Rh catalysts. Rapid deactivation was also observed in case of Pd coated monoliths as a result of coke deposition. Finally, Fe, Re, and Ru catalysts could not sustain the CPO reaction at the applied conditions. The authors thus concluded that Rh-based catalysts were the most suitable for synthesis gas production. Bodke et al. (1998) showed that H₂ selectivities on Rh monoliths could be further improved by addition of a washcoat. Also, it was found that small monolith pore sizes enhanced the selectivities: S(H₂) = 83 % on 20 ppi monoliths, increasing to 95 % on 80 ppi catalysts. The latter results were explained on the basis of differences in mass transfer rates. Finally, ZrO₂ monoliths gave slightly better performance than Al₂O₃.

In contrast to the work of Hickman and Schmidt (1992) and Hickman et al. (1993), Heitnes et al. (1994) showed that synthesis gas formation on Pt and Ni coated monoliths followed the indirect combustion/reforming mechanism. The CPO reaction was investigated using 5 wt% Ni and 1.5 wt% Pt supported by a γ -Al₂O₃ washcoat on cordierite extruded monoliths. Atmospheric pressure experiments were carried out at furnace temperatures of 873-1173 K, using 2:1:4 CH₄/O₂/He feed mixtures, and space times between 0.005 and 0.2 s. Equilibrium product distributions were obtained, except at very low space times. Measured axial temperature profiles, see Figure 5, showed a large temperature maximum at the reactor inlet, followed by a temperature decrease. Hence, the indirect CPO reaction mechanism was suggested. It should be noted, however, that the corresponding temperature profiles were obtained at space times considerably higher than the values applied by Schmidt and co-workers.

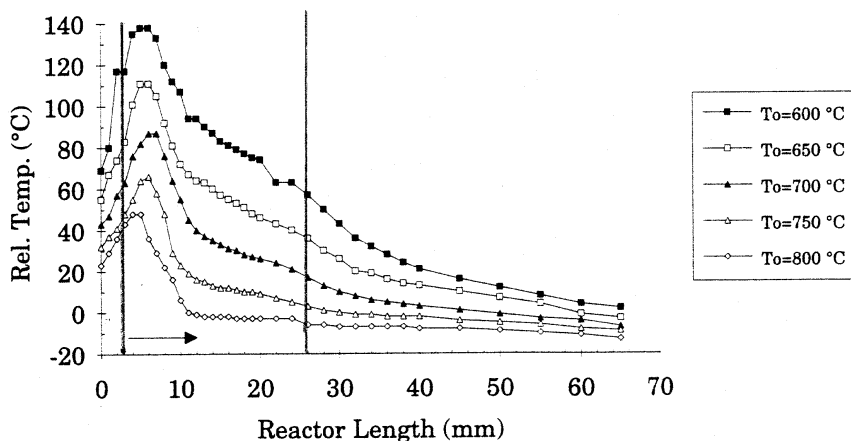


Figure 5. Axial temperature profiles over the Ni monolith at different furnace temperatures (Heitnes et al., 1994). The vertical lines indicate the position of the monolith reactor. Conditions: $\text{CH}_4/\text{O}_2/\text{He} = 2:1:4$, space time = 0.17 s.

Heitnes Hofstad et al. (1996) also investigated the performance of a single Pt gauze catalyst at space times of approximately 10^{-4} s. At the applied conditions, oxygen was only partly consumed, and CO, CO_2 , and H_2O were the main products. Very low selectivities to H_2 were observed. The reactant conversions were found to be independent of temperature, indicating that mass transport limitations were important. Both the H_2 and CO selectivities increased at increasing catalyst temperatures. The oxygen conversions increased significantly with time-on-stream, which was attributed to oxidation reactions on Pt, deposited downstream of the gauze catalyst due to Pt volatilization. The authors tentatively assumed that CO is a primary product of the CPO reaction, since high CO selectivities were observed at low space times.

Different group VIII metal gauzes (Pt, Pt-5%Rh, Pt-10%Rh, Pt-10%Ir, and Pd) were studied by Fahti et al. (1998). The experiments were carried out at 1 bar and temperatures between 973 and 1373 K, using $\text{CH}_4/\text{O}_2/\text{Ar}$ feed. Pd gauzes deactivated rapidly at the applied conditions due to PdO formation. High selectivities to CO were observed at high temperatures: $S(\text{CO}) = 95\%$ at 1373 K in case of Pt-10%Rh. The gauze catalysts alloyed with Rh also showed the highest stability. In accordance with the work of Heitnes Hofstad (1996), the selectivity to H_2 was always rather low, typically below 30% at conditions of incomplete oxygen conversion.

2.6 Fluidized-bed reactors

The fluidized-bed reactor for synthesis gas production is mentioned in the literature as a reactor concept with inherent advantages over conventional fixed-bed reactors. The intensive axial and radial mixing of solids can result in isothermal reactor operation, due to thermal coupling of exothermic oxidation and endothermic reforming zones during indirect CPO.

Pressure drop in fluidized-bed reactors is substantially lower compared to fixed-bed reactors of the same length and diameter. Also, carbon deposition can be minimized to a large extent: catalyst particles in the reforming zone are transported to the oxygen-rich oxidation zone where carbon deposits are burnt off.

Bharadwaj and Schmidt (1994) studied methane partial oxidation in autothermal fluidized bed reactors at atmospheric pressure using CH₄/air feed mixtures. The applied catalysts consisted of attrition resistant 100 μm Al₂O₃ particles coated with Pt, Rh, or Ni. The reactors were operated close to the turbulent regime: a maximum temperature difference over the catalyst bed of 50 K was found. At temperatures of 973-1073 K and residence times between 0.1 and 0.5 s, conversions in excess of 90 %, and CO and H₂ selectivities as high as 95 % were observed on Rh and Ni catalysts. In case of supported Pt, significantly lower conversions and selectivities were found, probably caused by higher oxidation and lower reforming rates. Although Rh and Ni resulted in similar conversions and selectivities, Rh was considered to be the optimum catalyst since Ni tends to be oxidized and volatilized at high temperatures.

Axial temperature profiles in fluidized-bed reactors were investigated in detail by Santos et al. (1994). The CPO reaction was studied using a NiO/NiAl₂O₄ catalyst at temperatures of 973-1173 K and a 2:1:1 CH₄/O₂/N₂ feed. Equilibrium product compositions were obtained without significant carbon formation. Essentially isothermal operating conditions were achieved with a maximum temperature difference of approximately 10 K, see Figure 6. Low temperatures and catalyst entrainment in the disengagement zone above the fluid bed resulted in methane production via the reverse steam-reforming reaction. Olsbye et al. (1997) showed, however, that the latter effect could be minimized to a large extent by using catalysts with low Ni loading, without loss of activity.

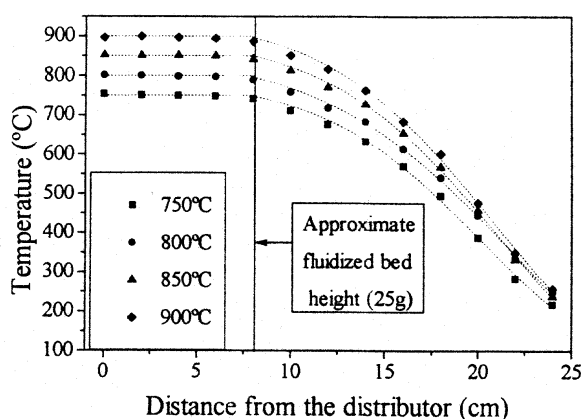


Figure 6. Axial temperature profiles in a fluidized-bed reactor at four different temperature setpoints (Santos et al., 1994).

Pugsley and Malcus (1997) proposed an internally circulating fluidized bed (ICFB) reactor for the partial oxidation of methane. In this reactor concept, the catalyst is transported vertically upward in a riser. Upon exiting the riser, the catalyst is separated from the gas and recirculated to the base of the riser. The ICFB reactor combines the advantages of both fixed-bed and bubbling fluidized-bed reactors for the CPO reaction: high throughputs can be realised, resulting in short space times, whereas the solids circulation promotes isothermal operation. Reactor simulations indicated that equilibrium conversions of methane could be obtained at high solid mass fluxes. Recently, Marschall and Mleczko (1999) investigated a laboratory-scale ICFB reactor. Both 1 and 5 wt% Ni-Al₂O₃ catalysts were studied at 1073 K and residence times varying from 0.07 to 0.24 s. Methane conversions and syngas selectivities in the range of the thermodynamic equilibrium values were obtained. Measured axial temperature profiles in the riser indicated isothermal reactor operation. However, the catalyst stability was influenced significantly by carbon deposition. On-line regeneration of the Ni catalyst by introducing carbon dioxide into the annulus surrounding the riser reactor was therefore proposed. The authors also indicated that a laboratory ICFB reactor can be scaled up in a straightforward way by applying the direct scale-up concept of multitubular reactors.

2.7 Membrane reactors

The catalytic partial oxidation of methane to synthesis gas for downstream production of methanol or liquid fuel requires high operating pressure in order to be commercially viable. At high pressures, however, thermodynamics predict significantly lower methane conversions compared to atmospheric conditions. For instance, the equilibrium conversion for a 2:1 CH₄/O₂ mixture is close to 80 % at 973 K and 1 bar, whereas at 20 bar the equilibrium conversion drops to 40 %. Also, oxygen-containing feeds are preferred over CH₄/air mixtures from industrial standpoint since downstream processing requires nitrogen-free product streams. Cryogenic oxygen separation from air, however, would add considerably to the total cost of the partial oxidation process. Novel reactor concepts have therefore been proposed in the literature to overcome the latter limitations. Hydrogen permeable membrane reactors have been investigated, which increase the methane conversions by a favorable shift in the thermodynamic equilibrium. Also, oxygen-transporting membranes have been proposed to eliminate the need for an oxygen separation plant by performing the oxygen-nitrogen separation inside the CPO reactor.

2.7.1 Hydrogen-permeable membrane reactors

Santos et al. (1995) performed experiments using a two-zone fixed-bed reactor containing a 10 wt% Ni/Al₂O₃ catalyst inside a ceramic membrane, see Figure 7. The first zone of the reactor

was surrounded by an impervious wall, and correspondingly behaved as a conventional fixed-bed reactor. This impervious wall was applied to achieve sufficiently high concentrations of the reaction products. In the second zone, hydrogen could permeate preferentially through the ceramic membrane, and was removed with nitrogen containing sweep gas. A comparison of conventional fixed-bed reactors and fixed-bed membrane reactors was presented. At 1073 K and atmospheric pressure, using 2:1:1 CH₄/O₂/N₂ mixtures, the methane conversion in the fixed-bed reactor amounted to an equilibrium value of 96 %, whereas the conversion in the membrane reactor amounted to 98 %. At 2 bar pressure, the increase of the methane conversion in the membrane reactor was more pronounced: the experimental values were close to the equilibrium values at 1 bar pressure.

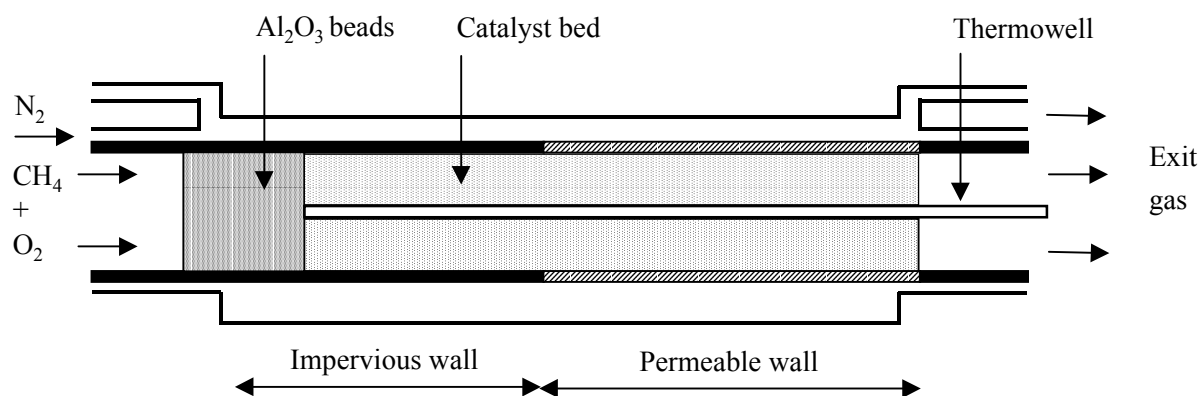


Figure 7. Schematic of the membrane reactor applied by Santos et al. (1995)

Kikuchi and Chen (1998) also studied the CPO reaction in a fixed-bed membrane reactor, using a 1 wt% Rh/Al₂O₃ catalyst. The catalyst bed was completely surrounded by a palladium membrane in the applied reactor setup. Conversions and selectivities in both conventional fixed-bed reactors and fixed-bed membrane reactors were reported, see Figure 8. The potential of fixed-bed membrane reactors was clearly illustrated: the methane conversions and product selectivities were significantly higher than the corresponding equilibrium values obtained in the fixed-bed reactor.

Mleczko et al. (1996) proposed a fluidized-bed membrane reactor to achieve both high methane conversions at elevated pressures and isothermal operating conditions. Simulation results indicated that higher methane conversions and synthesis gas yields could be obtained in the fluidized-bed membrane reactor compared to fixed-bed reactors at identical space times. Ostrowski et al. (1997) therefore investigated the potential of fluidized-bed membrane reactors for synthesis gas production on a laboratory scale. A single ceramic membrane tube was inserted into the fluidized bed reactor. At 1023 K and 1 bar pressure, using a Ni/Al₂O₃ catalyst, stable and isothermal reactor operation was obtained. The methane conversions, however, hardly improved

in the membrane reactor despite the high separation selectivity. The authors therefore suggested that membranes with even higher separation selectivity should be applied.

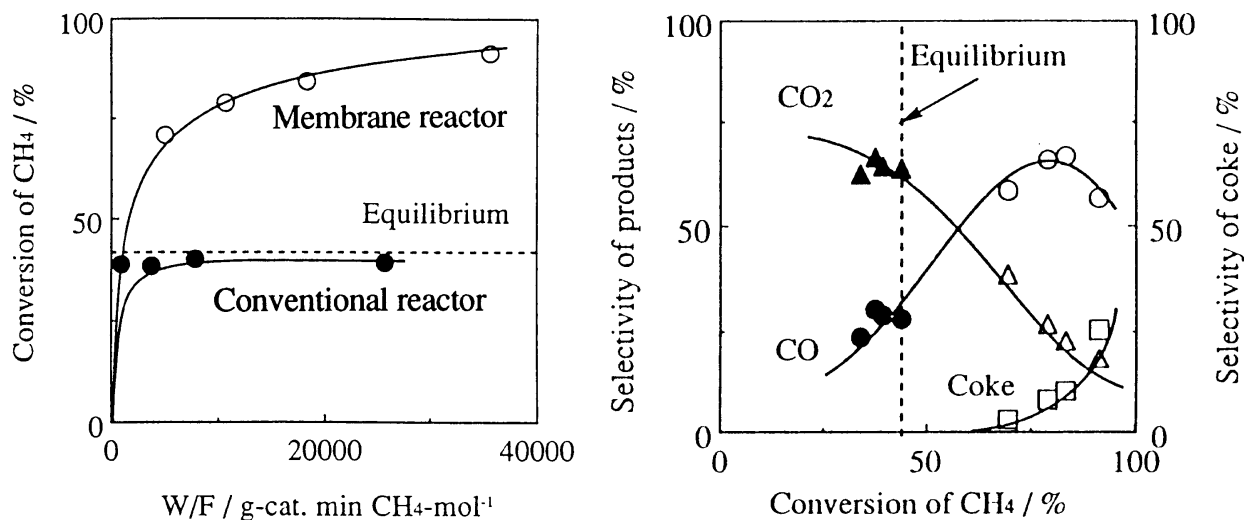


Figure 8. Conversion of methane vs. space time in a conventional fixed-bed reactor and a fixed-bed membrane reactor (left panel), and selectivities to CO, CO₂ and coke vs. methane conversion (right panel). Conditions: $T = 773\text{ K}$; $\text{air}/\text{CH}_4 = 2.5$. Open symbols: membrane reactor; Closed symbols: fixed-bed reactor.

2.7.2 Oxygen-transporting membrane reactors

Dense perovskite-type oxides have been proposed in the literature as effective oxygen-permeating membranes (Balachandran et al., 1995, Tsai et al., 1997). An oxygen-conducting membrane reactor, in which air separation and methane partial oxidation were carried out simultaneously, was investigated by Tsai et al. (1997). Three different reactor configurations were applied, containing disk-shaped perovskite membranes, see Figure 9. The membranes were located in the centre of the reactor: CH₄/He mixtures were fed at the top, whereas air was introduced in the bottom part of the reactor. In the absence of a catalyst, CO₂ and H₂O were the main products at a membrane temperature of 1123 K. The deep oxidation products could be reformed to synthesis gas when a Ni/Al₂O₃ catalyst was added downstream. The highest methane conversions and product selectivities were observed when the Ni catalyst was stacked directly on top of the membrane: $X(\text{CH}_4) = 80\%$, $S(\text{CO}) = 95\%$, $\text{H}_2/\text{CO} = 2$. The applied membrane reactors were found to be stable for at least 850 h time-on-stream.

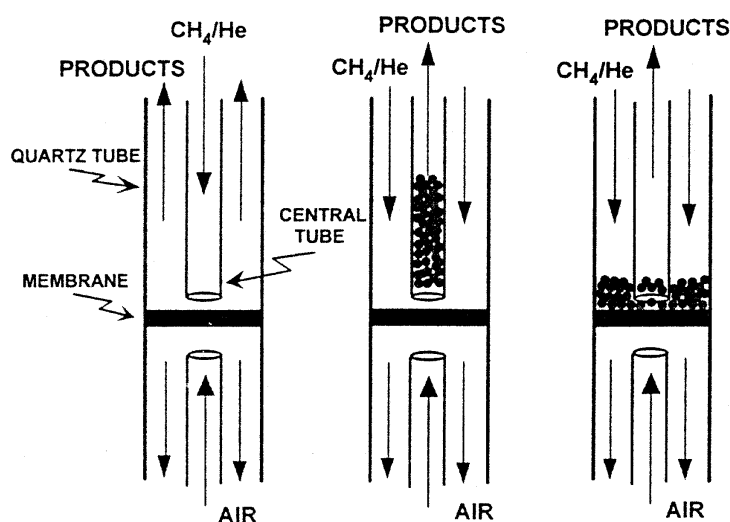


Figure 9. Disk-shaped perovskite membrane reactors applied by Tsai et al. (1997). Conditions: $T(\text{membrane}) = 1123 \text{ K}$.

2.8 CPO research in industry

At present, industry is closely involved in the development of gas-to-liquids technology (Exxon, Rentech, Shell, Syntroleum) and hydrogen production for fuel-cell-powered vehicles (Shell, Daimler Benz). Synthesis gas production via catalytic partial oxidation is expected to result in major cost reductions compared to established syngas processes. Industrial focus on CPO as a novel and economic route towards synthesis gas is clearly evidenced by the significant number of patents issued by for instance Exxon and Shell. In this section a short overview of CPO research in industry will therefore be presented.

Already in 1989, Exxon issued a patent on a fluidized-bed reactor for synthesis gas production (Goetsch and Say, 1989). The fluidized-bed reactor was selected because of the excellent mixing characteristics and high heat-transfer rates. The reactor was operated at about 1273 K, pressures up to 40 bar, methane/steam ratios of 1.5-2.5, and methane/oxygen ratios of 1.7-2.5, using a typical $\text{Ni}/\text{Al}_2\text{O}_3$ catalyst. Methane and steam were fed to the base of the fluidized-bed reactor while oxygen was fed in the middle of the fluidized bed to avoid premixing. Catalyst attrition, resulting in the deposition of catalyst fines in the cool sections of the equipment, was found to be a significant problem. Small catalyst particles in cool sections can promote methanation of CO and H_2 as well as carbon deposition due to the Boudouart reaction. To avoid methanation and carbon deposition, a process design was proposed in which the syngas product stream was rapidly quenched to low temperatures. At temperatures below 773 K, both methanation and carbon deposition did not occur to a significant extent. The design of coupled fluidized-bed and heat exchanger resulted in slightly lower than 90% methane conversion and equilibrium synthesis gas yields.

Exxon also reported on the application of the previously mentioned syngas preparation process in large pilot plant units (appr. 100 bbl/day) for the production of liquid hydrocarbons (Eisenberg et al., 1998). The fluidized-bed reactor is coupled to a slurry reactor containing a cobalt catalyst in which synthesis gas is converted to normal paraffins. The product slate contains substantial amounts of high boiling material which can be isomerized consecutively in a fixed-bed or trickle-bed reactor to slightly isomerized analogues. The final product is typically a mixture of diesel and naphtha. The diesel product fraction has a very low sulphur content, and can approach 80% of the total plant output.

Shell has pioneered the GTL process with a 12.500 BBP middle distillates plant in Bintulu Malaysia. Synthesis gas is produced in this plant via a high temperature non-catalytic gasification reactor. Considerable attention has also been directed towards the development of catalytic partial oxidation processes for syngas production. The patents issued by Shell illustrate the activities in the field of CPO at industrially relevant conditions, i.e. at high temperatures and pressures. At these conditions, it is recognized that formation of nitrogen containing products, e.g. NH_3 and HCN, can adversely affect downstream Fischer-Tropsch hydrocarbon synthesis or methanol production.

A process design was proposed (De Jong et al., 1993) for the production of synthesis gas with subsequent removal of NH_3 and HCN. The syngas production stage was based on a reactor with supported Rh or Ir catalysts, which were found to give significantly less nitrogen containing products compared to Ru. The process was operated at temperatures between 1000 and 1200 °C, methane-to-oxygen ratios between 1.3 - 2.2, and pressures between 3 and 100 bar. Ceramic foam monolith reactors were preferred since high conversions can be obtained in this configuration at very short contact times. A process design incorporating a packed liquid adsorption column and a secondary activated charcoal adsorber was proposed for syngas processing with trace amounts of NH_3 and HCN. In a separate patent (De Jong et al., 1994) it is additionally indicated that the presence of sulphur containing components can reduce the formation of nitrogen products even further. When the CPO reactor is used in conjunction with a Fischer-Tropsch process, however, sulphur removal via active carbon or zinc oxide is necessary.

Shell also proposed a novel process scheme for gas-to-liquids (Geerlings et al., 1998). The process is based on C_1 - C_4 feed streams, preferably containing at least 75 % of methane. The CPO unit is a monolithic type reactor (zirconia carrier) preferably coated with Rh or Ir. Oxygen enriched air is used as oxidant, produced from a membrane based air separation process. Syngas production is carried out between 1123 and 1323 K and pressures between 20 and 40 bar. The product stream is cooled to temperatures between 323 and 373 K before passing through a cobalt-based fixed-bed Fischer-Tropsch reactor. Typical temperatures of this reactor are in the range from 453 to 543 K with pressures of 10 to 70 bar. Approximately 70 wt% of C_5 - C_{20} linear paraffines are produced: the heavy paraffines can optionally be hydrocracked to middle

distillates. Also, other process layouts involving CO and H₂ recycle streams were proposed for more flexibility and improved carbon efficiency.

2.9 Conclusions

Catalysts The potential of synthesis gas production via catalytic partial oxidation of methane has been demonstrated unambiguously on a laboratory scale using different group VIII metal catalysts, atmospheric operation conditions, and temperatures above 1000 K. Both supported Ni and Rh presently appear to be the most promising catalysts. Ni-based catalysts result in high conversions and synthesis gas yields, but suffer from catalyst deactivation due to Ni oxidation and carbon deposition. Recent developments showed, however, that careful selection of the catalyst support could reduce the coke deposition rates to a considerable extent. Rh catalysts display both high activity and selectivity: the high cost and limited availability of the noble metal will probably determine whether commercial application is viable.

Reactors Different reactor concepts have been applied to investigate the feasibility of methane partial oxidation. Fixed-bed CPO reactors were used extensively due to operational flexibility and straightforward design. However, application of fixed-bed reactors appears to be limited to low pressures, due to the possible occurrence of hot spots in the catalyst bed. Fluidized-bed reactors appear to be more promising in this respect, since isothermal operating conditions can be obtained. Nevertheless, scale-up issues will have to be dealt with. Noble-metal-coated monolith reactors were shown to be highly active and selective at high temperature conditions and short residence times. Hence, this reactor concept appears to be the most promising for the production of large amounts of synthesis gas in compact reactors. In addition, successful pilot-scale operation has been demonstrated. Finally, membrane reactors were shown to have great potential to overcome the thermodynamic limitations of CPO at elevated pressures. The stability of membranes at high pressures and temperatures remains to be investigated in more detail.

Kinetics Kinetic studies revealed that the reduced metals in the catalyst are the active species for the CPO reaction. The reaction mechanism was found to depend primarily on the applied reaction conditions. At space times sufficiently high to obtain equilibrium methane conversions and synthesis gas selectivities, the indirect CPO reaction mechanism seems to prevail on Ni and Rh catalysts. At very short space times, however, Rh catalysts were found to give high non-equilibrium conversions and selectivities. In the latter case, direct formation of synthesis gas was proposed. The work on catalytic partial oxidation reported in the literature was mainly carried out at atmospheric pressure. Development of high-pressure CPO reactors still requires considerable attention to ensure complete heterogeneous production of synthesis gas in the absence of homogeneous gas-phase reactions.

2.10 Relation to present thesis

The research described in this thesis concerns kinetic investigations using *noble metal catalysts*, e.g. Pt and Rh, as well as fixed-bed reactor simulations using *Ni-based catalysts*. Kinetic investigations clearly remain essential, considering the ongoing debate with respect to the CPO reaction mechanism and the impact of the reaction mechanism on reactor operation. Reactor simulations are required to investigate the feasibility of CPO reactors at conditions which cannot be realised safely in a laboratory. Most kinetic studies indeed have been carried out conservatively, i.e. at atmospheric pressure and low catalyst temperatures.

Experimental studies reported in the literature were generally carried out at high reactant conversions. A clear distinction between direct and indirect synthesis gas production routes, however, requires experimental data at low oxygen conversions. The research described in this thesis therefore focuses on experimental investigations at low conversion levels. In Chapter 3, a kinetic study is presented using a 0.3 wt% Rh/ α -Al₂O₃ catalyst in a fixed-bed reactor. Oxygen conversions in the range of 0 – 100 % could be obtained by careful selection of the operating conditions. In addition, Chapters 4 and 5 report on an experimental reactor, containing a single Pt gauze catalyst, which allowed to investigate the CPO reaction at very low oxygen conversions. Low conversions could be obtained by applying high reactant flow rates, which could be realised in this reactor setup without large pressure drop.

Careful measurement of the catalyst temperature is essential in kinetic investigations. Formation of hot spots (Choudhary et al., 1992, 1993) can lead to different conclusions with respect to the reaction mechanism. Hu and Ruckenstein (1995) suppressed hot-spot formation in the reactor by using a pulse technique, involving very small amounts of reactants. The gauze reactor which was applied in the present thesis was constructed in such a way that the catalyst temperature could be measured directly, by means of a spotwelded thermocouple. Measurements of both gas-phase and catalyst temperatures indeed indicated that significant heat-transport limitations can occur at the applied conditions.

The relevance of homogeneous gas-phase reactions was discussed in section 2.2.2. Gas-phase reactions were generally suppressed during kinetic studies reported in the literature by performing experiments at rather low temperatures and at pressures close to atmospheric pressure. The kinetic study presented in Chapter 3, however, was carried out at conditions as close as possible to the industrially desired values, i.e. at high temperatures and pressure. Since homogeneous reactions can become important at these conditions, both homogeneous and heterogeneous reactions were investigated. The influence of gas-phase reactions in fixed-bed reactors operating at industrial conditions will also be addressed in Chapter 6.

References

- Ashcroft, A.I., Cheetham, A.K., Foord, J.S., Green, M.L.H., Grey, C.P., Murrell, A.J., & Vernon, P.D.F. (1990). Selective oxidation of methane to synthesis gas using transition metal catalysts. *Nature*, *344*, 319-321.
- Balachandran, U., Dusek, J.T., Mieville, R.L., Poeppel, R.B., Kleefisch, M.S., Pei, S., Kobylinski, T.P., Udovich, C.A., & Bose, A.C. (1995). Dense ceramic membranes for partial oxidation of methane to synthesis gas. *Appl. Catal. A*, *133*, 19-29.
- Berger, R.J., & Marin, G.B. (1999). Investigation of gas-phase reactions and ignition delay occurring at conditions typical for partial oxidation of methane to synthesis gas. *Ind. Engng. Chem. Res.*, *38*, 2582-2592.
- Bharadwaj, S.S., & Schmidt L.D. (1994). Synthesis gas formation by catalytic oxidation of methane in fluidized bed reactors. *J. Catal.*, *146*, 11-21.
- Bodke, A.S., Bharadwaj, S.S., & Schmidt, L.D. (1998). The effect of ceramic supports on partial oxidation of hydrocarbons over noble metal coated monoliths. *J. Catal.*, *179*, 138-149.
- Boucouvalas, Y., Zhang, Z., & Verikyos, X.E. (1994). Heat transport limitations and reaction scheme of partial oxidation of methane over supported rhodium catalysts. *Catal. Lett.*, *27*, 131-142.
- Boucouvalas, Y., Zhang, Z., & Verykios, X.E. (1996). Partial oxidation of methane to synthesis gas via the direct reaction scheme over Ru/TiO₂ catalyst. *Catal. Lett.*, *40*, 189-196.
- Buyevskaya, O.V., Wolf, D., & Baerns, M. (1994). Rhodium-catalyzed partial oxidation of methane to CO and H₂. Transient studies on its mechanism. *Catal. Lett.*, *29*, 249-260.
- Chen, Q., Couwenberg, P.M., & Marin, G.B. (1994). Effect of pressure on the oxidative coupling of methane in the absence of catalyst. *AIChE J.*, *40*, 521-535.
- Choudhary, V.R., Rajput, A.M., & Prabhakar, B. (1992). Low temperature oxidative conversion of methane to syngas over NiO-CaO catalyst. *Catal. Lett.*, *15*, 363-370.
- Choudhary, V.R., Rane, V.H., & Rajput, A.M. (1993). Selective oxidation of methane to CO and H₂ over unreduced NiO-rare earth oxide catalysts. *Catal. Lett.*, *22*, 289-297.
- Claridge, J.B., Green, M.L.H., Tsang, S.C., York, A.P.E., Ashcroft, A.T., Battle, P.B (1993). A study of carbon deposition on catalysts in the partial oxidation of CH₄ to syngas. *Catal. Lett.*, *22*, 299-305.
- Curry-Hyde, H.E., & Howe, R.F. (1993). Natural gas conversion II. *Stud. Surf. Sci. Catal.*, *81*, Elsevier, Amsterdam.
- De Jong, K.P., Schoonebeek, R.J., Vonkeman, K.A., Lednor, P.W., Oud, A.E., & Van der Zwet, G.P. (1993). A process for the preparation of carbon monoxide and/or hydrogen. WO 95/18063, assigned to Shell Internationale Research Maatschappij.
- De Jong, K.P., Schoonebeek, R.J., & Vonkeman, K.A. (1994). Process for the catalytic partial oxidation of hydrocarbons. WO 95/18062, assigned to Shell Internationale Research Maatschappij.
- Dietz III, A.G., & Schmidt, L.D. (1995). Effect of pressure on three catalytic partial oxidation reactions at milliseconds contact time. *Catal. Lett.*, *33*, 15-29.
- Dissanayake, D., Rosynek, M.P., Kharas, K.C.C., & Lunsford, J.H. (1991). Partial oxidation of methane to CO and H₂ over a Ni/Al₂O₃ catalyst. *J. Catal.*, *132*, 117-127.
- Dissanayake, D., Rosynek, M.P., & Lunsford, J.H. (1993). Are the equilibrium concentrations of CO and H₂ exceeded during oxidation of CH₄ over a Ni/Yb₂O₃ catalyst? *J. Chem. Phys.*, *97*, 3644-3646.
- Drago, R.S., Jurczyk, K., Kob, N., Bhattacharyya, A., & Masin, J. (1998). Partial oxidation of methane to synthesis gas using NiO-supported catalysts. *Catal. Lett.*, *51*, 177-181.
- Eisenberg, B., Fiato, R.A., Mauldin, C.H., Say, G.R., & Soled, S.L. (1998). Exxon's advanced gas-to-liquids technology. *Stud. Surf. Sci. Catal.*, *119*, 943-948.

- Fathi, M., Heitnes Hofstad, K., Sperle, T., Rokstad O.A., & Holmen, A. (1998). Partial oxidation of methane to synthesis gas at very short contact times. *Catal. Today*, 42, 205-209.
- Gavalas, G.R., Phichitkul, C., & Voecks, G.E. (1984). Structure and activity of NiO/ α -Al₂O₃ and Ni/ZrO₂ calcined at high temperatures. II. Activity in the fuel rich oxidation of methane. *J. Catal.*, 88, 65-72.
- Geerlings, J.J.C., Van Herwijnen, T., De Jong, K.P., Lange, J-P, Senden, M.M.G., & Van der Zwieter, G.P. (1998). Process for the production of liquid hydrocarbons. WO 99/15483, assigned to Shell Internationale Petroleum Maatschappij.
- Goetsch, D.A., & Say, G.R. (1989). Synthesis gas preparation and catalyst therefor. US 4877550, assigned to Exxon Research and Engineering Company.
- Heitnes, K., Lindberg, S., Rokstad, O.A., & Holmen, A. (1994). Catalytic partial oxidation of methane to synthesis gas using monolithic reactors. *Catal. Today*, 21, 471-480.
- Heitnes Hofstad, K., Rokstad, O.A., & Holmen, A. (1996). Partial oxidation of methane over platinum metal gauze. *Catal. Lett.*, 36, 25-30.
- Heitnes Hofstad, K., Hoebink, J.H.B.J., & Marin, G.B. (1998). Partial oxidation of methane to synthesis gas over rhodium catalysts. *Catal. Today*, 40, 157-170.
- Hickman, D.A., & Schmidt L.D. (1992). Synthesis gas formation by direct oxidation of methane over Pt monoliths. *J. Catal.*, 13, 267-282.
- Hickman, D.A., Hauptfear, E.A., & Schmidt L.D. (1993). Synthesis gas formation by direct oxidation of methane over Rh monoliths. *Catal. Lett.*, 17, 223-237.
- Hickman, D.A., & Schmidt, L.D. (1993). Steps in CH₄ oxidation on Pt and Rh surfaces: high temperature reactor simulations. *AIChE. J.*, 39, 1164-1177.
- Hochmut, J.K. (1992). Catalytic partial oxidation of methane over a monolith supported catalyst. *Appl. Catal. B: Environmental*, 1, 89-100.
- Holmen, A., Jens, K.-J., & Kolboe, S. (1990). Natural gas conversion, *Stud. Surf. Sci. Catal.*, 61, Elsevier, Amsterdam.
- Hu, Y.H., & Ruckenstein, E. (1995). Pulse-MS study of the partial oxidation of methane over Ni/La₂O₃ catalyst. *Catal. Lett.*, 34, 41-50.
- Huszar, K., Racz, G., & Szekely, G. (1971). Investigation of the partial catalytic oxidation of methane. I. Conversion rates in a single-grain reactor. *Acta Chim. Acad. Sci. Hung.*, 70, 287-299.
- Ito, M., Tagawa, T., & Goto, S. (1999). Partial oxidation of methane on supported nickel catalysts. *J. Chem. Engng. Jap.*, 32, 274-279.
- Kikuchi, E., & Chen, Y. (1998). Syngas formation by partial oxidation of methane in palladium membrane reactors. *Stud. Surf. Sci. Catal.*, 119, 441-446.
- Korchnak, J.D., Dunster, M., & English, A. (1990). Patent cooperation treaty WO90/06282, PCT/US89/05369, assigned to Davy McKee Corporation.
- Lemonidou, A.A., Stambouli, A.E., Tjatjopoulos, G.J., & Vasalos, I.A. (1997). Partial oxidation of methane to synthesis gas over unpromoted and (0.1-0.5 wt%) Ni-promoted calcium aluminate catalysts. *Catal. Lett.*, 43, 235-240.
- Mallens, E.P.J. (1996). A reaction path analysis of the catalytic partial oxidation of methane by transient experiments. *PhD Thesis*, Eindhoven University of Technology, Eindhoven.
- Mallens, E.P.J., Hoebink, J.H.B.J., & Marin, G.B. (1997). The reaction mechanism of the partial oxidation of methane to synthesis gas: a transient kinetic study over rhodium and a comparison with platinum. *J. Catal.*, 167, 43-53.
- Marschall, K.-J., & Mleczko, L. (1999). Short-contact-time reactor for catalytic partial oxidation of methane. *Ind. Eng. Chem. Res.*, 38, 1813-1821.
- Mleczko, L., Ostrowski, T., & Wurzel, T. (1996). A fluidized-bed membrane reactor for the catalytic partial oxidation of methane to synthesis gas. *Chem. Engng. Sci.*, 51, 3187-3192.

- Nakagawa, K., Ikenaga, N., Suzuki, T., Kobayashi, T., & Haruta, M. (1998). Partial oxidation of methane to synthesis gas over supported iridium catalysts. *Appl. Catal. A*, *169*, 281-290.
- Nakagawa, K., Ikenaga, N., Teng, Y., Kobayashi, T., & Suzuki, T. (1999). Partial oxidation of methane to synthesis gas over iridium-nickel bimetallic catalysts. *Appl. Catal. A*, *180*, 183-193.
- Olsbye, U., Dahl, I.M., Slagtern, A., Krogh, F., & Blom, R. (1997). Catalytic partial oxidation of methane to synthesis gas in a fluidized bed reactor. Proceedings of the 1st European Congress on Chemical Engineering, 367-370.
- Ostrowski, T., Mirodatos, C., Giroir-Fendler, A., Mleczko, L. (1997). Entwicklung eines Membran-Wirbelschichtreaktors für die katalytische partielle Oxidation von Methan zu Synthesegas. *Chem. Ing. Tech.*, *69*, 1624-1627.
- Parmaliana, A., Sanfilippo, D., Frusteri, F., Vaccari, A., & Arena, F. (1998). Natural gas conversion V, *Stud. Surf. Sci. Catal.*, *119*, Elsevier, Amsterdam.
- Prettre, M., Eichner, Ch., & Perrin, M. (1946). The catalytic oxidation of methane to carbon monoxide and hydrogen. *Trans. Farad. Soc.*, *43*, 335-340.
- Pugsley, T.S., & Malcus, S. (1997). Partial oxidation of methane in a circulating fluidized-bed catalytic reactor. *Ind. Eng. Chem. Res.*, *35*, 4567-4571.
- Ruckenstein, E., & Hu, Y.H. (1999). Methane partial oxidation over NiO/MgO solid solution catalysts. *Appl. Catal. A*, *183*, 85-92.
- Santos, A., Menendez, M., Santamaria, J. (1994). Partial oxidation of CH₄ to CO and H₂ in a fluidized bed reactor. *Catal. Today*, *21*, 481-488.
- Santos, A., Coronas, J., Menendez, M., & Santamaria, J. (1995). Catalytic partial oxidation of methane to synthesis gas in a ceramic membrane reactor. *Catal. Lett.*, *30*, 189-199.
- Slaa, J.C., Berger, R.J., & Marin, G.B. (1997). Partial oxidation of methane to synthesis gas over Rh/ α -Al₂O₃ at high temperatures. *Catal. Lett.*, *43*, 63-70.
- Tang, S., Lin, J., & Tan, K.L. (1998). Partial oxidation of methane to syngas over Ni/MgO, Ni/CaO and Ni/CeO₂. *Catal. Lett.*, *51*, 169-175.
- Tian, Z., Dewaele, O., & Marin, G.B. (1999). The state of Rh during the partial oxidation of methane into synthesis gas. *Catal. Lett.*, *57*, 9-17.
- Torniainen, P.M., Chu, X., & Schmidt L.D. (1994). Comparison of monolith-supported metals for the direct oxidation of methane to syngas. *J. Catal.*, *146*, 1-10.
- Tsai, C.-Y., Dixon, A.G., Moser, W.R., & Ma, Y.H. (1997). Dense perovskite membrane reactors for partial oxidation of methane to syngas. *AIChE J.*, *43*, 2741-2750.
- Tsang, W., & Hampson, R.F. (1986). Chemical kinetic database for combustion chemistry: Part I. Methane and related compounds. *J. Phys. Chem. Ref. Data*, *15*, 1087-1099.
- Vermeiren, W.J.M., Blomsma, E., & Jabobs, P.J. (1992). Catalytic and thermodynamic approach of the oxyreforming of methane. *Catal. Today*, *13*, 427-436.
- Vernon, P.D.F., Green, M.L.H. Cheetham, A.K., & Ashcroft, A.T. (1990). Partial oxidation of methane to synthesis gas. *Catal. Lett.*, *6*, 181-186.
- Walter, K., Buyevskaya, O.V., Wolf, D., & Baerns, M. (1994). Rhodium-catalyzed partial oxidation of methane to CO and H₂. In situ DRIFTS studies on surface intermediates. *Catal. Lett.*, *29*, 261-270.
- Wang, D., Dewaele, O., De Groote, A.M., & Froment, G.F. (1996). Reaction mechanism and role of the support in the partial oxidation of methane on Rh/Al₂O₃. *J. Catal.*, *159*, 418-426.
- Wang, H.Y., & Ruckenstein, E. (1999). Partial oxidation of methane to synthesis gas over MgO- and SiO₂-supported rhodium catalysts. *J. Catal.*, *186*, 181-187.

3

Partial oxidation of methane over Rh/ α -Al₂O₃ – Relative importance of heterogeneous catalytic and homogeneous gas-phase reactions at low conversions

This chapter has been submitted for publication in App. Catal. A

Abstract - The catalytic partial oxidation (CPO) of methane to synthesis gas was studied using a 0.3 wt% Rh/ α -Al₂O₃ catalyst. Special attention was paid to the relative importance of homogeneous gas-phase reactions and heterogeneous catalytic reactions at low oxygen conversions. Homogeneous gas-phase reactions and heterogeneous catalytic reactions were investigated in a continuous-flow reactor setup at temperatures between 1273 and 1345 K and pressures between 400 and 800 kPa, using 6.7/3.3/90 CH₄/O₂/He feed mixtures. At these conditions, both partial and total oxidation products as well as C₂-hydrocarbons were observed. An accurate description of the homogeneous gas-phase experiments was obtained with a kinetic model consisting of 40 reversible gas-phase reactions. Heterogeneous termination reactions could be neglected at the investigated surface area to volume ratio. In case of the α -Al₂O₃ support alone, homogeneous gas-phase reactions contributed at least 50% to the measured conversions. Production of C₂-hydrocarbons occurred primarily via homogeneous gas-phase reactions. Comparison of conversions obtained with the α -Al₂O₃ support alone and with the Rh/ α -Al₂O₃ catalyst indicated that both homogeneous gas-phase reactions and heterogeneous catalytic reactions were important in case of the Rh catalyst. The product yields measured with the α -Al₂O₃ support and Rh/ α -Al₂O₃ catalyst showed that the latter is primarily active towards total oxidation of methane at 1345 K. At 1273 K, however, Rh/ α -Al₂O₃ also catalyzes the direct partial oxidation of methane to synthesis gas.

Keywords: Partial oxidation; synthesis gas; Rh/ α -Al₂O₃; Catalytic reactions;
Gas-phase reactions

3.1 Introduction

Synthesis gas production via catalytic partial oxidation (CPO) of methane has developed into an important research area in the past decade as a result of the growing interest in natural gas conversion into liquid products and hydrogen-for-fuel-cells. The potential of the CPO reaction is reflected by the mild exothermicity and the favorable H_2/CO ratio of the product compared to the conventional steam-reforming process. Both Ni-based catalysts and noble-metal based catalysts have been mentioned in the literature to be active and selective towards partial oxidation. In particular, Rh catalysts have been reported to give high synthesis gas yields with good long-term stability (Vernon et al., 1990).

The mechanism of the catalytic partial oxidation of methane on Rh catalysts has been investigated extensively in the literature. Special attention has been paid to the influence of the state of the catalyst, the available surface oxygen species, and the role of the support (Mallens et al., 1997, Au and Wang, 1997, Heitnes Hofstad et al., 1998, Tian et al., 1999). However, final agreement on the reaction mechanism has not been reached yet. At short residence times, direct CPO mechanisms have been proposed, yielding synthesis gas in a single step (Hickman and Schmidt, 1993, Mallens et al., 1997). Indirect CPO reaction mechanisms, in which synthesis gas is produced via total oxidation and reforming in series, have also been suggested (Vernon et al., 1990, Boucouvalas et al., 1994, Wang et al., 1995).

Most kinetic studies have been performed at relatively low temperatures and operating pressures. In our laboratory, however, methane partial oxidation has been studied on a 0.3 wt% Rh/ α - Al_2O_3 catalyst at conditions as close as possible to those industrially relevant: pressures up to 800 kPa and temperatures above 1273 K (Slaa et al., 1997). Intrinsic kinetic data were obtained when the feed was diluted with helium. The experimental results indicated that the Rh catalyst could be present in two states: a low-activity oxidized state, and a high-activity reduced state. At low oxygen conversions, i.e. in the oxidized state, C_2H_6 , CO_2 , and H_2O were observed as the primary products. Significant amounts of CO , H_2 , and C_2H_4 were found at increasing oxygen conversions. At complete oxygen conversion, i.e. in the reduced state of the Rh catalyst, CO and H_2 were formed selectively by reforming of CH_4 with CO_2 and H_2O . An additional direct route to CO and H_2 at low oxygen conversions was not excluded by the authors. It was shown that the α - Al_2O_3 support was not inert at the applied conditions. Preliminary simulations with the slightly modified gas-phase kinetic model of Chen et al. (1994), obtained at conditions typical for oxidative coupling of methane, indicated that gas-phase reactions were not important. Slaa et al. (1997) thus concluded that the observed products were produced entirely via heterogeneous reactions on the Rh/ α - Al_2O_3 catalyst.

The present work was initiated to obtain more detailed insight into the activity of the 0.3 wt% Rh/ α -Al₂O₃ catalyst at low oxygen conversions, i.e. at conditions where the total and partial oxidation products as well as the C₂-hydrocarbons are observed. Homogeneous gas-phase experiments were performed and simulated at the conditions applied during the catalytic experiments, i.e. at high temperature and pressure using diluted CH₄/O₂/He feed mixtures. In addition, a comparison of experimental results obtained with the 0.3 wt% Rh/ α -Al₂O₃ catalyst and the α -Al₂O₃ support will be presented, with the aim to obtain insight into the activity of the Rh catalyst at low oxygen conversions. The relative importance of both homogeneous gas-phase reactions and heterogeneous catalytic reactions will be highlighted.

3.2 Experimental equipment, procedures, and conditions

The experimental results reported in this work were obtained using a continuous-flow reactor setup consisting of a sintered alumina tube ($l_r = 0.65$ m, $d_{r,i} = 8.5 \cdot 10^{-3}$ m). The tubular reactor could be operated at pressures up to 2500 kPa using a back-pressure controller, and heated up to 1500 K with an electrical furnace. A fluidized sand bed was positioned between the reactor and the electrical furnace to suppress axial temperature gradients. The axial temperature profile was measured with a movable thermocouple placed inside a sintered alumina thermowell in the centre of the reactor ($d_{w,e} = 4.0 \cdot 10^{-3}$ m). Sintered alumina was applied because of the inertness of the material. Several safety devices were used in the reactor setup to minimize the effects of possible explosions and flames (Slaa et al., 1997, Berger and Marin, 1999). The experiments were performed at steady-state conditions.

Runaway in the downstream part of the tubular reactor was prevented in case of the gas-phase experiments by introducing an alumina tube in the bottom part of the reactor ($l_{ft} = 0.24$ m, $d_{ft,e} = 7.65 \cdot 10^{-3}$ m, $d_{ft,i} = 4.75 \cdot 10^{-3}$ m), c.f. de Smet et al. (1998). The reactor configuration applied for the experiments with the Rh/ α -Al₂O₃ catalyst and the α -Al₂O₃ support is shown in Figure 1. The Rh catalyst particles ($0.08 < d_p < 0.11$ mm), diluted with non-porous alumina pellets ($0.11 < d_p < 0.15$ mm), were positioned in the centre of the reactor. Both at the top and bottom of the catalyst bed, non-porous alumina spheres ($0.5 < d_p < 1$ mm) were placed. In addition, sintered alumina filling tubes were used in the bottom and top parts of the reactor to fill up as much empty space as possible. In case of the experiments with the α -Al₂O₃ support, identical pellet sizes and reactor filling were applied.

The reactor tube, filling tubes, and non-porous alumina pellets were cleaned prior to the experiments in a 60% nitric acid solution in order to remove any impurities. The Rh/ α -Al₂O₃ catalyst and the α -Al₂O₃ support were pretreated in-situ using a flow of 2% H₂/He at 1140 K and with a 6.7/3.3/90 CH₄/O₂/He mixture at 1400 K, respectively. This procedure resulted in

stable operation for more than 15 days in case of the Rh/ α -Al₂O₃ catalyst. The conditions applied during the experiments are shown in Table 1. Helium is used as diluent in both the support and catalytic experiments to prevent large axial temperature gradients, and to allow for intrinsic kinetic measurements. A maximum temperature difference over the catalyst bed of 7 K was found. The gas-phase experiments were also carried out in the presence of helium, to investigate the homogeneous reactions at conditions as close as possible to those applied in the catalytic experiments. Additional details about the experimental analysis method, catalyst preparation procedure, and catalyst specifications can be found in Slaa et al. (1997).

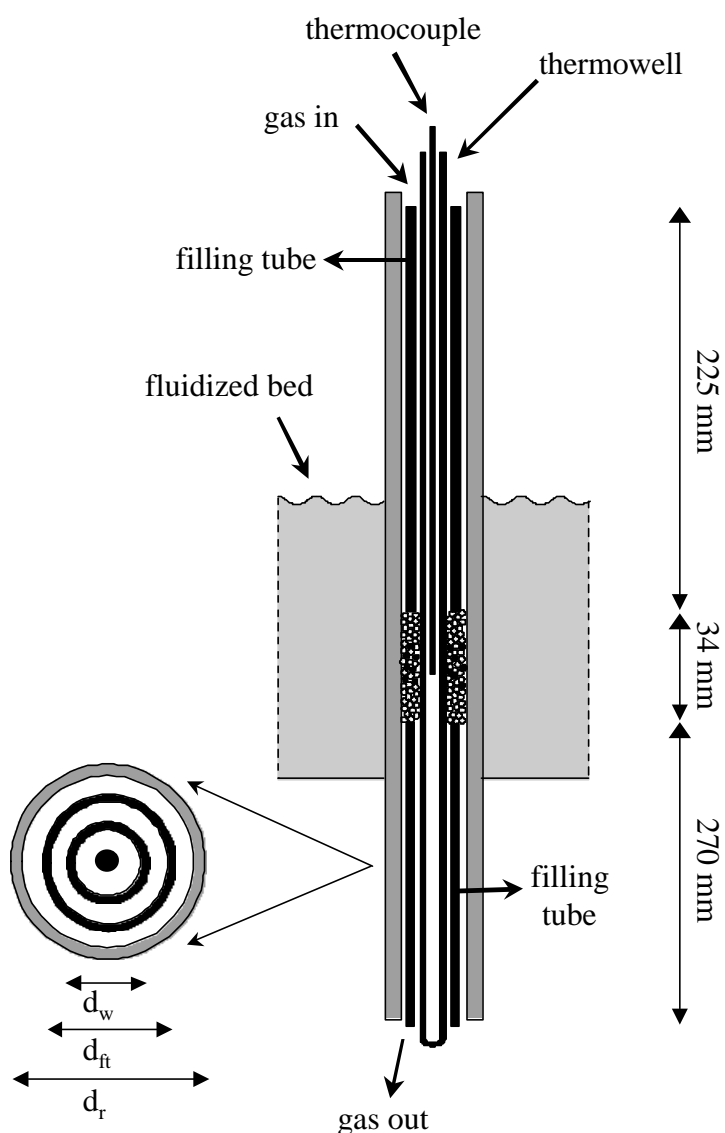


Figure 1. Schematic representation of the continuous-flow reactor setup used to investigate the heterogeneous catalytic reactions.

Table 1. Ranges of experimental conditions applied in the gas-phase, support, and catalytic experiments

		Gas-phase experiments	Al ₂ O ₃ -support experiments	Rh/Al ₂ O ₃ -catalyst experiments
P _{tot}	/ kPa	400, 600, 800	400	400
T _{max}	/ K	1273	1273 - 1345	1273 - 1345
CH ₄ /O ₂ /He	/ %	6.7/3.3/90	6.7/3.3/90	6.7/3.3/90
F _{tot} *10 ³	/ mol s ⁻¹	3.4	0.1 - 2.2	0.4 - 4.3
V/F _{tot} *10 ³	/ m ³ s mol ⁻¹	3.6	-	-
W/F _{CH_{4,0}}	/ kg s mol ⁻¹	-	0.4 - 8	0.2 - 2.5

3.3 Investigation of homogeneous gas-phase reactions at low reactant partial pressures

The kinetics of the homogeneous gas-phase reactions have been studied in detail by Berger and Marin (1999) at conditions typical for the partial oxidation of methane to synthesis gas. Pressures in the range from 300 to 800 kPa, temperatures between 1030 and 1300 K, and undiluted feed mixtures with CH₄/O₂ ratios of 2.1 to 3.1 were applied. The experimental results were described using a free-radical mechanism featuring 40 reversible gas-phase reactions between 13 molecular (H₂, H₂O, H₂O₂, O₂, CH₄, C₂H₆, C₂H₄, C₂H₂, C₃H₈, C₃H₆, CH₂O, CO, and CO₂) and 10 radical species (H•, O•, OH•, HO₂•, CH₃•, C₂H₅•, C₂H₃•, C₃H₇•, CH₃O•, and CHO•). The effect of pressure falloff on the rate of unimolecular reactions was taken into account explicitly in the model. The proposed reaction mechanism will be referred to in the following as the BM gas-phase kinetic model. In the present work, the experiments with the α -Al₂O₃ support and Rh/ α -Al₂O₃ catalyst were carried out with helium as diluent, see Table 1. At 90% He dilution, the partial pressures of methane and oxygen are a factor 10 lower than in case of undiluted feed mixtures. Hence, additional gas-phase experiments were carried out and simulated at conditions corresponding to those applied in the support and catalytic experiments, i.e. at low reactant partial pressures. This was done to evaluate the applicability of the BM gas-phase kinetic model at low reactant partial pressures.

3.3.1 Experimental results

The measured conversions and selectivities obtained with diluted feed mixtures at different total pressures are shown in Table 2 together with typical results reported by Berger

and Marin (1999). In case of the gas-phase experiments with helium-dilution, both the methane and oxygen conversions increase at increasing total pressure. The C_2H_6 selectivity decreases considerably, whereas the CO, H_2 , and C_2H_4 selectivities increase at higher pressures. Identical trends have been found in case of undiluted CH_4/O_2 mixtures, at lower values of the maximum gas-phase temperature. The conversions observed in case of the experiments with helium are, as expected, considerably lower than the experimental values obtained with undiluted CH_4/O_2 feed mixtures, at comparable space-times, pressures, and temperatures.

Table 2. Measured and simulated conversions and selectivities of nine gas-phase experiments in case of feed mixtures with and without He-dilution at various pressures, temperatures, and residence times. Simulation results obtained with the BM gas-phase kinetic model with extended validity range.

Experimental conditions				Measured and simulated (between brackets) conversions and selectivities							
P_{tot} [kPa]	T_{max} [K]	τ [s]	$CH_4/O_2/He$ [%]	X(CH_4) [%]	X(O_2) [%]	S(H_2) [%]	S(H_2O) [%]	S(CO) [%]	S(CO_2) [%]	S(C_2H_6) [%]	S(C_2H_4) [%]
400	1277	0.164	6.7/3.3/90	2.9 (3.8)	6.0 (5.7)	10.3 (21.3)	59.4 (46.5)	36.9 (47.6)	2.3 (1.6)	43.3 (32.6)	17.5 (14.3)
600	1273	0.258	6.7/3.3/90	11.1 (11.0)	21.5 (19.2)	16.6 (25.8)	51.8 (57.6)	43.5 (56.6)	3.2 (6.0)	24.1 (16.6)	29.2 (17.3)
800	1281	0.355	6.7/3.3/90	21.8 (22.1)	43.4 (47.3)	18.9 (29.5)	60.8 (58.9)	51.5 (62.0)	4.8 (10.4)	13.6 (7.6)	30.3 (18.1)
300	1112	0.094	67/33/0	1.3 (1.5)	3.4 (2.9)	8.5 (9.7)	60.4 (52.1)	37.6 (44.4)	2.5 (1.4)	42.3 (42.1)	15.2 (8.9)
500	1107	0.103	67/33/0	3.4 (3.7)	9.5 (9.1)	10.4 (8.8)	65.2 (61.3)	50.8 (49.7)	4.6 (4.4)	22.7 (24.3)	18.3 (17.7)
750	1109	0.086	67/33/0	6.4 (6.5)	17.5 (18.5)	19.3 (8.2)	63.2 (73.4)	59.5 (58.6)	7.7 (8.5)	9.3 (8.7)	19.4 (19.6)
500	1207	0.100	67/33/0	7.5 (7.8)	19.4 (19.8)	12.2 (16.7)	61.6 (62.3)	54.5 (49.5)	6.5 (8.6)	14.8 (16.1)	21.3 (21.9)
500	1300	0.107	67/33/0	14.1 (11.8)	34.4 (28.2)	28.6 (17.2)	53.1 (60.3)	59.4 (52.8)	7.6 (11.3)	9.4 (12.7)	21.6 (21.7)
500	1109	0.297	67/33/0	14.2 (17.1)	43.2 (41.9)	12.1 (9.0)	65.4 (76.1)	59.2 (53.3)	5.9 (19.4)	15.7 (10.2)	16.3 (14.3)

3.3.2 Comparison with simulation results

The experimental and simulated oxygen conversions in case of the feed mixtures with He-dilution are shown in Table 3. The simulation results were obtained using the BM gas-phase kinetic model together with a 1-dimensional reactor model. The method developed by

Dente et al. (1979), applying the pseudo-steady-state assumption for the reactive radical species, was used for integration of the continuity equations. The measured axial temperature profiles were accounted for explicitly in the simulations.

Table 3. Measured and calculated oxygen conversions in case of the gas-phase experiments with He-dilution vs. total pressure. Calculated results: (A) BM gas-phase kinetic model, (B) BM gas-phase kinetic model including quench reactions (5) and (6). Conditions: $CH_4/O_2/He = 6.7/3.3/90$, $T_{max} = 1277$ K, $F_{tot} = 3.4 \cdot 10^{-3} \text{ mol s}^{-1}$.

P_{tot} / kPa	Experiment	A	B ¹
400	6.0	32.4	17.0
600	21.5	72.7	59.2
800	43.4	88.9	83.2

¹ $s_{i,0} = 1.0$

The calculated oxygen conversions are considerably higher than the corresponding experimental values. This clearly illustrates that the BM gas-phase kinetic model cannot be extrapolated in a straightforward way to low reactant partial pressures. However, the observed discrepancy between the measured and simulated conversions can be caused by heterogeneous termination reactions of radical species at the reactor walls. The latter effect is not accounted for in the simulations and can result in significantly lower oxygen conversions. In case of undiluted CH₄/O₂ feed mixtures, the influence of heterogeneous termination reactions was neglected as a result of high homogeneous termination rates compared to heterogeneous termination rates at the reactor wall (Berger and Marin, 1999, Chen et al., 1991). At low reactant partial pressures, however, heterogeneous termination reactions will be more important. This will be illustrated in detail in the next section.

3.3.3 Influence of heterogeneous termination reactions

Heterogeneous termination reactions at the reactor walls can result in significant radial concentration profiles of the involved molecular and radical species. Hence, a two-dimensional reactor model was developed to investigate the effect of heterogeneous termination reactions on reactant conversions. The corresponding continuity equations were written as:

$$\phi_m \frac{\partial}{\partial z} \left(\frac{C_i}{\rho_f} \right) = \frac{D_{m,i} \rho_f}{r} \frac{\partial}{\partial r} \left(r \frac{\partial}{\partial r} \left(\frac{C_i}{\rho_f} \right) \right) + R_{i,g} \quad (1)$$

Axial convection and radial diffusion of both molecules and radical species were taken into account. The gas-phase production rates, $R_{i,g}$, were calculated using the BM gas-phase kinetic model. The following initial and boundary conditions were used:

$$z = 0, r_0 < r < r_1 \quad C_i = C_{i,o} \quad (2)$$

$$r = r_0 \quad D_{m,i} \rho_f \frac{\partial}{\partial r} \left(\frac{C_i}{\rho_f} \right) = R_{i,t} \quad (3)$$

$$r = r_1 \quad D_{m,i} \rho_f \frac{\partial}{\partial r} \left(\frac{C_i}{\rho_f} \right) = -R_{i,t} \quad (4)$$

At the reactor wall, the thermowell wall, and at the external and internal surfaces of the downstream filling tube, termination reactions can take place, see Eq. (3) and (4). The resulting set of 24 partial differential equations (14 molecular species, including He, and 10 radical species), together with the initial and boundary conditions, was solved numerically using the method of lines and the method of Gear in the standard NAG-library routine D03PGF (NAG Fortran Library, 1997).

The experimental reactor, applied during the gas-phase experiments, contains two distinct zones. The first annular zone is bounded by the thermowell and reactor walls ($r_0 = d_{w,e}/2$; $r_1 = d_{r,i}/2$). The second zone consists of two annular spaces, bounded by (i) the thermowell wall and internal surface of the downstream filling tube ($r_0 = d_{w,e}/2$; $r_1 = d_{f,i}/2$), and (ii) the external surface of the downstream filling tube and the reactor wall ($r_0 = d_{f,e}/2$; $r_1 = d_{r,i}/2$). In order to calculate the concentration profiles at the reactor outlet, the set of partial differential equations was solved first in case of the annular zone bounded by the thermowell and reactor walls. A small initial value of the radical concentrations, typically in the order of 10^{-12} mol %, was applied at the reactor inlet to start the integration. The influence of the initial radical concentrations on the simulation results could be neglected. Radially averaged concentrations were taken at the outlet of the first zone and used next to solve the continuity equations in case of the annular spaces of the second zone. Finally, radially averaged concentrations at the outlet of both annular spaces were used to calculate the resulting concentrations at the reactor outlet.

Simulations with the reactor model and the BM gas-phase kinetic model in the absence of heterogeneous termination reactions indicated that the methyl and hydrogen peroxy radicals are most abundant at the applied conditions. The $\text{CH}_3\bullet$ and $\text{HO}_2\bullet$ radical concentrations typically amounted to 10^{-5} and 10^{-6} mol % at the maximum gas-phase

temperature, whereas the concentration of the other radicals were of the order of 10⁻⁸ mol % or lower. Two heterogeneous termination reactions were thus considered:



The heterogeneous termination reaction of hydrogen peroxy radicals was also used by Couwenberg et al. (1995) to model the oxidative coupling of methane over Li/MgO-based catalysts. The termination reaction of methyl radicals towards ethane also occurs homogeneously (Berger and Marin, 1999). The heterogeneous termination rates of both HO₂• and CH₃• were considered to be first order in the respective radical concentrations. The corresponding rate coefficient was calculated from:

$$k_{t,i} = s_{i,0} \frac{1}{4} \sqrt{\frac{8RT}{\pi M_i}} \quad (7)$$

with $s_{i,0}$ the sticking coefficient on a clean surface.

The calculated oxygen conversions in case of the methyl or hydrogen peroxy termination reactions are shown in Figure 2 as a function of the sticking coefficients.

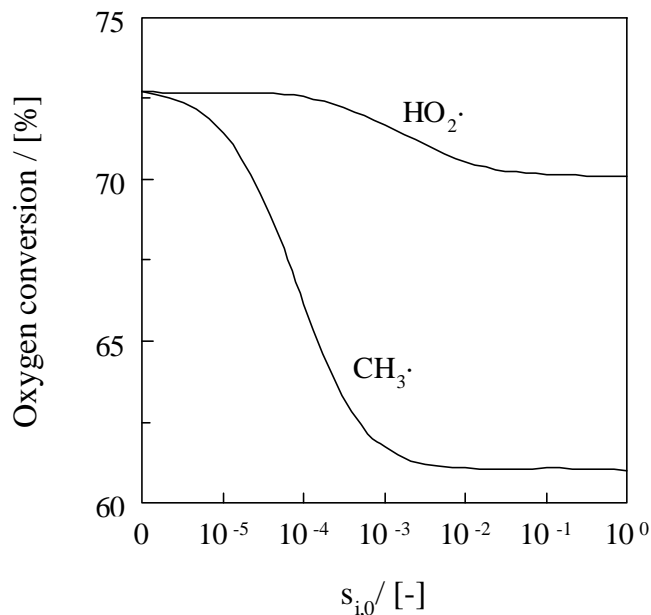


Figure 2. Calculated oxygen conversions in case of the gas-phase kinetic model of Berger and Marin (1999) including heterogeneous termination of hydrogen peroxy or methyl radicals vs initial sticking coefficient. Conditions: $P_{\text{tot}} = 600 \text{ kPa}$, $T_{\text{max}} = 1274 \text{ K}$, $F_{\text{tot}} = 3.4 \times 10^{-3} \text{ mol s}^{-1}$, $\text{CH}_4/\text{O}_2/\text{He} \frac{1}{2}_0 = 6.7/3.3/90$.

Reaction (5) resulted in a minor decrease of the calculated oxygen conversions: at a sticking coefficient of 1.0, the oxygen conversion decreased from 72.7 to 70.0 %. The heterogeneous termination reaction of methyl radicals, however, had a considerable influence on the calculated oxygen conversions. In the latter case, the oxygen conversion amounted to 61.1% for a sticking coefficient of 1.0.

Table 3 (see section 3.3.2) shows the calculated oxygen conversions at different total pressures in case of maximum sticking coefficients of the hydrogen peroxy and/or methyl radicals. The effect of the heterogeneous termination reactions is most pronounced at low operating pressure. At increasing total pressure, the homogeneous termination rates are considerably enhanced, thereby decreasing the influence of the heterogeneous termination reactions. Even in case of maximum heterogeneous termination rates, the calculated oxygen conversions are still considerably higher than the measured values. This clearly indicates that the BM gas-phase kinetic model has to be modified in order to describe the oxygen conversions in case of diluted feed mixtures. Couwenberg et al. (1995) obtained a sticking coefficient of $5 \cdot 10^{-5}$ for the hydrogen peroxy termination reaction. Application of this value of $s_{i,0}$ in case of either $\text{HO}_2\bullet$ or $\text{CH}_3\bullet$ termination results in only a minor decrease of the calculated oxygen conversions, see Figure 2. Hence, the influence of the heterogeneous termination reactions will be neglected in the following.

3.3.4 Extension of the validity of the BM gas-phase kinetic model to low reactant partial pressures

Modification of the BM gas-phase kinetic model was carried out using the total number of nine experiments listed in Table 2. Experimental data both in the presence and absence of He were taken into account to obtain a kinetic model valid over the entire range of partial pressures. A 1-dimensional reactor model was used in the calculations. A total number of 15 pre-exponential factors was adjusted, see Table 4. It should be noted that the latter parameters were allowed to change only within a fixed window having a width approximately equal to the uncertainties of the corresponding literature values, c.f. Berger and Marin (1999). The radical reactions shown in Table 4 were selected because of the large influence of the corresponding reaction rates on the reactant conversions. The pre-exponential factors were optimized using a minimization routine based on an algorithm from Rosenbrock (Rosenbrock, 1961). A simplified form of the generalized least-squares criterion was used as objective function:

$$S(\mathbf{b}) = \sum_{j=1}^n w_j \sum_{k=1}^n \frac{(y_{kj} - f_j(\mathbf{x}_k, \mathbf{b}))^2}{(y_{kj} f_j(\mathbf{x}_k, \mathbf{b}))} \quad (8)$$

The reactant conversions and product selectivities were taken as responses, y_{kj} , with the exception of H₂O₂ which was not detected experimentally. The corresponding weighting factors, w_j , were taken from Berger and Marin (1999). The weighting factors of CH₄ and O₂ were increased by a factor of 2 in order to improve the description of the reactant conversions in particular.

Table 4. Pre-exponential factors in case of the BM gas-phase kinetic model, and the gas-phase kinetic model with extended validity that covers the entire range of partial pressures. The values corresponding to the latter gas-phase model were obtained after minimization of the conversions and selectivities. The numbers of the reactions correspond to the numbers used by Berger and Marin (1999).

No.	Reaction		$k_{0,g}^*$ (BM model)	$k_{0,g}^*$ (extended validity)
1	CH ₄ + M	\rightleftharpoons CH ₃ [•] + H [•] + M	0.240·10 ¹⁷	0.874·10 ¹⁶
3	CH ₄ + H [•]	\rightleftharpoons CH ₃ [•] + H ₂	0.473·10 ⁸	0.624·10 ⁸
5	CH ₄ + OH [•]	\rightleftharpoons CH ₃ [•] + H ₂ O	0.659·10 ⁸	0.221·10 ⁸
6	CH ₄ + HO ₂ [•]	\rightleftharpoons CH ₃ [•] + H ₂ O ₂	0.128·10 ⁸	0.592·10 ⁷
7	CH ₃ [•] + O ₂	\rightleftharpoons CH ₂ O + OH [•]	0.396·10 ⁶	0.258·10 ⁶
8	CH ₃ [•] + O ₂	\rightleftharpoons CH ₃ O [•] + O [•]	0.102·10 ¹⁰	0.208·10 ⁹
9	CH ₃ [•] + HO ₂ [•]	\rightleftharpoons CH ₃ O [•] + OH [•]	0.255·10 ⁸	0.116·10 ⁸
10	2 CH ₃ [•] + M	\rightleftharpoons C ₂ H ₆ + M	0.329·10 ⁷	0.352·10 ⁷
17	CHO [•] + O ₂	\rightleftharpoons CO + HO ₂ [•]	0.305·10 ⁸	0.196·10 ⁹
18	CO + HO ₂ [•]	\rightleftharpoons CO ₂ + OH [•]	0.474·10 ⁸	0.204·10 ⁸
19	C ₂ H ₆ + H [•]	\rightleftharpoons C ₂ H ₅ [•] + H ₂	0.223·10 ⁹	0.446·10 ⁸
20	C ₂ H ₆ + OH [•]	\rightleftharpoons C ₂ H ₅ [•] + H ₂ O	0.230·10 ⁹	0.132·10 ⁹
21	C ₂ H ₆ + CH ₃ [•]	\rightleftharpoons C ₂ H ₅ [•] + CH ₄	0.874·10 ⁹	0.262·10 ⁹
35	O ₂ + H [•]	\rightleftharpoons OH [•] + O [•]	0.728·10 ⁹	0.202·10 ⁹
36	O ₂ + H [•] + M	\rightleftharpoons HO ₂ [•] + M	0.150·10 ³	0.414·10 ³

* k_0 is expressed in units [m³ mol⁻¹ s⁻¹] or [m⁶ mol⁻² s⁻¹]

The calculated conversions and selectivities obtained after minimization are shown in Table 2. The experimental conversions are simulated accurately over the entire range of operating pressures, reactant partial pressures, temperatures, and residence times. Clearly, the present gas-phase kinetic model can account for the observed reactant conversions in case of the experiments with He, without incorporating heterogeneous termination reactions. The trends in the observed selectivities are well reproduced by the model. In case of the experiments

with He, the calculated CO and H₂ selectivities are slightly higher than the measured values, whereas the C₂H₆ and C₂H₄ selectivities are too low. The pre-exponential factors obtained after minimization are generally in the same order of magnitude as the values reported in case of the BM kinetic model, see Table 4. In case of reactions (8) and (19), the pre-exponential factors decreased by a factor of 5, whereas the pre-exponential factor of reaction (17) increased with a factor of 6. The present gas-phase kinetic model will be used now to investigate the influence of gas-phase reactions during the catalytic experiments.

3.4 Investigation of heterogeneous catalytic reactions in the presence of supported catalyst

3.4.1 Experimental results

The heterogeneous reactions were investigated by performing experiments using both the α -Al₂O₃ support and the 0.3 wt% Rh/ α -Al₂O₃ catalyst. The conversions and selectivities on the Rh/ α -Al₂O₃ catalyst at a fixed temperature of 1273 K are shown in Figure 3 as a function of space time, $W/F_{\text{CH}_4,0}$. The reactant conversions first increase gradually with increasing space time. The selectivities to CO, H₂, and C₂H₄ increase, whereas those to C₂H₆ and CO₂ decrease at higher values of the space time. The selectivity to H₂O remains approximately constant. Slaa et al. (1997) showed that addition of CO₂ and H₂O did not influence the experimental results at low oxygen conversions, suggesting that reforming reactions on the Rh/ α -Al₂O₃ catalyst are not important at these conditions. The presence of significant amounts of CO and H₂ thus indicates that direct formation of synthesis gas is possible at low conversions.

The heterogeneous reaction rates are strongly accelerated at $W/F_{\text{CH}_4,0}$ ratios greater than 2, resulting in a sudden transition to complete oxygen conversion. This transition is not due to heat transfer limitations, as a simultaneous increase of the catalyst bed temperature was not observed. High selectivities to CO and H₂ are found, and C₂-hydrocarbons are no longer detected. This sudden transition to complete oxygen conversion was also observed by Slaa et al. (1997) and Heitnes Hofstad et al. (1998) and was ascribed to complete reduction of Rh-oxide, formed at low oxygen conversions. Metallic rhodium obviously is very active towards oxidation of CH₄, C₂H₄, and C₂H₆, which explains the disappearance of the higher hydrocarbons and the sudden increase of the methane conversion at high space times. Experimental results at high space times (Slaa et al., 1997) showed that the remaining CH₄ is reformed with CO₂ and H₂O towards synthesis gas. The experimental trends shown in Figure 3 were also observed at higher catalyst temperatures. At higher temperatures, however, the

transition to complete oxygen conversion occurred at lower space times. This can be expected from a thermodynamic point of view, since reduction of Rh-oxide is governed by the partial pressure of oxygen. Due to increased oxygen conversions at 1345 K, the oxygen partial pressure is significantly lower at comparable space times. Hence, Rh-oxide is reduced at lower $W/F_{\text{CH}_4,0}$. Also, Rh-oxide is less stable at higher temperatures (Mallens et al., 1997).

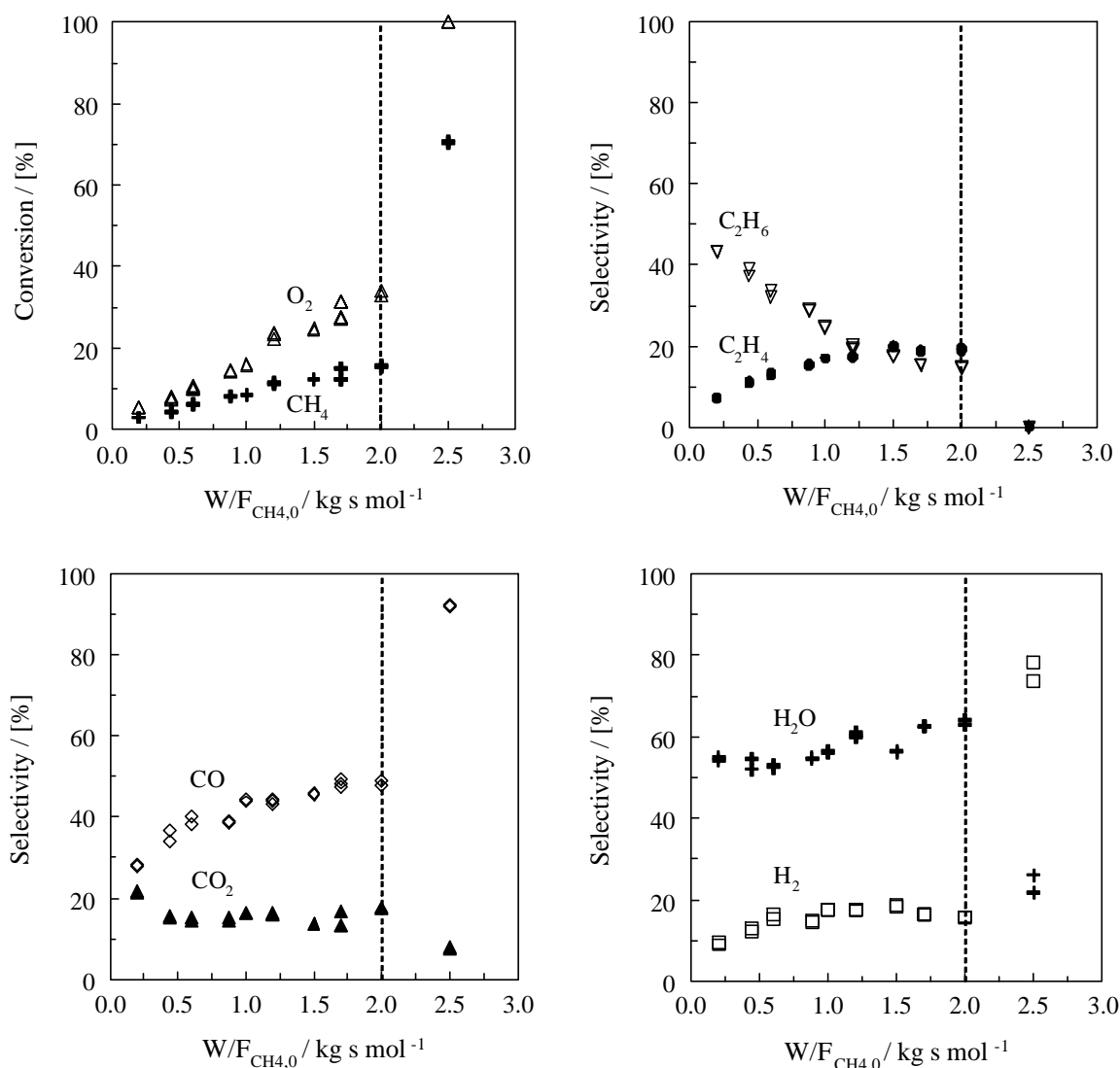


Figure 3. Measured conversions and selectivities on Rh/ α -Al₂O₃ vs space time. Conditions: $P_{\text{tot}} = 400 \text{ kPa}$, $T_s = 1273 \text{ K}$, $\text{CH}_4/\text{O}_2/\text{He} \text{ } \nu_{\text{0}} = 6.7/3.3/90$.

The results obtained with the α -Al₂O₃ support at 1273 K are shown in Figure 4. The observed trends in the conversions and selectivities at low space times are identical to those shown in Figure 3 for the Rh/ α -Al₂O₃ catalyst. The methane and oxygen conversions in case of the support experiments approximately amount to 11 and 17% at a $W/F_{\text{CH}_4,0}$ ratio of 2.0. In

case of the Rh/ α -Al₂O₃ catalyst, however, the conversions amounted to 16 and 34%, respectively. Figure 4 also indicates, that the reactant conversions and synthesis gas selectivity increase gradually at higher space times. This clearly contrasts with the results shown in Figure 3, in which a sudden transition to complete oxygen conversion and high synthesis gas selectivity is observed at W/F_{CH_{4,0}} ratios larger than 2.0.

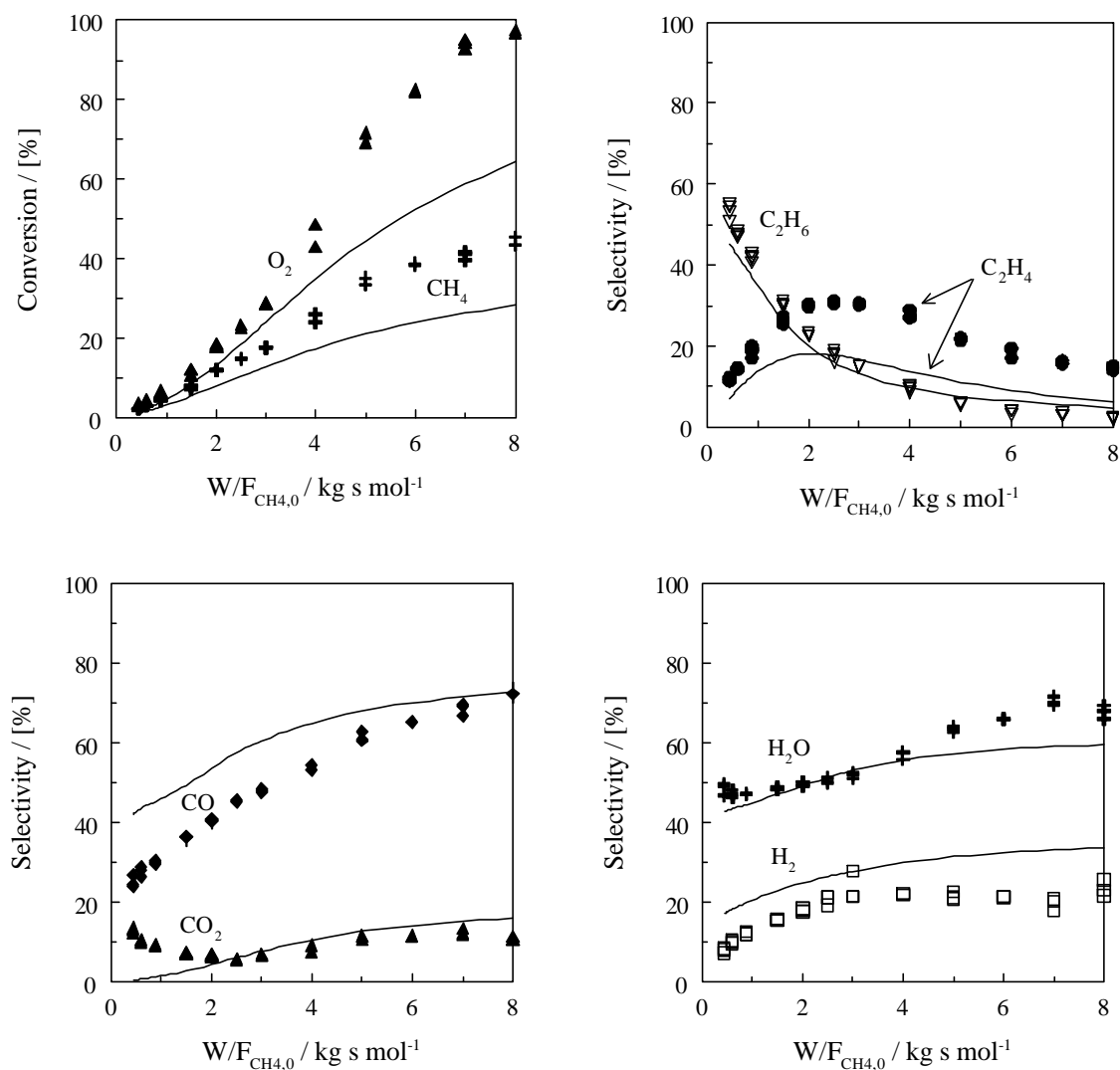


Figure 4. Conversions and selectivities on α -Al₂O₃ vs space time. Lines: calculated results using the extended BM gas-phase kinetic model and a 1-dimensional reactor model. Points: experimental results. Conditions: $P_{tot} = 400$ kPa, $T_s = 1273$ K, $CH_4/O_2/He^{1/2}_0 = 6.7/3.3/90$.

The production of C₂ hydrocarbons during the support and catalytic experiments suggests that gas-phase reactions could be important even in the presence of large amounts of He. Slaa et al. (1997) concluded, however, that gas-phase reactions do not occur at the

applied conditions. The products observed in case of the experiments with the α -Al₂O₃ support were thus assigned to heterogeneous activity of the support material. The authors however, did not rule out the possible occurrence of surface initiated gas-phase reactions, e.g. by the heterogeneous production of methyl radicals. Heitnes Hofstad et al. (1998) also investigated the activity of the α -Al₂O₃ support using a Temporal Analysis of Products setup, i.e. at pressures sufficiently low to suppress any homogeneous reactions. The results indicated that the support shows no activity for the partial oxidation of methane in the temperature range of 673 to 1123 K. The latter observations clearly are not in line with the results obtained by Slaa et al. (1997). The influence of gas-phase reactions will therefore be re-evaluated, using the extended gas-phase kinetic model presented in section 3.3.4, valid at conditions corresponding to those applied in the present catalytic experiments.

3.4.2 Influence of gas-phase reactions during the α -Al₂O₃ support experiments

The experiments performed with the α -Al₂O₃ support were simulated using the extended gas-phase kinetic model and a 1-dimensional reactor model. The calculated conversions and selectivities are shown in Figure 4 together with the corresponding experimental values. The simulated methane and oxygen conversions are lower than the measured values. At low space times, the gas-phase reactions contribute 50% to the measured conversions, which increases to 70 % at high W/F_{CH_{4,0}} ratios. The observed trends in the CO and H₂ selectivities are well reproduced by the model. The calculated selectivities, however, are higher than the experimental values. Note that the calculated selectivities to CO₂ and H₂O increase with increasing space-times, whereas the experimental curves display a minimum. The maximum in the C₂H₄ selectivity is described qualitatively. At the highest temperature applied during the support experiments, 1345 K, similar trends were found. At these conditions, the calculated conversions amounted to 90% of the measured values at the highest space time applied. The latter observation indicates that gas-phase reactions become increasingly important at higher temperatures.

The present analysis thus indicates that the contribution of gas-phase reactions is considerable at the applied reaction conditions, despite the low partial pressures of methane and oxygen. The observed production of C₂-hydrocarbons and partial oxidation products occurs primarily through the homogeneous gas-phase reactions. However, the difference between the measured and calculated conversions indicates that heterogeneous activity of the α -Al₂O₃ support cannot be ruled out completely. The difference in the trends between the experimental and simulated selectivities to CO₂ and H₂O at low space times, suggests that the support catalyzes the total oxidation of methane.

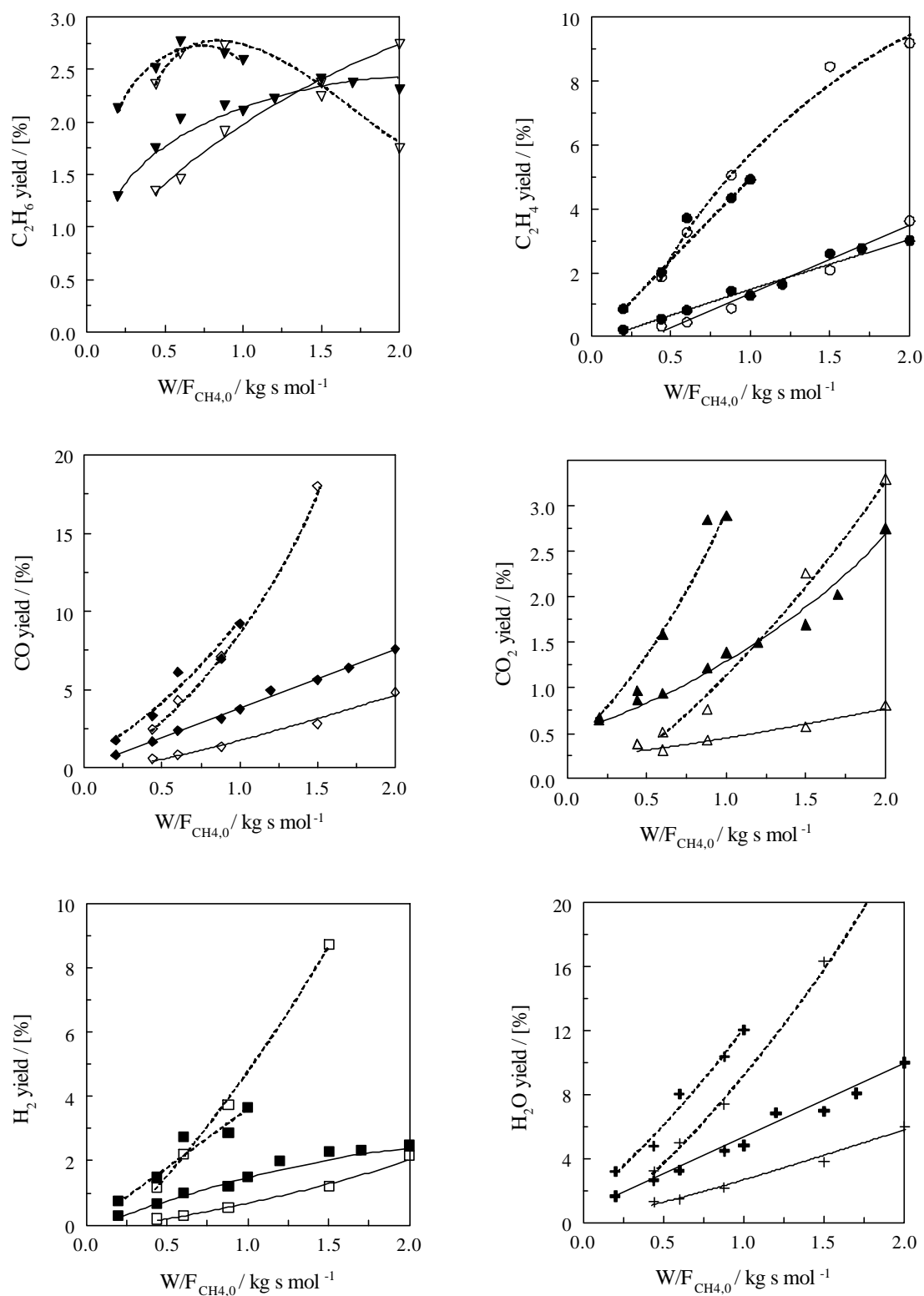


Figure 5. Measured product yields vs space time. Closed symbols: results obtained with $Rh/a-Al_2O_3$; Open symbols: results obtained with $a-Al_2O_3$; Solid lines: $T_S = 1273\ K$; Dashed lines: $T_S = 1345\ K$. Lines are drawn to guide the eye. Conditions: see Figures 3 and 4.

Figures 3 and 4 indicate that the trends in conversions and selectivities are similar in case of the experiments with the support and Rh catalyst at incomplete oxygen conversion. This suggests that gas-phase reactions will also contribute significantly in case of the Rh/ α -Al₂O₃ catalyst. However, the measured reactant conversions in case of the catalytic experiments were approximately 50 % higher than the values obtained during the support experiments. This illustrates that heterogeneous reactions in the presence of the Rh/ α -Al₂O₃ catalyst also occur to a significant extent. This will be investigated in the next section.

3.4.3 Comparison of α -Al₂O₃ support and Rh/ α -Al₂O₃ catalyst

The heterogeneous reactions occurring at the surface of the Rh catalyst were investigated by comparing experimental yields obtained in case of the α -Al₂O₃ support and the Rh/ α -Al₂O₃ catalyst. The comparison is based on product yields to account for the observed difference in reactant conversions. The corresponding experimental yields are shown in Figure 5 as a function of space time at temperatures of 1273 and 1345 K. First of all, it is clear that the C₂H₆ and C₂H₄ yields are approximately the same for the support and catalyst. This observation clearly justifies the assumption that C₂-hydrocarbon production occurs primarily via homogeneous gas-phase reactions, see section 3.4.2. The yields to the CO_x products at 1273 K are considerably higher in case of the Rh/ α -Al₂O₃ experiments. The same result is found in case of the H₂ and H₂O yields. The observed difference between the experimental CO and H₂ yields is significantly smaller at a temperature of 1345 K. This might be a result of the increased gas-phase reaction rates at these conditions. The experimental yields of CO₂ and H₂O obtained with the Rh/ α -Al₂O₃ catalyst, however, remain higher than those found in case of the support. This clearly illustrates that the Rh/ α -Al₂O₃ catalyst is primarily active towards the total oxidation of methane. At the lower temperature of 1273 K, however, direct partial oxidation towards CO and H₂ also occurs to a significant extent.

3.4.4 Discussion

The relative importance of homogeneous gas-phase reactions and heterogeneous catalytic reactions was also addressed by Schmidt et al. (1998) and Faravelli et al. (1998). Schmidt et al. (1998) investigated the catalytic partial oxidation of methane towards acetylene at very low space times, using Pt foam monoliths. As a result of the exothermic catalytic oxidation reactions, the outlet of the monolith reactor reached a temperature of almost 1773 K, which was considered to

be sufficiently high to initiate homogeneous gas-phase reactions. The calculated acetylene selectivities, obtained from reactor simulations using a homogeneous gas-phase model, were found to be similar to the experimental values. Faravelli et al. (1998) compared the results of homogeneous gas-phase simulations with experimental results of oxidative dehydrogenation of alkanes from propane up to hexanes. They found that both homogeneous gas-phase reactions as well as heterogeneous catalytic reactions occurred to a significant extent. The catalyst provided higher conversion rates and promoted the formation of dehydrogenated products. A few simplified catalytic reaction steps, coupled with a homogeneous reaction mechanism, allowed the authors to describe the experimental results. Deutschmann and Schmidt (1998) modelled the partial oxidation of methane in Rh coated monolith reactors using both gas-phase and catalytic reaction mechanisms. The catalytic oxidation rates were always significantly higher than the gas-phase reaction rates. At a pressure of 10 bar, gas-phase reactions led to a small increase of the production of complete oxidation products and to formation of ethane.

In the present work, gas-phase reactions also contributed significantly to the observed conversions and selectivities, even in case of significant dilution with helium. The strong influence of gas-phase reactions mainly results from the relatively low activity of the Rh/ α -Al₂O₃ catalyst and the high temperatures. The selectivities towards the C₂-products in case of the Rh/ α -Al₂O₃ catalyst and the α -Al₂O₃ support alone were approximately the same, indicating that surface initiated gas-phase reactions did not occur. In addition, initiation of gas-phase reactions due to local hot spots (c.f. Schmidt et al., 1998) could be ruled out, since the experiments were carried out isothermally. Hence, the homogeneous gas-phase reactions and the heterogeneous catalytic reactions occur independent of each other, in contrast to the findings of Schmidt et al. (1998) and Faravelli et al. (1998).

3.5 Conclusions

A gas-phase kinetic model was derived resulting in an accurate description of homogeneous gas-phase experiments, performed at conditions corresponding to those applied in the heterogeneous experiments, i.e. at high temperatures and pressures, using CH₄/O₂/He feed mixtures. Heterogeneous termination reactions could be neglected at the investigated surface area to volume ratio. Reactor simulations with the gas-phase kinetic model indicated that homogeneous reactions are very important at the applied reaction conditions. In case of the experiments with the α -Al₂O₃ support alone, the gas-phase reactions contributed at least 50% to the measured conversions. Production of C₂-hydrocarbons was assigned primarily to homogeneous gas-phase reactions. Comparison of the measured conversions obtained in the α -Al₂O₃ support and Rh/ α -Al₂O₃ catalytic experiments, indicated that both homogeneous

gas-phase reactions and heterogeneous catalytic reactions are important in case of the Rh/ α -Al₂O₃ catalyst. A quantitative description of the conversions and selectivities in case of the Rh/ α -Al₂O₃ catalyst thus requires the simultaneous consideration of both heterogeneous and homogeneous reactions. The Rh/ α -Al₂O₃ catalyst is primarily active towards the total oxidation of methane at 1345 K. At 1273 K, however, there are strong indications that Rh/ α -Al₂O₃ also catalyzes the direct partial oxidation of methane to synthesis gas.

Notation

\mathbf{b}	Parameter vector
C_i	molar concentration of species i , mol m ⁻³
d_p	particle size, mm
$d_{r,i}$	inner diameter of the tubular reactor, m
$d_{ft,i}$	inner diameter of the filling tube, m
$d_{ft,e}$	external diameter of the filling tube, m
$d_{w,e}$	external diameter of the thermowell, m
$D_{m,i}$	Effective binary diffusion coefficient of species i , m ² s ⁻¹
$f_j(x_k, \mathbf{b})$	Calculated response value for response j in experiment k
F_{tot}	total molar flow rate, mol s ⁻¹
$k_{0,g}$	rate coefficient of gas-phase reaction, m ³ mol ⁻¹ s ⁻¹ or m ⁶ mol ⁻² s ⁻¹
$k_{t,i}$	rate coefficient of heterogeneous termination reaction, m s ⁻¹
l_r	length of the tubular reactor, m
l_{ft}	length of the filling tube, m
P_{tot}	total pressure, kPa
r	radial reactor coordinate, m
R	gas constant, J mol ⁻¹ K ⁻¹
$R_{i,g}$	net gas-phase production rate of species i , mol m ⁻³ s ⁻¹
$R_{i,t}$	Heterogeneous termination rate of species i , mol m ⁻² s ⁻¹
$s_{i,0}$	initial sticking coefficient, -
$S(\mathbf{b})$	Objective function, -
$S(i)$	Selectivity of species i , -
T_{max}	Maximum temperature, K
$V/F_{tot,0}$	space time in gas-phase experiment, m ³ s mol ⁻¹
w_j	Weighting factor for response j , -
$W/F_{CH_4,0}$	space time in carrier and catalytic experiments, kg s mol ⁻¹
x_k	vector of independent variables, -

X(i)	Conversion of reactant i, -
y _{kj}	Experimentally observed response value of response j in experiment k
z	axial reactor coordinate, m

Greek symbols

ϕ_m	mass flux, $\text{kg m}^{-2} \text{s}^{-1}$
ρ_f	fluid density, kg m^{-3}
τ	gas-phase residence time, s

References

- Au, C.T., & Wang, H.Y. (1997). Mechanistic studies of methane partial oxidation to syngas over SiO₂-supported rhodium catalysts. *J. Catal.*, *167*, 337-345.
- Berger, R.J., & Marin, G.B. (1999). Investigation of gas-phase reactions and ignition delay occurring at conditions typical for partial oxidation of methane to synthesis gas. *Ind. Engng. Chem. Res.*, *38*, 2582-2592.
- Boucouvalas, Y., Zhang, Z., & Verykios, X.E. (1994). Heat transport limitations and reaction scheme of partial oxidation of methane to synthesis gas over supported rhodium catalysts. *Catal. Lett.*, *27*, 131-142.
- Chen, Q., Hoebink, J.H.B.J., & Marin, G.B. (1991). Kinetics of the oxidative coupling of methane at atmospheric pressure in the absence of catalyst. *Ind. Engng. Chem. Res.*, *30*, 2088-2097.
- Chen, Q., Couwenberg, P.M., & Marin, G.B. (1994). Effect of pressure on the oxidative coupling of methane in the absence of catalyst. *AIChE J.*, *40*, 521-535.
- Couwenberg, P.M., Chen, Q., & Marin, G.B. (1996). Kinetics of a gas-phase chain reaction catalyzed by a solid: The oxidative coupling of methane over Li/MgO-based catalysts. *Ind. Engng. Chem. Res.*, *35*, 3999-4011.
- De Smet, C.R.H., Berger, R.J., Slaa, J.C., & Marin, G.B. (1998). Kinetic modelling of the partial oxidation of methane to syn-gas at high temperatures. *Stud. Surf. Sci. Catal.*, *119*, 825-829.
- Dente, M., Ranzi, E., & Goossens, A.G. (1979). Detailed prediction of olefine yields from hydrocarbon pyrolysis through a fundamental simulation model (SPYRO). *Comput. Chem. Eng.*, *3*, 61-75.
- Deutschmann, O., & Schmidt, L.D. (1998). Modeling the partial oxidation of methane in a short-contact-time reactor. *AIChE J.*, *44*, 2465-2477.
- Faravelli, T., Goldaniga, A., Ranzi, E., Dietz, A., Davis, M., & Schmidt, L.D. (1998). Partial oxidation of hydrocarbons: an experimental and kinetic modelling study. *Stud. Surf. Sci. Catal.*, *199*, 575-580.
- Heitnes Hofstad, K., Hoebink, J.H.B.J., Holmen, A., & Marin, G.B. (1998). Partial oxidation of methane to synthesis gas over rhodium catalysts. *Catal. Today*, *40*, 157-170.
- Hickman, D.A., & Schmidt, L.D. (1993). Steps in CH₄ oxidation on Pt and Rh surfaces: High-temperature reactor simulations. *AIChE J.*, *39*, 1164-1177.
- Mallens, E.P.J., Hoebink, J.H.B.J., & Marin, G.B. (1997). The reaction mechanism of the partial oxidation of methane to synthesis gas: a transient kinetic study over rhodium and a comparison with platinum. *J. Catal.*, *167*, 43-53.

- NAG, Numerical Algorithm Group (1997). NAG Fortran Library Manual (Mark 18). Oxford: Wilkinson House.
- Rosenbrock, H.H. (1961). An automated method for finding the greatest or least value of a function. *Comput. J.*, *3*, 175-184.
- Slaa, J.C., Berger, R.J., & Marin, G.B. (1997). Partial oxidation of methane to synthesis gas over Rh/ α -Al₂O₃ at high temperatures. *Catal. Lett.*, *43*, 63-70.
- Schmidt, L.D., Hohn, K.L., & Davis, M.B. (1998). Catalytic partial oxidation of methane at extremely short contact times: production of acetylene. *Stud. Surf. Sci. Catal.*, *119*, 397-402.
- Tian, Z., Dewaele, O., & Marin, G.B. (1999). The state of Rh during the partial oxidation of methane into synthesis gas. *Catal. Lett.*, *57*, 9-17.
- Vernon, P.D.F., Green, M.L.H., Cheetham, A.K., & Ashcroft, A.T. (1990). Partial oxidation of methane to synthesis gas. *Catal. Lett.*, *6*, 181-186.
- Wang, D., Dewaele, O., De Groot, A.M., & Froment, G.F. (1995). Reaction mechanism and role of the support in the partial oxidation of methane on Rh/Al₂O₃. *J. Catal.*, *159*, 418-426.

4

An experimental reactor to study the intrinsic kinetics of the catalytic partial oxidation of methane in the presence of heat-transport limitations

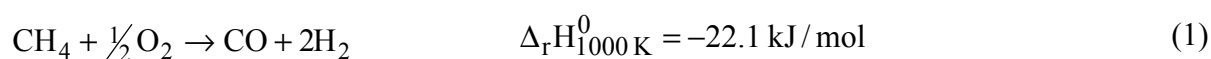
This chapter was published in Appl. Catal. A., 187, 33-48 (1999).

Abstract -The catalytic partial oxidation (CPO) of methane with oxygen was studied at atmospheric pressure in a continuous-flow reactor containing a single Pt metal gauze. Experiments were performed at catalyst temperatures and residence times in the range of 950-1200 K and 0.02-0.2 milliseconds, respectively. Heat-transport limitations are taken into account explicitly, by measuring the catalyst temperature directly by means of a surface thermocouple. The experimental results indicated that the conversions of methane and oxygen were determined by transport phenomena; however, the CO selectivity appeared to be influenced significantly by the kinetics of the catalytic reactions. Hydrogen was found only at temperatures above 1273 K. In order to be able to derive intrinsic kinetic information from the experimental data, a reactor model consisting of two rows of parallel flat plates in series was developed, taking into account the relevant transport phenomena. This flat-plate reactor model was validated by comparing the model results to 3D FLUENT simulations of simultaneous heat and mass transfer in case of a simple surface reaction on the gauze catalyst. A series-parallel CPO reaction mechanism allowed simulating the observed conversions and selectivities at different space-times. More detailed elementary-step reaction mechanisms can be developed, using both the experimental data and the flat-plate reactor model.

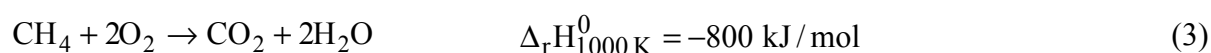
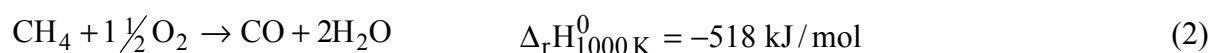
Keywords: Methane partial oxidation; heat-transport limitations; Pt metal gauze; reactor model

4.1 Introduction

In the past decade, global research activities have been unfolded both in industry and academia to develop economic processes for the chemical conversion of large natural gas reserves to valuable liquid products, such as methanol and higher hydrocarbons. These chemicals can be produced either via direct conversion routes, such as oxidative coupling, or via indirect routes, with synthesis gas as an intermediate. At present, synthesis gas is mainly produced via endothermic steam reforming, using a Ni-Al₂O₃ catalyst (Rostrup-Nielsen, 1993). The catalytic partial oxidation of methane with oxygen to synthesis gas, which is thermodynamically favoured at sufficiently high temperatures, has recently received increasing attention as a fast and energy-efficient alternative to steam reforming:



Highly exothermic partial or total oxidation reactions, such as:



can also occur. These exothermic, non-selective oxidation reactions can result in high catalyst temperatures, which can have detrimental effects on the stability of the catalytic material and can cause severe heat-transport limitations.

Already in 1946, Prettre et al. (1946) reported high selectivities to synthesis gas during the catalytic partial oxidation of methane using a Ni-Al₂O₃ catalyst. The reaction is considered to proceed via a two-step mechanism: total oxidation of part of the methane, followed by reforming of the remaining methane with steam and carbon dioxide to synthesis gas. This mechanism is supported by the work of Vernon et al. (1990), using supported transition metal catalysts, and by Vermeiren et al. (1992), using measured temperature profiles over a nickel catalyst. Hickman et al. (1992a, 1993), however, showed that synthesis gas can be produced directly from methane and oxygen at very short residence times, using both noble metal coated monoliths and Pt-10%Rh gauzes. Mallens et al. (1997) also showed that CO and H₂ are the primary products of the CPO reaction in case of Pt and Rh sponges, using the Transient Analysis of Products (TAP) technique.

In order to determine the intrinsic kinetics of a heterogeneous catalytic reaction, experiments have to be performed in which both internal and external concentration and temperature gradients at the scale of the catalyst can be neglected. Since the CPO reaction is reported to be very fast (Hickman et al., 1992, 1993), high mass-transfer rates are required to

avoid large concentration gradients. In case of the indirect CPO mechanism, however, the total combustion reactions inevitably result in large temperature gradients at the scale of the catalyst. Even in case of the direct route, with synthesis gas selectivities up to 90 % (Hickman and Schmidt, 1992a, Hickman et al., 1993), the heat of reaction is sufficiently high to cause severe heat-transport limitations. This indicates that the intrinsic kinetics of the partial oxidation of methane to synthesis gas can only be studied accurately when experimental reactors are used in which high mass-transfer rates can be realised, and in which special attention is paid to the measurement of the catalyst temperature.

The present work reports on an experimental reactor to study the intrinsic kinetics of the catalytic partial oxidation of methane in the presence of heat-transport limitations. The reactor contains a single Pt metal gauze, which enables high mass-transfer rates without significant pressure drop. Heat-transport limitations can be taken into account explicitly, since the catalyst temperature is measured directly by means of a Pt/Pt-10%Rh surface thermocouple. Experimental results indicate, however, that it is impossible to perform experiments at conditions where both reactant conversions and product selectivities are determined by chemical phenomena alone. Therefore, a reactor model taking into account the relevant transport phenomena is developed to determine the intrinsic kinetic parameters of the CPO reaction. This reactor model will be used to calculate conversions and selectivities in case of a series-parallel CPO reaction mechanism. However, the experimental set-up, together with the flat-plate reactor model, based upon the actual mesh size of the gauze catalyst, can be used as a tool to study the intrinsic kinetics of any heterogeneous reaction in the presence of transport limitations.

4.2 Experimental equipment and procedures

The partial oxidation of methane with oxygen to synthesis gas was studied by performing steady-state experiments in a continuous flow reactor set-up containing a single Pt metal gauze. A schematic drawing of the reactor, together with the layout of the gauze catalyst is shown in Figure 1. The gauze catalyst is constructed by using a single Pt wire ($d_w = 0.20$ mm) and consists of two rows of six parallel wires placed on top of each other. The average distance between the centres of two individual wires, D_{w-w} , amounts to $8.2 \cdot 10^{-4}$ m, which corresponds to a mesh size of approximately 150 meshes/cm². To ensure mechanical stability, the wires were spotwelded at the intersection points.

The quartz reactor contains three distinct zones. The reactant gases are preheated in the annular preheating zone ($d_e = 15$ mm, $d_i = 12$ mm). Then, the gas mixture passes over the Pt gauze catalyst, which is located at the end of the preheating zone. Finally, the product gas is

cooled in the annular cooling zone ($d_e = 8$ mm, $d_i = 7$ mm), which is placed perpendicular to the heating zone. This perpendicular orientation of the annular tubes enables the use of an optical pyrometer to determine the surface temperature of the Pt gauze and provides a means to monitor the performance of the gauze catalyst as well as possible Pt deposits due to the formation of volatile Pt oxide species.

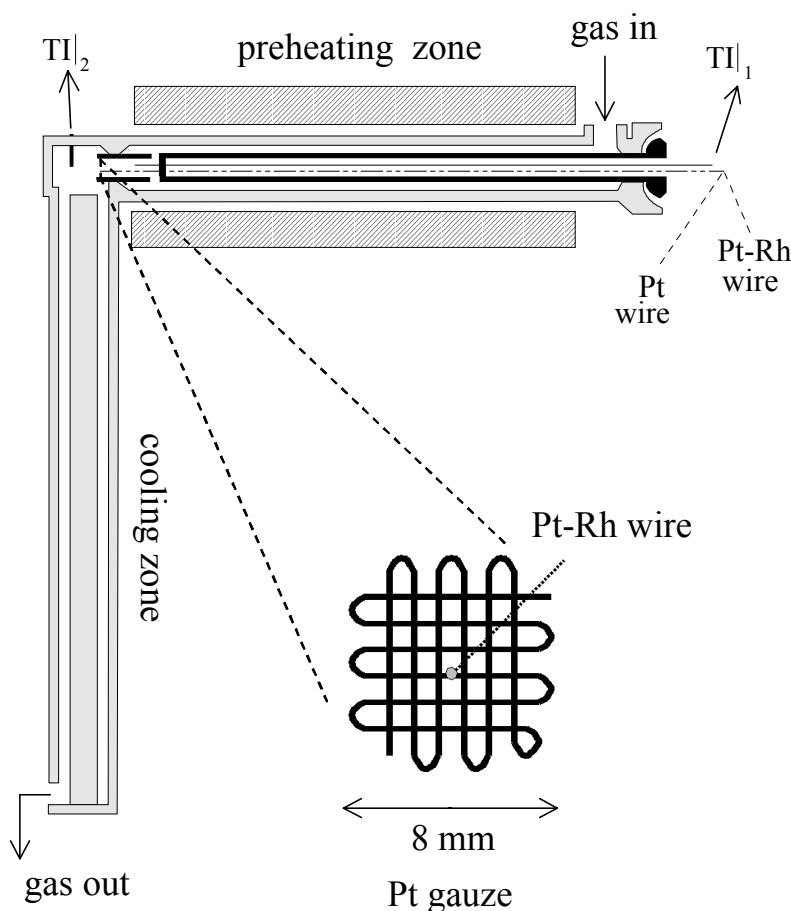


Figure 1. Schematic drawing of the laboratory reactor. $TI|_1$, $TI|_2$ = Nisil/nicrosil thermocouples, used to measure the gas-phase temperature upstream and downstream of the gauze catalyst, respectively.

Special attention was paid to the temperature measurement. The gas-phase temperature was measured upstream and downstream of the Pt gauze by Nisil/Nicrosil thermocouples, located in quartz thermocouple wells. In addition to the surface temperature measurement via the optical pyrometer, the catalyst temperature was also determined directly by means of a surface thermocouple. This thermocouple was constructed by spotwelding a thin Pt-10%Rh wire ($d_w = 0.10$ mm) to the centre of the gauze catalyst. The temperatures measured with the

optical pyrometer were always within 10 K of those obtained via the surface thermocouple. The optical pyrometer was also used to monitor the temperature uniformity of the gauze catalyst during the experiments. The maximum temperature difference between the centre and the perimeter of the gauze catalyst approximately amounted to 10 K.

A typical example of measured catalyst and bulk gas-phase temperatures at reaction conditions is shown in Figure 2. The bulk gas-phase temperature is defined as the average of the gas-phase temperatures measured upstream and downstream of the gauze catalyst. It is clear that the catalyst surface temperatures are at least 200 K higher than the average gas-phase bulk temperature, indicating that strong heat-transfer limitations indeed occur. Therefore, the measured catalyst temperature will be used to determine the intrinsic kinetics of the CPO reaction at a given temperature.

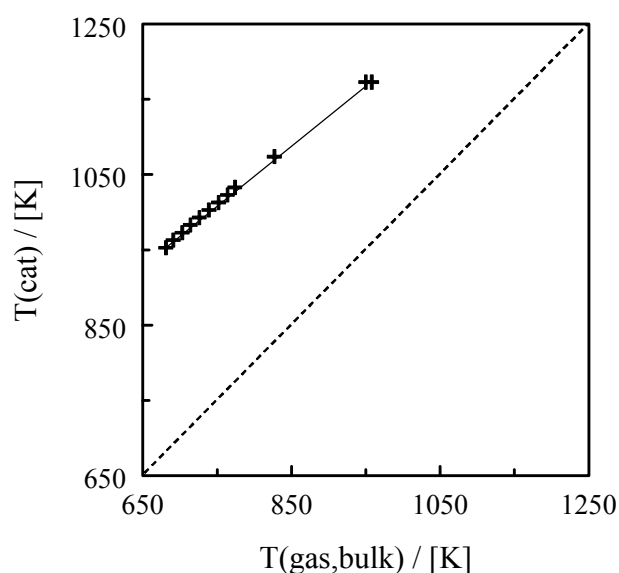


Figure 2. Comparison of measured catalyst and gas-phase bulk temperatures. Conditions: $P_{tot} = 130$ kPa, $F_{tot} = 1 \cdot 10^{-2}$ mol s^{-1} , $W/F_{CH_4,0} = 39.9$ g s mol $^{-1}$, $CH_4/O_2/He|_0 = 14.3/5.7/80$.

The experiments were carried out using gases with purities of 99.995% for CH₄, 99.5% for C₂H₆, 99.999% for O₂, 99.996% for H₂, 99.996% for He, and 99.999% for N₂. All the products were analysed using a HP 5890 series II gas chromatograph, equipped with Molsieve 5A and Poraplot Q columns and TCD detectors. Nitrogen was used as an internal standard. The reactant conversions and product selectivities were calculated based on the total number of moles of C, O, and H in the product stream. The component mass balances were closed within 5 %.

Prior to the experiments, the gauze catalyst was reduced for one hour with a 10% H₂/He mixture at 973 K. In order to activate the catalyst, a standard pre-treatment procedure was applied. The catalytic reactions were ignited at a gas-phase temperature of approximately 950 K by flowing a gas mixture containing 30% C₂H₆, 20% O₂, and 50% He. C₂H₆ was used to ignite the reactions, as the ignition temperature of C₂H₆/O₂ mixtures is considerably lower than the ignition temperature of CH₄/O₂ mixtures. After ignition, C₂H₆ was gradually replaced by CH₄, and the gauze temperature was maintained at 1173 K for one hour. The reactions were extinguished by adding a surplus of He and, if necessary, by switching off the pre-heater. Finally, the Pt gauze was exposed to a 10% H₂O/He mixture at 973 K to remove residual carbon deposits. An analogous start-up and shutdown procedure was applied prior to each experimental series, which resulted in reproducible results. An experimental series consisted of a number of experiments in which the influence of a single process variable was investigated.

The range of experimental conditions covered during the catalytic experiments is shown in Table 1. The total molar flow rate was varied in the range of 1.5 to 20 mmol s⁻¹, which resulted in linear gas velocities of 1.5 to 20 m s⁻¹ at the position of the gauze catalyst. The corresponding Reynolds numbers, based upon the velocity, density, and viscosity at the position of the gauze catalyst, and the reactor diameter, amounted to a maximum value of approximately 1000, which indicates that the flow pattern is laminar.

Table 1. *Ranges of experimental conditions covered during the catalytic experiments.*

Catalyst temperature (K)	950 - 1200
Total pressure (kPa)	130 - 240
Total flow rate (mmol s ⁻¹)	1.5 - 20
W/F _{CH_{4,0}} (g s mol ⁻¹)	10 - 130
CH ₄ /O ₂ ₀	2 - 5
He-dilution (%)	40 - 80
CH ₄ conversion (-)	0.02 - 0.12
O ₂ conversion (-)	0.09 - 0.46

The maximum catalyst temperature applied during the experiments amounts to 1200 K. At such high temperatures, gas-phase reactions may become important. Berger and Marin (1999) developed a kinetic model for gas-phase chain reactions at typical CPO conditions.

Simulations were carried out using this kinetic model together with a plug-flow reactor model at the most severe conditions encountered during the experiments, i.e. at the highest catalyst temperature and the highest space-time W/F. The calculated methane and oxygen conversions amounted to 0.14 and 0.23 %, respectively, indicating that the effect of gas-phase reactions can be neglected at the conditions applied. This is mainly caused by the high total molar flow rates and the low reactant partial pressures applied during the experiments.

4.3 Experimental results

At all conditions investigated, CO, CO₂, and H₂O were the main products, indicating that the oxidation reactions are far from thermodynamic equilibrium. H₂ was found only at catalyst temperatures above 1273 K. It is known that a single Pt metal gauze is a poor catalyst for hydrogen production, even at high catalyst temperatures (Heitnes et al., 1995, Heitnes et al., 1996, Fahti et al., 1998). This is a result of the surface reaction of adsorbed hydrogen and oxygen species towards adsorbed hydroxyl species, which is a precursor for water formation. The latter reaction is extremely fast on Pt (Hickman and Schmidt, 1993). Significant amounts of hydrogen have only been detected in case of multiple gauzes in series, when the oxygen conversion is complete (Hickman and Schmidt, 1992a).

At catalyst temperatures above 1273 K the gauze catalyst did not exhibit a stable performance with time on stream. A slow increase of the methane and oxygen conversions, a decrease of the CO selectivity, and an appreciable evaporation of Pt was observed. Pt evaporation as a result of the formation of volatile Pt oxide species is a well-known phenomenon in industrial ammonia oxidation (Thieman et al., 1985, Twigg, 1996). In addition, the observed changes in conversions and selectivities are generally ascribed to morphological changes of the Pt catalyst, which lead to a significant roughening of the Pt surface (Bergene et al., 1996). In order to perform experiments at constant catalyst activity, and to decrease the risk of Pt evaporation, the catalyst temperature was always kept below 1200 K.

The influence of the catalyst temperature and the reactant space-time, W/F_{CH₄,0}, on conversions and selectivities is shown in Figures 3 and 4. Both the methane and oxygen conversions are hardly temperature dependent. From the results of Figure 3 an apparent activation energy of the methane and oxygen conversion rates of approximately 10 kJ mol⁻¹ follows, which indicates that the reaction rates are completely determined by transport phenomena. The selectivity to CO, however, varied strongly with the catalyst temperature. The formation rate of CO thus appears to be determined significantly by the kinetics of the catalytic reactions, in contrast to the conversions of methane and oxygen. Identical trends

were also found by Heitnes Hofstad et al. (1996) and by Hickman and Schmidt (1992a) using both Pt and Pt/10%Rh gauzes.

Figure 4 shows that the methane and oxygen conversions increase with increasing space-times at a fixed catalyst temperature of 1123 K. The catalyst temperature was kept at a constant value of 1123 K by decreasing the preheat temperature at increasing space-times. The selectivity to CO decreases at increasing space-time, which indicates that CO is a primary product of the oxidation reaction. As indicated in the introduction, much debate has been going on in the literature concerning primary product formation. In case of supported fixed-bed transition metal catalysts, the total oxidation products are generally considered as the primary products (Vernon et al., 1990), which subsequently react with methane to synthesis gas. Hickman and Schmidt (1992a, 1993) have shown that in case of noble metal coated monoliths and noble metal gauzes, CO and H₂ are the primary products.

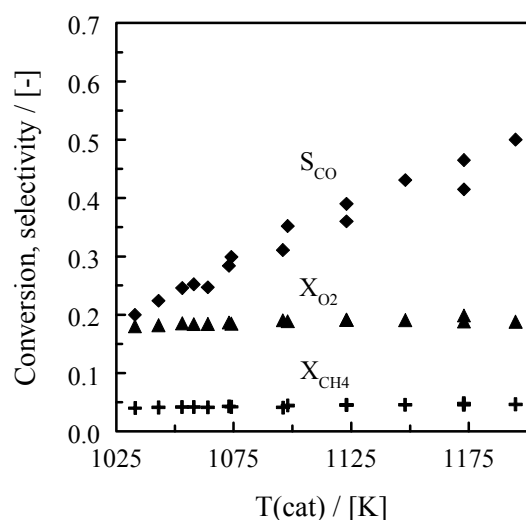


Figure 3. Conversion and selectivity as a function of the catalyst temperature. Points: experiments. Conditions: $P_{tot} = 130$ kPa, $F_{tot} = 1 \cdot 10^{-2}$ mol s⁻¹, $W/F_{CH_4,0} = 39.9$ g s mol⁻¹, $CH_4/O_2/He|_0 = 14.3/5.7/80$.

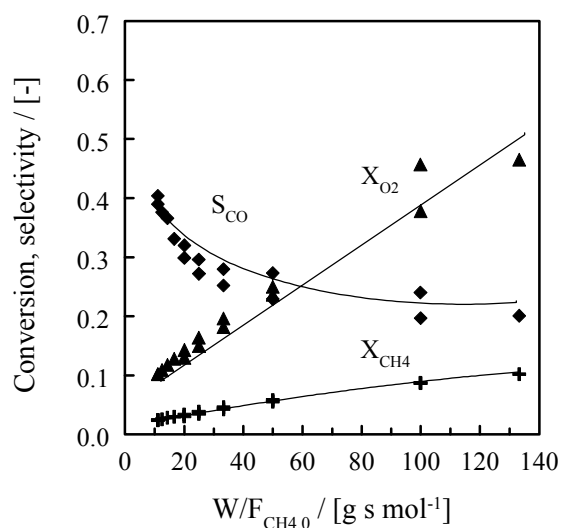


Figure 4. Conversion and selectivity as a function of the space-time. Lines: calculated using the flat-plate reactor model and the series-parallel CPO reaction mechanism. Points: experiments. Conditions: $P_{tot} = 160$ kPa, $T_{cat} = 1123$ K, $CH_4/O_2/He|_0 = 28.6/11.4/60$.

4.4 Reactor model development

4.4.1 Approach

The experimental results indicated that both the methane and oxygen conversion rates are completely determined by mass transport at the conditions applied. The CO formation rate, however, was influenced significantly by the kinetics of the catalytic reactions. Therefore, a reactor model taking into account the transport phenomena in an appropriate way should allow determining the intrinsic kinetics of the CO formation.

The computational fluid dynamics program FLUENT (Fluent User Manual, 1995) was used to calculate gas-phase temperature and mole fraction profiles in case of a model surface reaction taking into account the 3D geometry of the gauze. The model surface reaction and the corresponding rate equation used in the simulations can be written as:



$$r_{\text{w,CH}_4} = k_{\text{intr}} C_{\text{CH}_4}^n M_{\text{CH}_4} \quad (5)$$

The surface reaction concerns the deposition of a solid hydrogen atom, from gaseous methane, which can be readily implemented in the FLUENT simulations. More detailed surface kinetics could not be taken into account, since the standard FLUENT code cannot be used in conjunction with external subroutines that model elementary step surface reaction mechanisms.

FLUENT simultaneously solves the momentum equation, the continuity equations for the gas-phase components ($\text{CH}_4(\text{g})$ and $\text{CH}_3(\text{g})$), and the energy equation by means of the control-volume based finite-difference method. The control volumes are defined by means of a computational grid, describing the geometry of the gauze catalyst. A total number of (22 x 22 x 57) gridpoints was used in the (x, y, z) directions. As indicated in section 2, the temperature of the gauze catalyst is measured in-situ by means of the surface thermocouple. The measured surface temperatures were imposed at the wire surface in the FLUENT calculations.

Typical gas-phase temperature and reactant mole fraction profiles are shown in Figure 5. Because of symmetry considerations, only a quarter of a single mesh of the gauze catalyst has to be taken into account during the calculations. From both profiles it is clear, that strong heat and mass-transfer resistances occur at the conditions applied. In addition, gas-phase temperature and reactant mole fraction profiles along the axis of the cylinders can be observed, which result from the interaction between the different wires.

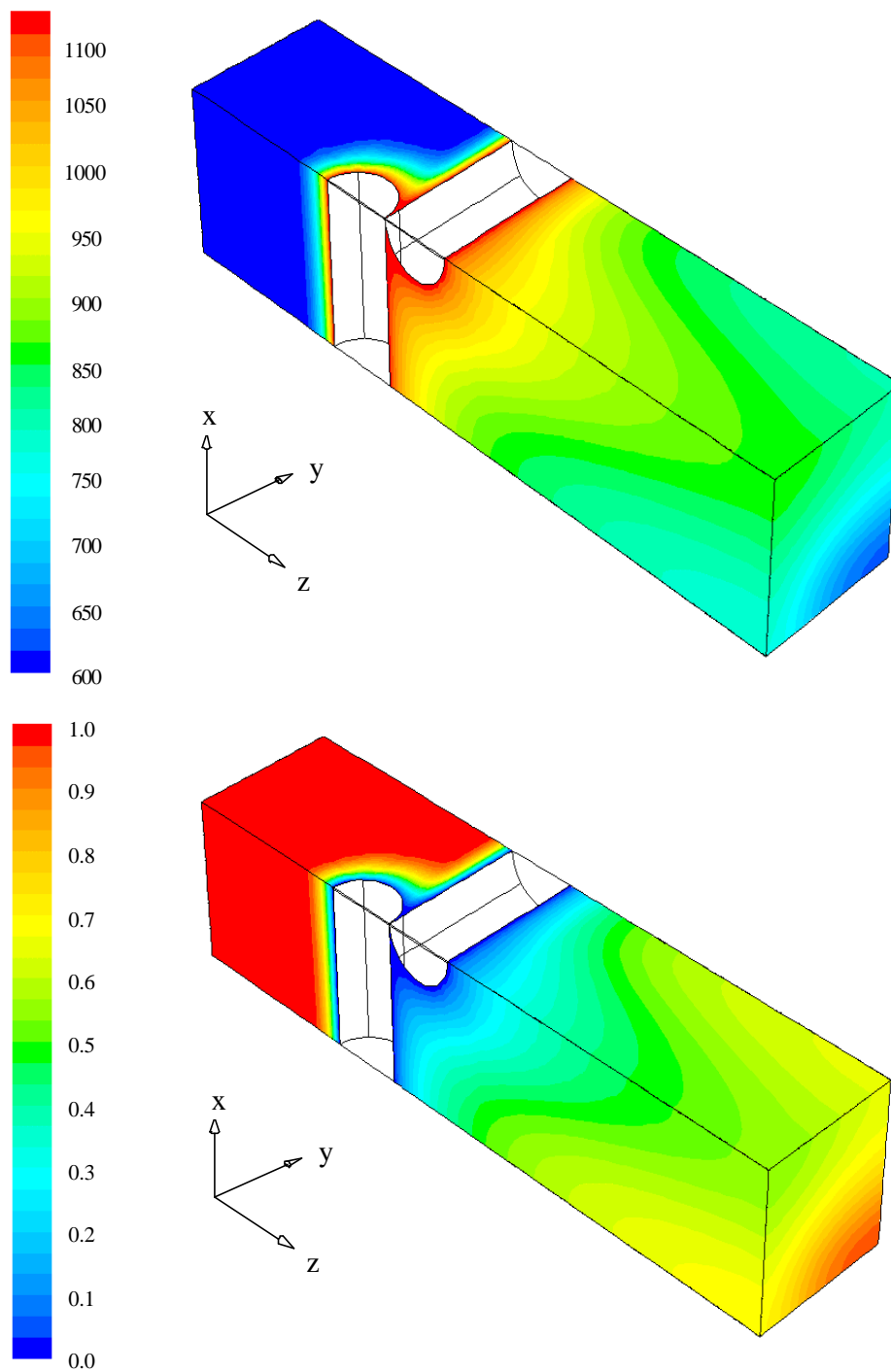


Figure 5. (a) Gas-phase temperature profile, and (b) CH₄ mole-fraction profile obtained from a FLUENT simulation taking into account the 3D gauze geometry. Conditions: $T_{in}=600$ K, $T_{cat}=1123$ K, $u_{in}=10$ m s⁻¹, $k_{intr}=1 \times 10^4$ m s⁻¹, $n=1$.

The CPU time required to calculate the temperature and mole fraction profiles approximately amounts to 10 ks, using a Silicon Graphics Power Challenge computer. FLUENT simulations thus are not suited to estimate intrinsic kinetic parameters via regression analysis due to large computational times. Therefore, there is a need for a simpler reactor model. A schematic representation of the approach used to derive such a reactor model is shown in Figure 6.

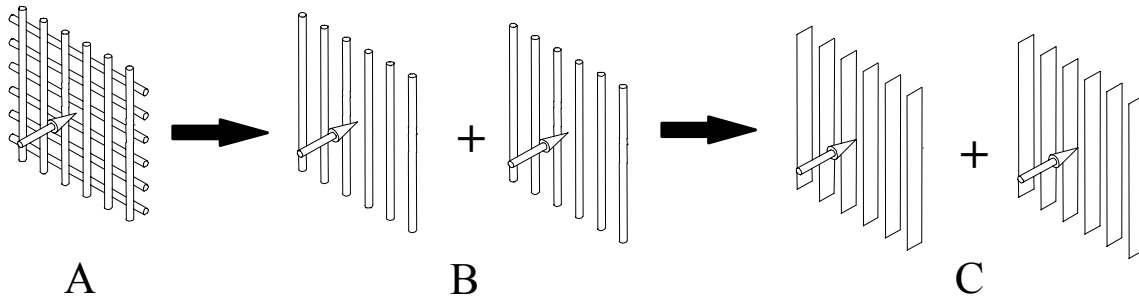


Figure 6. Derivation of the flat-plate reactor model: (a) gauze catalyst, (b) 2D approximation using two rows of parallel cylinders in series, and (c) the flat-plate reactor model, consisting of two rows of parallel flat plates in series.

First, the computational complexity of the gauze catalyst is reduced from 3D to 2D, by considering (1) two identical rows of parallel cylinders of infinite length in series, and (2) using the mean gas-phase temperature and mole fractions at the outlet of the first row of cylinders as input conditions for the second row of cylinders (Figure 6-B). This reactor configuration, consisting of two rows of cylinders of infinite length in series, was described mathematically by means of two identical rows of parallel flat plates of infinite length in series (Figure 6-C). The latter configuration of parallel flat plates will be referred to as the flat-plate reactor model.

A considerable reduction of the computational time was obtained in case of the flat-plate reactor model by solving the continuity and energy equations numerically for both rows of plates separately, using a uniform flow field. The CPU time required in case of a simple surface reaction approximately amounts to 1 s. The numerical solution procedure followed in case of the flat-plate reactor model is shown in detail in Figure 7. The characteristic dimensions of a single row of cylinders of the gauze catalyst, d_w and D_{w-w} , and a single row of plates of the flat-plate reactor model, b (length of a single flat plate) and h (distance between two flat plates), are shown in Figure 8, together with the corresponding heat and mass fluxes.

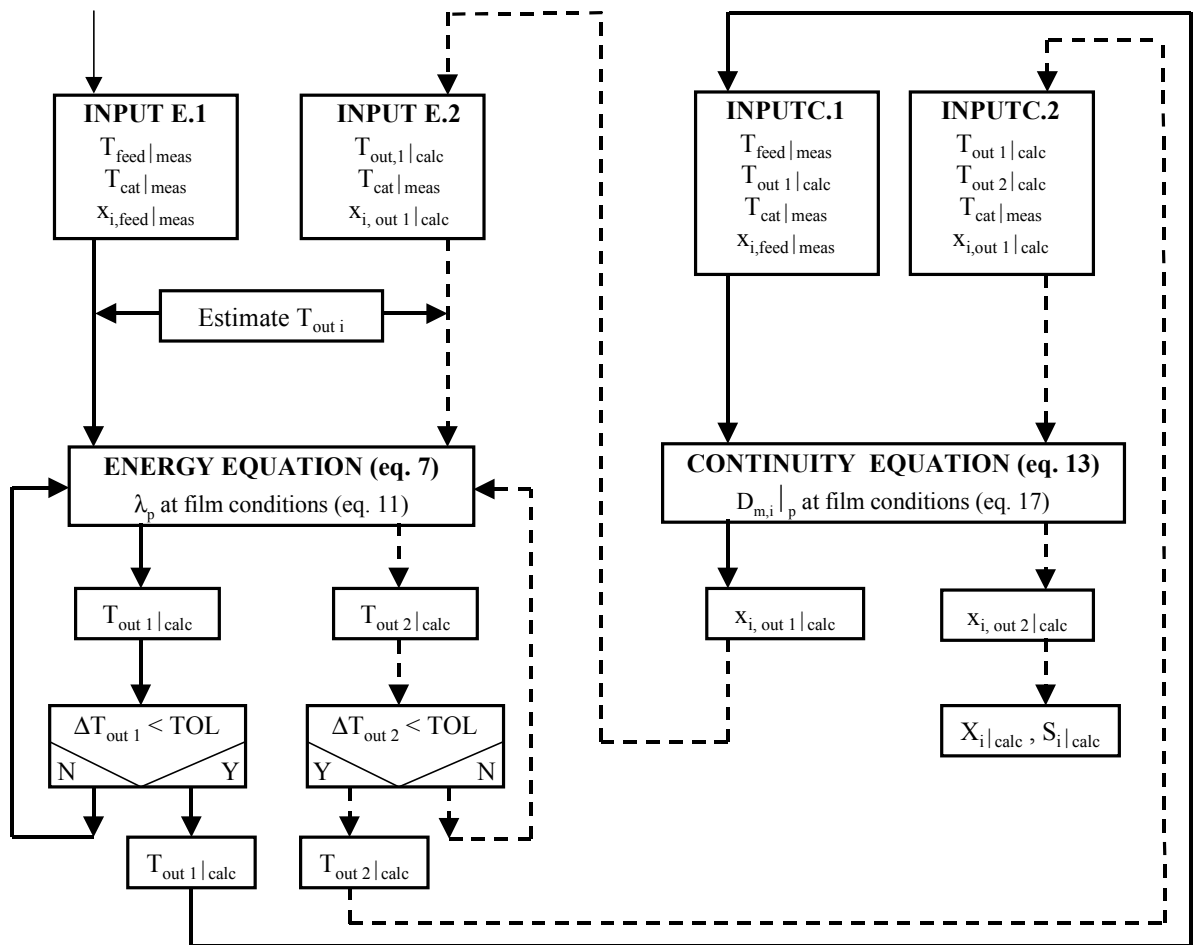


Figure 7. Flow diagram of the solution procedure applied in case of the flat-plate reactor model. Solid arrows: procedure in case of the first row of flat plates. Dotted arrows: second row of flat plates. TOL = tolerance used to calculate the outlet gas-phase temperature.

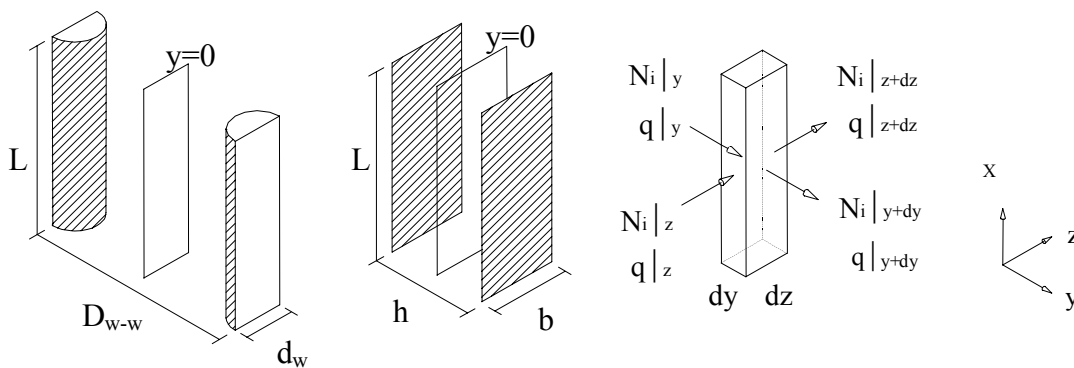


Figure 8. Characteristic dimensions of: (a) a single row of cylinders of the gauze catalyst, (b) a single row of flat plates in the flat-plate reactor model, and (c) the heat and mass fluxes considered in case of a single row of flat plates.

The gas-phase temperature at the outlet of the first row of flat plates ($T_{\text{out1|calc}}$) is calculated first, by solving the energy equation. Both convective heat transport in the axial direction (z-direction, Figure 8) of the flat plates and conductive heat transport in the radial direction (y-direction, Figure 8) are taken into account. The measured feed temperature ($T_{\text{feed|meas}}$), the measured catalyst temperature ($T_{\text{cat|meas}}$), and the inlet mole fractions ($x_{i,\text{feed|meas}}$), together with the initial estimate of the mean outlet temperature (T_{out1}), are used as input (INPUT E.1, Figure 7). The mean outlet temperature is solved via the method of successive substitution, as the heat conductivity λ_p is defined at film temperature, the arithmetic average of the gas-phase bulk and surface temperature. The energy equation, together with the corresponding initial and boundary conditions are shown in Section 4.2.

The continuity equation in case of the first row of plates is solved next, using $T_{\text{feed|meas}}$, $T_{\text{out1|calc}}$, $T_{\text{cat|meas}}$, and $x_{i,\text{feed|meas}}$ as input (INPUT C.1, Figure 7). Mass transport by means of axial convection and radial diffusion are taken into account. The inlet, outlet, and catalyst temperatures are required to calculate the diffusion coefficient at film temperature. The mean mole fractions at the outlet of the first row of flat plates ($x_{i,\text{out1|calc}}$) are obtained by integrating the resulting mole fraction profiles. The continuity equation, together with the corresponding initial and boundary conditions are presented in Section 4.3. The energy and continuity equations in case of the second row of plates are solved using an analogous procedure. In case of the energy equation, however, $T_{\text{out1|calc}}$ and $x_{i,\text{out1|calc}}$ are used as input to the second row of plates, together with $T_{\text{cat|meas}}$ (INPUT E.2, Figure 7). The value of the measured catalyst temperature is identical to the value used to solve the first row of flat plates. In case of the continuity equation, $T_{\text{out1|calc}}$ and $x_{i,\text{out1|calc}}$ together with $T_{\text{cat|meas}}$ and the calculated temperature at the outlet of the second row of plates, $T_{\text{out2|calc}}$, are used as input (INPUT C.2, Figure 7). The mean mole fractions at the outlet of the second row of plates are finally determined and result in the calculated values of conversions and selectivities.

The results of the 3D FLUENT simulations were used to validate the flat-plate reactor model (Section 4.4) by comparing the outlet temperatures and reactant conversions as calculated from the 3D FLUENT simulations to the temperatures and conversions obtained with the flat-plate reactor model. The input parameters used in the 3D FLUENT simulations and the corresponding ranges applied during validation are shown in Table 2. The large window of the intrinsic reaction rate constant covers the entire range from intrinsic to mass-transfer limited conditions.

Table 2 Parameters used in the 3D FLUENT simulations.

Inlet velocity (m s ⁻¹)	2.5 - 25
Total pressure (kPa)	100
Inlet temperature (K)	300 - 1100
Catalyst temperature (K)	1123
Intrinsic reaction rate constant (*)	0.1 - 1·10 ⁴
Reaction order (-)	0.5 - 2
Diameter cylinder (m)	2.0·10 ⁻⁴
Distance between cylinders (m)	8.2·10 ⁻⁴

* unit depends on reaction order

4.4.2 Energy equation

In case of gases flowing perpendicularly to a single cylinder, complex flow patterns can develop as a function of the Reynolds (Re) number (Schlichting, 1979). For instance, at $5 < \text{Re} < 40$, a fixed pair of vortices are formed behind the cylinder. The flow pattern has a profound effect on the amount of heat transferred between the cylinder and the surrounding gas. In order to account for the effect of these flow patterns on heat transfer, a mean heat-transfer coefficient is introduced. This heat-transfer coefficient can be calculated from a Nusselt equation for forced convection of gases and liquids to a cylinder in crossflow (Churchill and Bernstein, 1977):

$$\text{Nu} = \frac{\alpha d_w}{\lambda_f} = \text{Nu}_0 + \frac{\gamma_1 \cdot \text{Re}^{1/2} \cdot \text{Pr}^{1/3}}{\left[1 + (0.4/\text{Pr})^{2/3}\right]^{1/4}} \cdot \left[1 + \left(\frac{\text{Re}}{282000}\right)^{5/8}\right]^{4/5} \cdot \left[\frac{T_b}{T_f}\right]^{0.17} \quad (6)$$

in which Nu_0 corresponds to the extrapolated Nusselt number at $\text{Re} \rightarrow 0$, and γ_1 to the slope of the experimentally determined Nu versus $\left\{(\text{Re}^{1/2} \text{Pr}^{1/3}) / (1 + (0.4/\text{Pr})^{2/3})^{1/4}\right\}$ curve. Churchill and Bernstein (1977) suggest values of 0.3 for Nu_0 and 0.62 for γ_1 . The equation is valid for $\text{Re} \cdot \text{Pr} > 0.2$; the Nu, Re, and Pr numbers are all calculated at film temperature.

In order to solve the mean outlet temperature at the outlet of both the first and second row of plates, the energy equation is solved, taking into account both axial heat convection and radial heat conduction. The energy equation, using the dimensionless coordinates q (z/b) and p (y/h), can be written as:

$$\frac{2 \cdot F_{w,0} \cdot c_{p,b} \cdot h}{A_{cat}} \cdot \frac{\partial T}{\partial q} = \lambda_p \cdot \frac{\partial^2 T}{\partial p^2} \quad (7)$$

in which λ_p corresponds to the effective gas-phase heat conductivity between the flat plates. The following initial and boundary conditions apply here:

$$q = 0 \wedge 0 < p < 1/2: \quad T = T_{in} \quad (8)$$

$$q > 0 \wedge p = 0: \quad \frac{\partial T}{\partial p} = 0 \quad (9)$$

$$q > 0 \wedge p = 1/2: \quad T = T_{cat} \quad (10)$$

The temperature profile is symmetric around radial position $p=0$ (the centreline between two plates) and the plate surface is considered to be isothermal at temperature T_{cat} . The effect of the flow pattern on the heat transfer from the cylinder to the gas is taken into account in the flat-plate reactor model by calculating λ_p from the Nu-number according to:

$$\lambda_p = \frac{\pi^2}{8} \cdot \lambda_f \cdot \left(\frac{h}{D_{w-w}} \right) \cdot \frac{Nu^2}{Re \cdot Pr} \cdot \frac{c_{p,f}}{c_{p,b}} \quad (11)$$

The derivation of equation (11) is presented in Appendix A.

The partial differential equation (7) together with the corresponding initial and boundary conditions (8,9,10) is solved numerically by using the standard NAG-library routine D03PGF (NAG Fortran Library, 1991). The temperature profile at the reactor outlet can only be calculated when the mean outlet temperature is known, as the effective heat conductivity (11) is defined at film temperature. Therefore, the mean outlet temperature is solved numerically via the method of successive substitution (Figure 7).

The best description of the mean outlet temperature is obtained when the coefficients Nu_0 and γ_1 in equation (6) are taken as: $Nu_0 = 0.39$ and $\gamma_1 = 0.66$. These values were obtained by comparing the calculated mean outlet temperatures in case of a single row of flat plates to the temperatures obtained from 2D FLUENT simulations of heat transfer in case of a single row of infinite cylinders.

4.4.3 Continuity equation

From Figures 5-a and 5-b it is clear, that the gas-phase temperature and reactant mole fraction profiles obtained from the 3D FLUENT simulations are very similar. This indicates

that the Chilton-Colburn analogy between heat and mass transfer applies. This analogy implies that at constant physical properties and moderate mass-transfer rates, a Sherwood correlation for mass transfer can be obtained from a Nusselt correlation for heat transfer by replacing the dimensionless Pr number by the Sc number in equation (6):

$$\text{Sh} = \frac{k_x d_w}{C_t D_{m,i}} = \text{Sh}_0 + \frac{\gamma_2 \cdot \text{Re}^{1/2} \cdot \text{Sc}^{1/3}}{\left[1 + (0.4/\text{Sc})^{2/3}\right]^{1/4}} \cdot \left[1 + \left(\frac{\text{Re}}{282000}\right)^{5/8}\right]^{4/5} \cdot \left[\frac{T_b}{T_f}\right]^{0.17} \quad (12)$$

in which Sh, Re, and Sc are calculated at film temperature. Because of the analogy between heat and mass transfer, the coefficients Sh_0 and γ_2 in equation (12) are taken as: $\text{Sh}_0 = \text{Nu}_0 = 0.39$ and $\gamma_1 = \gamma_2 = 0.66$.

The continuity equation, used to calculate the mean mole fractions at the outlet of both the first and second row of plates, can be written as:

$$\frac{2 \cdot F_{v,b} \cdot h}{A_{\text{cat}}} \cdot \frac{\partial x_i}{\partial q} = D_{m,i} \Big|_p \cdot \frac{\partial^2 x_i}{\partial p^2} \quad (13)$$

in which $D_{m,i} \Big|_p$ corresponds to the effective molecular diffusion coefficient between the flat plates. The following initial and boundary conditions apply here:

$$q = 0 \wedge 0 < p < 1/2: \quad x_i = x_{i,0} \quad (14)$$

$$q > 0 \wedge p = 0: \quad \frac{\partial x_i}{\partial p} = 0 \quad (15)$$

$$q > 0 \wedge p = 1/2: \quad -D_{m,i} \Big|_p \cdot \frac{C_{t,b}}{h} \cdot \frac{\partial x_i}{\partial p} = r_{i,A} \quad (16)$$

The mole fraction profile is symmetric around radial position $p=0$. At the plate surface, the flux to the surface is equal to the areal reaction rate.

The effect of the flow pattern on mass transfer between the gas and the cylinders is taken into account by calculating $D_{m,i} \Big|_p$ from the Sherwood correlation (12) according to:

$$D_{m,i} \Big|_p = \frac{\pi^2}{8} \cdot D_{m,i} \Big|_f \cdot \left(\frac{h}{D_{w-w}}\right) \cdot \left(\frac{C_{t,f}}{C_{t,b}}\right) \cdot \frac{\text{Sh}^2}{\text{Re} \cdot \text{Sc}} \quad (17)$$

The derivation of equation (17) is presented in Appendix B.

In order to calculate the mole fraction profiles, the mean outlet temperature is calculated first by solving the heat equation (7). The resulting outlet temperature is used to

determine the effective diffusion coefficient at film conditions (17). Next, the continuity equation (13) is solved together with the corresponding initial and boundary conditions (14,15,16) with the NAG-library routine D03PGF (NAG Fortran Library, 1991).

4.4.4 Validation of the flat-plate reactor model

The 3D FLUENT simulations indicated, that a strong hydrodynamic interaction exists between the two rows of cylinders of the gauze catalyst, which resulted in gas-phase temperature and reactant mole fraction profiles along the axis of the cylinders near the intersection points. The influence of these temperature and mole fraction profiles on the heat and mass-transfer rates is illustrated in Table 3. In this table, the total heat and mass-transfer rates on the cylinders of the first and the second row in case of the 3D FLUENT simulations are compared to the total heat and mass-transfer rates in case of 2D FLUENT simulations, using a single row of infinite cylinders.

Table 3. Total heat and mass transfer rates per cylinder obtained from 2D and 3D FLUENT simulations. Conditions: $T_{in} = 600$ K, $T_{cat} = 1123$ K, $u_{in} = 5$ m s⁻¹, $k_{intr} = 1 \cdot 10^4$ m s⁻¹, $n = 1$, $d_w = 2.0 \cdot 10^{-4}$ m, $D_{w-w} = 8.2 \cdot 10^{-4}$ m.

Transfer rate to/from	Heat transfer rate (MW m ⁻²)	Mass transfer rate (kg m ⁻² s ⁻¹)
Row of infinite cylinders (2D)	0.923	0.433
1 st row of cylinders of 3D gauze	0.874	0.401
2nd row of cylinders of 3D gauze	0.663	0.299
3D gauze	0.768	0.350

The transfer rates per cylinder in case of the first row of cylinders of the 3D gauze are slightly smaller than the rates for a single row of infinite cylinders. In case of the second row of cylinders of the 3D gauze, however, the heat and mass-transfer rates are much smaller compared to the 2D simulations. This is caused by the large influence of the first row of cylinders on the temperature and the reactant mole fraction at the position of the second row of cylinders. As a result, the overall effectiveness of heat and mass transfer is smaller in case of the 3D gauze.

The observed decrease in heat and mass-transfer rates as a result of the interaction between the rows of cylinders is taken into account in the flat-plate reactor model by introducing effectiveness factors for both the Nusselt and Sherwood number in case of the first and the second row of flat plates:

$$\text{Nu}_{\text{gauze}} = \eta_h \cdot \text{Nu}_{\text{cylinder}} \quad (18)$$

$$\text{Sh}_{\text{gauze}} = \eta_m \cdot \text{Sh}_{\text{cylinder}} \quad (19)$$

Similar effectiveness factors for Nusselt are used in the design of shell and tube heat exchangers (Coulson and Richardson, 1990), to account for the influence of the orientation (inline or staggered) of the parallel heat exchanging tubes on the overall heat-transfer rate.

Because of the analogy between heat and mass transfer, the values of η_h and η_m are assumed to be identical. The single effectiveness factor, $\eta_h = \eta_m$, was obtained by minimisation of the residual sum of squares (Draper and Smith, 1966) applied to the calculated reactant conversions in case of the flat-plate reactor model and the reactant conversions obtained from the 3D FLUENT simulations. A value of 0.71 was found to describe the 3D FLUENT results best. It should be noted, that the obtained value of the effectiveness factor is only valid for this specific case. Application of different wire diameters (d_w) and distances between the centres of the wires (D_{w-w}) results in a different value for the effectiveness factor.

Figure 9 shows the parity plots for both the outlet gas-phase temperature and the reactant conversion. It is clear, that the flat-plate reactor model accurately describes simultaneous heat and mass transfer in case of a surface reaction. For that reason, it will be a valuable tool to obtain intrinsic kinetic data from experimental results.

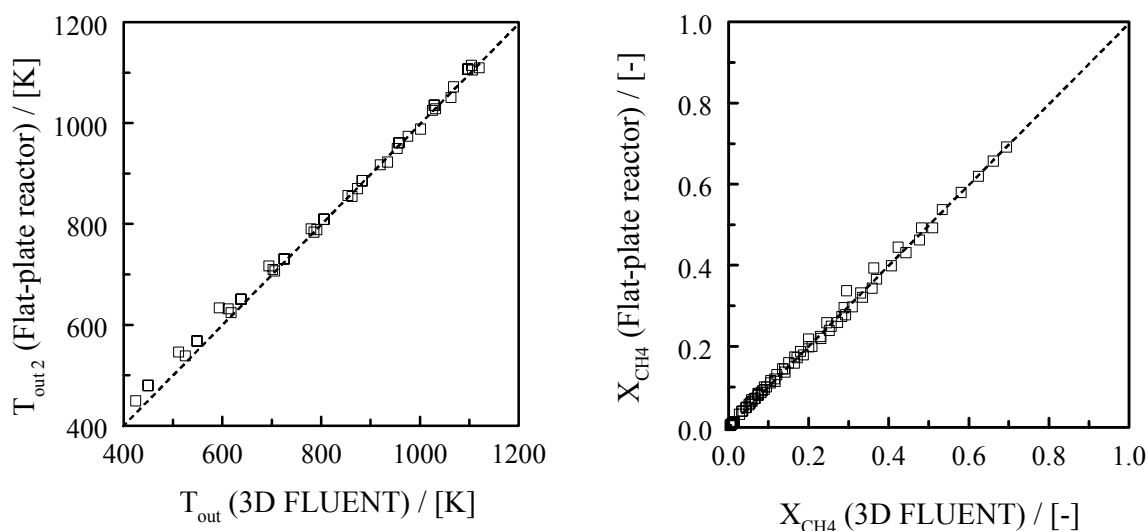
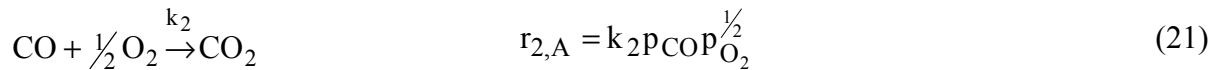
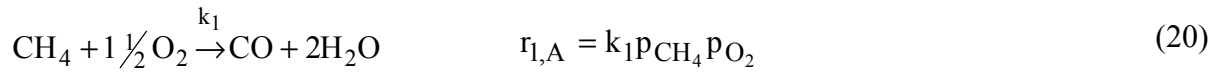


Figure 9. Comparison of (a) the outlet gas-phase temperatures, and (b) the methane conversions calculated in case of the flat-plate reactor model, and the 3D FLUENT simulations using the gauze geometry. Conditions: see Table 2.

4.5 Application of the flat-plate reactor model using a series-parallel CPO reaction mechanism

At present, only few reaction mechanisms for the catalytic partial oxidation of methane to synthesis gas on Pt metal catalysts are available in the literature. Hickman and Schmidt (1993) simulated the direct oxidation of methane to CO and H₂ in case of Pt coated monoliths using a 19-step elementary reaction mechanism. The reaction rate parameters were obtained from literature and from regression of experimental data. Deutschmann et al. (1994) and Bui et al. (1997) used an analogous 19-step reaction mechanism to model the catalytic ignition of methane/air and methane/oxygen mixtures on a Pt metal foil. Mallens et al. (1995) proposed a reaction network for the partial oxidation of methane over Pt sponges without values for the kinetic parameters, based upon experimental results obtained with the Temporal Analysis of Products set-up.

Hickman and Schmidt (1992b) also considered a series-parallel CPO reaction mechanism to determine the influence of boundary-layer mass transfer on the selectivity to synthesis gas. An analogous mechanism was used in this work to calculate conversions and selectivities in case of the flat-plate reactor model. The reactions considered, and the corresponding rate equations can be written as:



Reactions (20) and (21) are in series with respect to the partial oxidation product CO, and are parallel with respect to O₂. The oxidation of CH₄ to CO and H₂O is considered to be first order in the partial pressures of both CH₄ and O₂. The reaction of CO with O₂ towards CO₂ is first order in the partial pressure of CO and ½ order in the partial pressure of O₂.

The methane conversion, oxygen conversion, and the selectivity to CO were calculated in case of this series-parallel mechanism according to the procedure outlined in Figure 7. The reaction mechanism resulted in a set of five continuity equations (13), which were solved simultaneously, together with the corresponding initial and boundary conditions (14-16). The net fluxes of the reactants and products at the surface of the flat plates (equation 16) are calculated from the areal reaction rates ($r_{1,A}$ and $r_{2,A}$).

The physical properties (λ , μ , C_p) of the CH₄/O₂/He feed mixture, and of the gas mixture at the outlet of the first row of plates, were used to solve the energy and continuity equations in case of the first and second row of plates. The diffusion of the reactants and products was described using Fick's law, as in all experiments He was present in large excess.

The series-parallel reaction mechanism was implemented in the flat-plate reactor model and was used to simulate the conversions and selectivities at different space-times, $W/F_{CH_4,0}$. The lines in Figure 4 show the calculated conversions and selectivities as a function of space-time. The corresponding values of the intrinsic kinetic rate parameters k_1 and k_2 amount to $1.5 \cdot 10^{-8} \text{ mol Pa}^{-2} \text{ m}^{-2} \text{ s}^{-1}$ and $6.0 \cdot 10^{-6} \text{ mol Pa}^{-1.5} \text{ m}^{-2} \text{ s}^{-1}$, respectively. It is clear, that the reaction mechanism results in an adequate description of the measured methane and oxygen conversions. In addition, the model correctly predicts a decrease in the CO selectivity with increasing space-time.

Typical reactant and product mole fraction profiles at the outlet of the first row of plates are shown in Figure 10 as a function of the dimensionless radial coordinate p . Close to the surface of the flat plates, at $p = 1/2$, a rapid decrease in the oxygen mole fraction can be observed, which indicates that the oxygen consumption rate is strongly influenced by mass transfer to the surface. The methane mole fraction profile is completely determined by the oxygen consumption rate, since methane is always present in excess. In addition, significant mole fraction profiles exist for the reaction products.

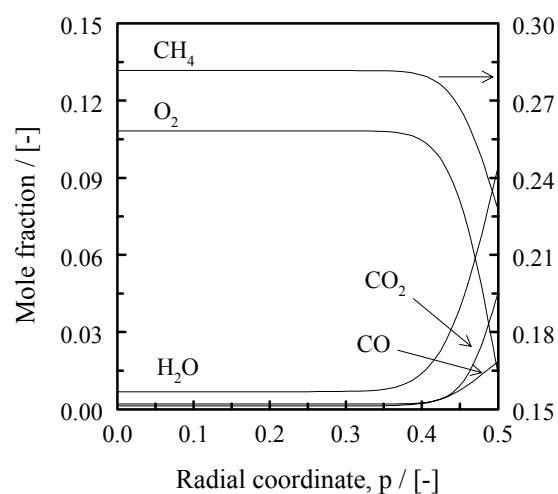


Figure 10. Radial mole fraction profiles at the outlet of the first row of flat plates in case of the series-parallel CPO reaction mechanism. Conditions: $P_{tot} = 160 \text{ kPa}$, $T_{cat} = 1123 \text{ K}$, $W/F_{CH_4,0} = 20 \text{ g s mol}^{-1}$, $CH_4/O_2/He|_0 = 28.6/11.4/60$.

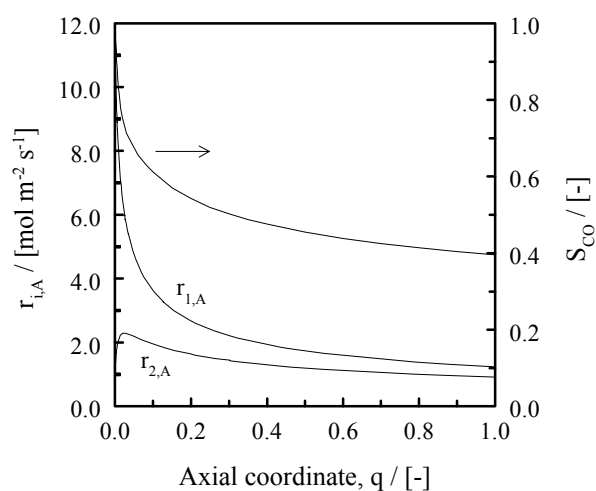


Figure 11. Calculated areal reaction rates at the plate surface and selectivity to CO in case of the first row of flat plates as a function of the dimensionless axial coordinate. Conditions: $P_{tot} = 160 \text{ kPa}$, $T_{cat} = 1123 \text{ K}$, $W/F_{CH_4,0} = 11.1 \text{ g s mol}^{-1}$, $CH_4/O_2/He|_0 = 28.6/11.4/60$.

Figure 11 shows the calculated reaction rates at the plate surface, together with the selectivity to CO as a function of the dimensionless axial coordinate q in case of the first row of plates at $W/F_{CH_4,0} = 11.1 \text{ g s mol}^{-1}$. The initial methane oxidation rate ($r_{1,A}$) is very high,

and decreases rapidly at increasing values of the axial coordinate. The CO oxidation rate ($r_{2,A}$) shows a maximum value near the inlet, and approaches the value of $r_{1,A}$ near the outlet. The selectivity to CO approaches 100 % at the inlet, as the CO oxidation rate is approximately equal to zero. The difference between the reaction rates ($r_{1,A} - r_{2,A}$), corresponding to the net CO production rate, decreases rapidly at increasing values of the axial coordinate q . As a result, the CO selectivity decreases.

At increasing space-times, the initial decrease in the methane oxidation rate becomes much more pronounced. In addition, the maximum in the CO oxidation rate is progressively shifted to the inlet of the row of plates. As a result, the difference between the reaction rates $r_{1,A}$ and $r_{2,A}$ is much smaller at increasing space-time, which results in a decrease of the CO selectivity.

Introduction of a positive activation energy in case of the oxidation of CO, results in a decrease of the CO selectivity with increasing catalyst temperatures. The experimental results indicated, however, that the CO selectivity increases with increasing catalyst temperature. In order to describe the influence of the catalyst temperature on the CO selectivity accurately, more detailed elementary-step reaction mechanisms have to be considered. As indicated above, the CPU time required to solve the flat-plate reactor model in case of a simple surface reaction approximately amounts to 1 s. This indicates that calculations involving more detailed elementary-step reaction mechanisms can probably be performed within acceptable computational times as well.

4.6 Conclusions

During the catalytic partial oxidation of methane with oxygen to synthesis gas strong heat-transport limitations can occur as a result of non-selective, exothermic oxidation reactions. In order to study the intrinsic kinetics of the CPO reaction in the presence of heat-transport limitations an experimental reactor containing a single Pt gauze catalyst was used. Heat-transport limitations are taken into account explicitly in this reactor, by measuring the catalyst temperature directly by means of a surface thermocouple.

At all conditions investigated, CO, CO₂ and H₂O were the main products. Hydrogen was found only at temperatures above 1273 K. At these conditions, however, the catalyst did not exhibit a stable performance with time on stream. Both the methane and oxygen conversion rates were completely determined by mass-transport phenomena. The CO formation rate, however, was influenced significantly by the kinetics of the surface reactions. In addition, the experimental results showed that at increasing space-time, the selectivity to CO decreases, which indicated that CO is a primary product of the oxidation reactions.

In order to determine the intrinsic kinetics of the CO formation, a reactor model was developed, consisting of two rows of flat plates in series. This flat-plate reactor model was validated by comparing calculated conversions and gas-phase temperatures to the results obtained from FLUENT simulations using the 3D geometry of the gauze catalyst. The reactor model resulted in a considerable reduction of the computational time required during the 3D FLUENT simulations.

A series-parallel CPO reaction mechanism was used to calculate conversions and selectivities in case of the flat-plate reactor model at different space-times, $W/F_{\text{CH}_4,0}$. This reaction mechanism, together with the corresponding intrinsic kinetic parameters resulted in an accurate description of the experimental results. More detailed elementary-step kinetic models can be developed, using the experimental results obtained with the laboratory reactor together with the flat-plate reactor model.

Notation

A_{cat}	catalyst surface area (m^2)
b	length of flat plates (m)
C	concentration (mol m^{-3})
c_p	specific heat ($\text{J kg}^{-1} \text{K}^{-1}$)
d	diameter (m)
$D_{\text{w-w}}$	distance between the centres of two wires (m)
$D_{\text{m,i}}$	molecular diffusion coefficient in mixture ($\text{m}^2 \text{s}^{-1}$)
$F_{\text{CH}_4,0}$	inlet methane molar flow rate (mol s^{-1})
$F_{\text{v,b}}$	volumetric flow rate at bulk conditions ($\text{m}^3 \text{s}^{-1}$)
$F_{\text{w},0}$	inlet mass flow rate (kg s^{-1})
$\Delta_{\text{r}}H^0_{1300}$	reaction enthalpy at 1300 K and 1 bar pressure ($\text{kJ mol}_{\text{CH}_4}^{-1}$)
h	distance between two flat plates (m)
k_{intr}	intrinsic reaction rate constant (reaction dependent)
k_x	mass transfer coefficient ($\text{mol m}^{-2} \text{s}^{-1}$)
M_{CH_4}	methane molar weight (kg mol^{-1})
n	reaction order of model surface reaction (-)
N	mass flux ($\text{kg m}^{-2} \text{s}^{-1}$)
Nu	Nusselt number (-)
Nu_0	extrapolated Nu number at $Re \rightarrow 0$ (-)
P_{tot}	total pressure (kPa)
p	dimensionless radial coordinate (-), partial pressure (Pa)

Pr	Prandtl number (-)
q	dimensionless axial coordinate (-), heat flux ($\text{J m}^{-2} \text{s}^{-1}$)
r_{w,CH_4}	specific methane consumption rate ($\text{kg m}^{-2} \text{s}^{-1}$)
$r_{i,A}$	areal consumption rate ($\text{mol m}^{-2} \text{s}^{-1}$)
Re	Reynolds number (-)
Sc	Schmidt number (-)
Sh	Sherwood number (-)
Sh_0	extrapolated Sh number at $Re \rightarrow 0$ (-)
S_i	selectivity of component i (-)
T	temperature (K)
u_{in}	inlet velocity (m s^{-1})
W	catalyst weight (kg)
X_i	conversion of reactant i (-)
x	mole fraction (-)
y	radial coordinate (m)
z	axial coordinate (m)

Greek symbols

α	heat transfer coefficient ($\text{W m}^{-2} \text{K}^{-1}$)
γ_1, γ_2	coefficients in Nu and Sh correlations (-)
$\phi_{m,0}$	initial molar flux ($\text{mol m}^{-2} \text{s}^{-1}$)
$\phi_{w,0}$	initial mass flux ($\text{kg m}^{-2} \text{s}^{-1}$)
λ	gas-phase heat conductivity ($\text{W m}^{-1} \text{K}^{-1}$)
η_h, η_m	effectiveness factors for Nu and Sh numbers (-)
μ	viscosity ($\text{kg m}^{-1} \text{s}^{-1}$)

Subscripts

0	Initial
b	at bulk conditions
calc	Calculated
cat	Catalyst
e	External
f	at film conditions
i	internal, component I

in	Inlet
meas	Measured
out	Outlet
p	between the flat plates
t	Total
y	in y-direction
w	Wire
z	in z-direction

References

- Bergene, E., Trondstad, O., & Holmen, A. (1996). Surface areas of Pt-Rh catalyst gauzes used for ammonia oxidation. *J. Catal.*, *160*, 141-147.
- Berger, R.J., & Marin, G.B. (1999). Investigation of gas-phase reactions and ignition delay occurring at conditions typical for partial oxidation of methane to synthesis gas. *Ind. Eng. Chem. Res.*, *38*, 2582-2592.
- Bui, P.-A., Vlachos, D.G., & Westmoreland, P.R. (1997). Catalytic ignition of methane/oxygen mixtures over platinum surfaces: comparison of detailed simulations and experiments. *Surf. Sci.*, *385*, L1029-L1034.
- Churchill, S.W., & Bernstein, M. (1977). A correlating equation for forced convection from gases and liquids to a circular cylinder in crossflow. *J. Heat Trans.*, *99*, 300-306.
- Coulson, J.M., & Richardson, J.F. (1990). *Chemical Engineering*, p. 351, Pergamon Press, Oxford.
- Deutschman, O., Behrendt, F., & Warnatz, J. (1994). Modelling and simulation of heterogeneous oxidation of methane on a Pt foil. *Catal. Today*, *21*, 461-470.
- Draper, N.R., & Smith, H. (1966). *Applied Regression Analysis*, John Wiley & Sons, New York.
- Fathi, M., Heitnes Hofstad, K., Sperle, T., Rokstad O.A., & Holmen, A. (1998). Partial oxidation of methane to synthesis gas at very short contact times. *Catal. Today*, *42*, 205-209.
- FLUENT version 4.3, User Manual (1995). Flow Simulation International Limited, Sheffield.
- Heitnes, K., Lindberg, S., Rokstad, O.A., & Holmen, A. (1995). Catalytic partial oxidation of methane to synthesis gas. *Catal. Today*, *24*, 211-216.
- Heitnes Hofstad, K., Rokstad, O.A., & Holmen, A. (1996). Partial oxidation of methane over platinum metal gauze. *Catal. Lett.*, *36*, 25-30.
- Hickman, D.A., & Schmidt L.D. (1992a). Synthesis gas formation by direct oxidation of methane over Pt monoliths. *J. Catal.*, *13*, 267-282.
- Hickman, D.A., & Schmidt, L.D. (1992b). The role of boundary layer mass transfer in partial oxidation selectivity. *J. Catal.*, *13*, 300-308.
- Hickman, D.A., & Schmidt, L.D. (1993). Steps in CH₄ oxidation on Pt and Rh surfaces: High-temperature reactor simulations. *AIChE J.*, *39*, 1164-1177.
- Hickman, D.A., Hauptfear, E.A., & Schmidt L.D. (1993). Synthesis gas formation by direct oxidation of methane over Rh monoliths. *Catal. Lett.*, *17*, 223-237.
- Mallens, E.P.J., Hoebink, J.H.B.J., & Marin, G.B. (1995). An investigation on the reaction mechanism for the partial oxidation of methane to synthesis gas over platinum. *Catal. Lett.*, *33*, 291-304.

- Mallens, E.P.J., Hoebink, J.H.B.J., & Marin, G.B. (1997). The reaction mechanism of the partial oxidation of methane to synthesis gas: A transient kinetic study over rhodium and a comparison with platinum. *J. Catal.*, *167*, 43-56.
- NAG, Numerical Algorithm Group (1991). Fortran Library Manual, Mark 15, Wilkinson House, Oxford.
- Prettre, M., Eichner, C., & Perrin, M. (1946). The catalytic oxidation of methane to carbon monoxide and hydrogen. *Trans. Farad. Soc.*, *43*, 335-340.
- Rostrup-Nielsen, J.R. (1993). Production of synthesis gas. *Catal. Today*, *18*, 305-324.
- Schlichting, H. (1979). Boundary layer theory, p. 29, McGraw-Hill, New York.
- Thiemann, M., Scheibler, E., & Wiegand, K.W. (1985). Nitric acid, nitrous acid, and nitrogen oxides. In Ullmann's Encyclopedia of Industrial Chemistry, vol. 17, pp. 297-298, VCH, Weinheim.
- Twigg, M.V. (1996). Catalyst Handbook, p. 408, Manson Publishing, London.
- Vermeiren, W.J.M., Blomsma, E., & Jabobs, P.J. (1992). Catalytic and thermodynamic approach of the oxyreforming of methane. *Catal. Today*, *13*, 427-436.
- Vernon, P.D.F., Green, M.L.H., Cheetham, A.K., & Ashcroft, A.T. (1990). Partial oxidation of methane to synthesis gas. *Catal. Lett.*, *6*, 181-186.

Appendix A: Derivation of Eq. (11) for calculation of λ_p

In order to describe the dimensions used in the flat-plate reactor model in terms of the characteristic dimensions of the gauze catalyst, d_w and D_{w-w} , it is assumed that the volumetric surface area and residence time in case of a single row of cylinders (Figure 8-A) and in case of a single row of flat plates (Figure 8-B) are identical. At constant volumetric flow rate, this results in:

$$b = \frac{\pi \cdot d_w}{2}; \quad h = \frac{2}{\pi} \cdot \left[D_{w-w} - \frac{\pi}{4} \cdot d_w \right] \quad (\text{A.1})$$

The effect of the flow pattern on the heat transfer from a single cylinder to the gas is taken into account in the flat-plate reactor model by calculating the effective gas-phase heat conductivity, λ_p , from the Nu-number according to equation (11). In order to derive this equation, the energy equation for a single row of flat plates (equation 7) was solved analytically, at conditions where the temperature profile in the gas phase near the plate surface is not influenced by the presence of another flat plate. The dimensionless outlet gas-phase temperature can be written as:

$$\frac{T_{\text{cat}} - T_{\text{out}}}{T_{\text{cat}} - T_{\text{in}}} = 1 - \frac{4}{\sqrt{\pi}} \cdot \frac{\sqrt{\lambda_p \cdot b}}{\sqrt{\varphi_{w,0} \cdot c_{p,b} \cdot h^2}} = 1 - \frac{\sqrt{8 \cdot d_w \cdot \lambda_p}}{\sqrt{\varphi_{w,0} \cdot c_{p,b} \cdot D_{w-w} \cdot h}} \quad (\text{A.2})$$

In addition, the energy equation in case of heat transfer between a gas and a single row of cylinders (Figure 8-A) is used to calculate the outlet gas-phase temperature. Heat transfer between the cylinder surface and the surrounding gas is taken into account via the film model:

$$\varphi_{w,0} \cdot D_{w-w} \cdot L \cdot c_{p,b} \cdot dT = \alpha \cdot (T_{\text{cat}} - T) \cdot d(S(z)) \quad (\text{A.3})$$

In equation (A.3), α is the heat-transfer coefficient for forced convection in case of a single cylinder and $d(S(z))$ the cylinder surface area between z and $z+dz$. Integrating T from T_{in} to T_{out} and $d(S(z))$ from 0 to A_{cat} yields:

$$\frac{T_{\text{cat}} - T_{\text{out}}}{T_{\text{cat}} - T_{\text{in}}} = \exp \left[- \frac{\alpha \cdot \pi \cdot d_w}{\varphi_{w,0} \cdot c_{p,b} \cdot D_{w-w}} \right] \quad (\text{A.4})$$

When the term between brackets is small, corresponding to the situation where the temperature profile in the gas phase near the surface of the cylinder is not influenced by the other cylinders, equation (A.4) can be written as:

$$\frac{T_{\text{cat}} - T_{\text{out}}}{T_{\text{cat}} - T_{\text{in}}} \approx 1 - \frac{\alpha \cdot \pi \cdot d_w}{\varphi_{w,0} \cdot c_{p,b} \cdot D_{w-w}} \quad (\text{A.5})$$

Substitution of equation (A.5) into (A.2) results in an equation for λ_p :

$$\lambda_p = \frac{\pi^2}{8} \cdot \frac{\alpha^2 \cdot d_w \cdot h}{\varphi_{w,0} \cdot c_{p,b} \cdot D_{w-w}} \quad (\text{A.6})$$

Substitution of the dimensionless Re, Pr, and Nu-numbers:

$$\text{Re} = \frac{\varphi_{w,0} \cdot d_w}{\mu_f} ; \text{Pr} = \frac{c_{p,f} \cdot \mu_f}{\lambda_f} ; \text{Nu} = \frac{\alpha \cdot d_w}{\lambda_f} \quad (\text{A.7})$$

finally results in:

$$\lambda_p = \frac{\pi^2}{8} \cdot \lambda_f \cdot \left(\frac{h}{D_{w-w}} \right) \cdot \frac{\text{Nu}^2}{\text{Re Pr}} \cdot \frac{c_{p,f}}{c_{p,b}} \quad (11)$$

Appendix B: Derivation of Eq. (17) for calculation of $D_{m,i}|_p$

The effective diffusion coefficients of the gases between the flat plates, $D_{m,i}|_p$, are calculated from the Sh-number according to equation (17). In order to derive this equation, the continuity equation (13) for a single row of plates was solved analytically, at conditions where the mole fraction profile near the plate surface is not influenced by the presence of the other plate. The conversion at the outlet can be written as:

$$X_i = \frac{4}{\sqrt{\pi}} \cdot \sqrt{\frac{D_{m,i}|_p \cdot C_{t,b} \cdot b}{\varphi_{m,0} \cdot h^2}} = \sqrt{\frac{8 \cdot d_w \cdot D_{m,i}|_p \cdot C_{t,b}}{\varphi_{m,0} \cdot D_{w-w} \cdot h}} \quad (\text{A.8})$$

In addition, the continuity equation in case of mass transfer and a surface reaction in series is used to calculate the conversion for a single row of cylinders. Assuming a constant molar flow rate and mass-transfer limited conditions ($x_{i,\text{cat}} = 0$), the following continuity equation applies:

$$\varphi_{m,0} \cdot D_{w-w} \cdot L \cdot dx_i = k_x \cdot x_i \cdot d(S(z)) \quad (\text{A.9})$$

in which k_x is the mass transfer coefficient for forced convection to a single cylinder in cross-flow and $d(S(z))$ is the cylinder surface area between z and $z+dz$. Integrating x_i from $x_{i,\text{in}}$ to $x_{i,\text{out}}$ and $d(S(z))$ from 0 to A_{cat} yields:

$$X_i = 1 - \frac{x_{i,\text{out}}}{x_{i,\text{in}}} = 1 - \exp\left[-\frac{k_x \cdot \pi \cdot d_w}{\varphi_{m,0} \cdot D_{w-w}}\right] \quad (\text{A.10})$$

When the term between brackets is small, corresponding to a situation where the mole fractions profiles near the cylinder surface are not influenced by the other cylinder, equation (A.11) can be written as:

$$X_i \approx \frac{k_x \cdot \pi \cdot d_w}{\varphi_{m,0} \cdot D_{w-w}} \quad (\text{A.11})$$

Substitution of equation (A.12) into equation (A.9) results in:

$$D_{m,i}|_p = \frac{\pi^2}{8} \cdot \frac{k_x^2 \cdot d_w \cdot h}{\varphi_{m,0} \cdot C_{t,b} \cdot D_{w-w}} \quad (\text{A.12})$$

Substitution of the dimensionless Re, Sc, and Sh-numbers:

$$\text{Re} = \frac{\varphi_{m,0} \cdot \overline{M}_w \cdot d_w}{\mu_f} ; \text{Sc} = \frac{\mu_f}{\rho_f \cdot D_{m,i}|_p} ; \text{Sh} = \frac{k_x \cdot d_w}{C_{t,f} \cdot D_{m,i}|_f} \quad (\text{A.13})$$

finally gives:

$$D_{m,i}|_p = \frac{\pi^2}{8} \cdot D_{m,i}|_f \cdot \left(\frac{h}{D_{w-w}} \right) \cdot \left(\frac{C_{t,f}}{C_{t,b}} \right) \cdot \frac{\text{Sh}^2}{\text{Re} \cdot \text{Sc}} \quad (17)$$

5

Intrinsic kinetics for the partial oxidation of methane on a Pt gauze at low conversions

This chapter has been submitted for publication in AIChE J.

Abstract - The intrinsic kinetics of the catalytic partial oxidation of methane were studied at atmospheric pressure in the presence of transport limitations using a single Pt gauze. The catalyst temperature as well as the gas-phase temperature were measured directly. CO, CO₂, and H₂O were the main products at catalyst temperatures between 1030 and 1200 K, residence times of 0.02 to 0.2 milliseconds, CH₄/O₂ ratios between 1.8 and 5.0, and O₂ conversions between 9 and 46%. A kinetic model consisting of six reaction steps was developed. Methane adsorption had to be considered as oxygen-assisted in order to describe the experimental data, in particular the decrease of the selectivity for CO with increasing space-times, adequately. The corresponding intrinsic kinetic parameters were obtained from literature and from regression of the experimental CO selectivities. The calculated conversions and selectivities were obtained using the intrinsic kinetic model, together with a reactor model accounting for the transport limitations in a quantitative way without any adjustable parameter. Simulations indicate initial CO selectivities between 86 and 96% over the investigated range of conditions, and illustrate the relevance of both surface kinetics and mass transport in CO formation.

Keywords: Methane partial oxidation; Pt gauze; kinetic model; transport limitations

5.1 Introduction

The availability of large natural gas resources has been a key driving force in the past years to investigate and develop efficient natural gas conversion routes for the production of valuable chemicals. At present, commercial processes for natural gas conversion are mainly based on synthesis gas, i.e. a mixture of CO and H₂ (Christensen and Primdahl, 1994). Steam reforming still remains the major industrial route for synthesis gas production. However, catalytic partial oxidation (CPO) of methane by oxygen has attracted widespread attention as energy-efficient alternative to steam reforming. Supported transition-metal catalysts (Prettre et al., 1946, Vernon et al., 1990, Vermeiren et al., 1992), as well as noble metal-based catalysts (Hickman and Schmidt, 1992) have been reported to give high activity and selectivity towards synthesis gas.

On supported transition-metal catalysts, synthesis gas formation is considered to proceed indirectly, i.e. via total oxidation and reforming in series (Prettre et al., 1946, Vernon et al., 1990). At short residence times, using noble metal catalysts, direct CPO mechanisms were proposed, yielding CO and H₂ in a single step (Hickman and Schmidt, 1992, Mallens et al., 1995). Relatively few studies provide insights into the intrinsic kinetics that determine reactant conversions and synthesis gas selectivity. Hickman and Schmidt (1993) published detailed elementary step kinetic models, used to simulate the CPO reaction at high temperatures (1100-1500 K) and atmospheric pressure on Pt and Rh coated monoliths. The rate parameters of the individual surface reactions were obtained from literature and from fits to experiments. Analogous elementary step kinetic models were used to model short-contact-time CPO reactors (Deutschmann et al., 1998a) and the ignition behaviour of methane/oxygen mixtures (Bui et al., 1997, Deutschmann et al., 1994, Deutschmann et al., 1998b, Treviño, 1999).

At a methane to oxygen ratio of 2 and sufficiently high temperatures, the equilibrium composition corresponds to complete methane and oxygen conversions and 100 % selectivity to synthesis gas. This makes the distinction between the direct and indirect formation of synthesis gas difficult. In addition, the kinetics of the catalytic partial oxidation of methane cannot be determined in a straightforward way. First of all, the CPO reaction is extremely fast, which indicates that mass-transport limitations are likely to occur. Also, non-selective, exothermic oxidation reactions can lead to severe heat-transport limitations, resulting in high catalyst temperatures. Heitnes Hofstad et al. (1996) and Hickman and Schmidt (1992) used an optical pyrometer to determine the catalyst temperature at reaction conditions. However, in most kinetic studies heat-transfer resistances are not taken into account, since only gas-phase temperatures are measured.

Several experimental reactor configurations have been used to study the reaction kinetics of CPO at short residence times and high temperatures. These configurations have in common that the catalytic material is, in contrast to fixed beds, present in a structured way. A catalytic annular reactor was applied by Beretta et al. (1999). In order to study the intrinsic kinetics of the CPO reaction in the presence of heat-transport limitations, de Smet et al. (1999) developed an experimental reactor, containing a single Pt gauze catalyst. Heat-transport limitations were taken into account explicitly, since the catalyst temperature was measured directly, using a thermocouple spotwelded to the Pt gauze. It was demonstrated that experiments could not be performed at conditions where both conversions and selectivities are determined by chemical phenomena alone. Therefore, de Smet et al. (1999) developed a reactor model, taking into account the relevant transport phenomena, to obtain the intrinsic kinetic parameters of the CPO reaction.

The present paper reports on the development of a kinetic model for the catalytic partial oxidation of methane on a single Pt metal gauze, in the presence of irreducible transport phenomena. Experiments have been performed in which the influence of the catalyst temperature, the reactant space-time, and the inlet methane-to-oxygen ratio was investigated. The experimental data, together with the reactor model presented by de Smet et al. (1999), will be used to estimate the corresponding intrinsic kinetic parameters. Special attention will be paid to primary products, and the importance of mass-transport limitations. Hence, the conversions of methane and oxygen were maintained well below 100%.

5.2 Experimental equipment, procedures, and conditions

The partial oxidation of methane was studied in a continuous flow reactor set-up containing a single Pt gauze catalyst (150 meshes/cm², $W_{\text{cat}} = 5.72 \cdot 10^{-2}$ g, $d_w = 0.2$ mm). The reactant gases were preheated, and subsequently passed over the Pt gauze catalyst. Heat-transfer resistances were taken into account explicitly, since both the gas-phase temperature and the temperature of the catalyst were measured directly during the experiments. The catalyst temperature was determined by means of a surface thermocouple, constructed by spotwelding a thin Pt-10%Rh wire ($d_w = 0.1$ mm) to the centre of the gauze catalyst. An optical pyrometer was used to validate the catalyst temperature measurements and to verify the uniformity of the gauze temperature.

At typical experimental conditions, the measured catalyst temperatures were always significantly higher than the bulk gas-phase temperatures, indicating that strong heat-transfer limitations indeed occur. Consequently, the measured catalyst temperature was used to determine the intrinsic kinetic parameters of the CPO reaction. A total number of 40

atmospheric pressure experiments was performed at the range of conditions shown in Table 1. Note that the highest oxygen conversion amounts to 46%.

Table 1. Range of experimental conditions.

Catalyst temperature (K)	1023 - 1200
Total pressure (kPa)	130 - 165
Total flow rate (mmol s ⁻¹)	1.5 - 20
W/F _{CH_{4,0}} (g s mol ⁻¹)	10 - 130
CH ₄ /O ₂ ₀	1.8 - 5.0
He dilution (%)	35 - 80
CH ₄ conversion (-)	0.02 - 0.12
O ₂ conversion (-)	0.09 - 0.46

The influence of the reactant space-time, W/F_{CH_{4,0}}, and the inlet methane-to-oxygen ratio on conversions and selectivities was investigated at a fixed catalyst temperature of 1123 K. The space-time was varied by adjusting the inlet total molar flow rate. The catalyst temperature was kept at a constant value by decreasing the preheat temperature at increasing space-times and decreasing CH₄/O₂ |₀ ratios. The influence of the inlet methane-to-oxygen ratio was studied at constant total molar flow rate. The CH₄/O₂ ratio was varied by adjusting both the inlet molar flow rates of methane and helium, since the inlet molar flow rate of oxygen was fixed. Additional details about the experimental equipment and procedures can be found in de Smet et al. (1999).

At the high-temperature conditions applied in this study, gas-phase reactions may become important. Berger and Marin (1999) developed a kinetic model for gas-phase chain reactions at typical CPO conditions. Simulations using this kinetic model, together with a plug-flow reactor model resulted in very low methane and oxygen conversions. This indicates that gas-phase reactions can be neglected at the conditions applied. This is mainly caused by the high total molar flow rates and the low reactant partial pressures applied during the experiments.

5.3 Modelling procedures

5.3.1 Reactor model

In order to obtain the intrinsic kinetic parameters that determine the CO production rate, the reactor model developed by de Smet et al. (1999) was used. In this reactor model, which takes into account the transport limitations, the complex 3D geometry of the gauze catalyst was described by two rows of parallel flat plates in series (flat-plate reactor model, see Figure 1).

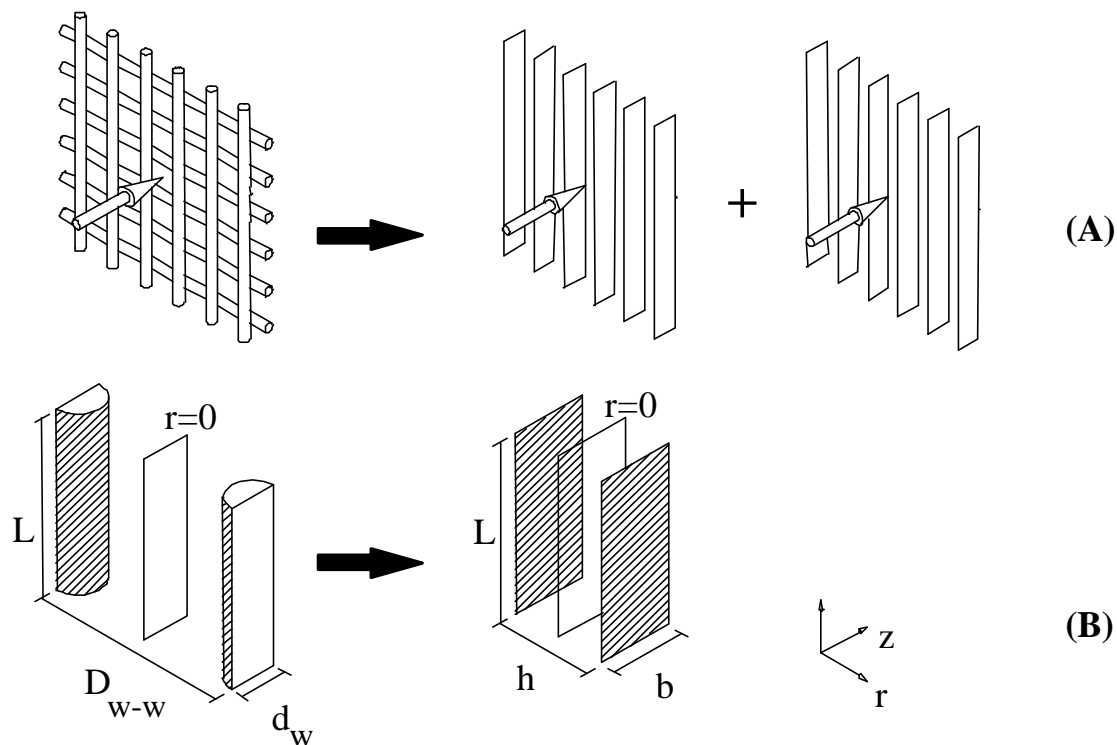


Figure 1. Schematic representation of the gauze catalyst and the flat-plate reactor model (A), together with the characteristic dimensions of a single row of cylinders of the gauze catalyst and a single row of flat plates in the flat-plate reactor model (B).

The volumetric surface area and the residence time in case of the actual gauze catalyst, and as applied in the flat-plate reactor model are required to be identical. Consequently, the characteristic dimensions of the flat-plate reactor model, i.e. the distance between the flat plates, h , and the length of the flat plates, b , can be calculated from the gauze wire diameter and the distance between the centres of two wires. The continuity equations account for mass transport by means of axial convection and radial diffusion:

$$\frac{2 \cdot F_{v,b} \cdot h}{A_{cat}} \cdot \frac{\int y_i}{\int z} = D_{m,i}|_{eff} \cdot \frac{\int^2 y_i}{\int r^2} \quad (1)$$

where z and r correspond to the dimensionless axial and radial coordinates, and $D_{m,i}|_{eff}$ is the effective diffusion coefficient. The following initial and boundary conditions are used:

$$z = 0 \wedge 0 < r < 1/2: \quad y_i = y_{i,0} \quad (2)$$

$$z > 0 \wedge r = 0: \quad \frac{\partial y_i}{\partial r} = 0 \quad (3)$$

$$z > 0 \wedge r = 1/2: \quad -D_{m,i}|_{eff} \cdot \frac{C_{t,b}}{h} \cdot \frac{\partial y_i}{\partial r} = r_{i,A} \quad (4)$$

The mole fraction profiles are symmetric around the radial position $r = 0$. At the catalyst surface, the molar flux is equal to the areal reaction rate, which is governed by the reaction kinetics.

Since the reactant gases are flowing perpendicularly to the wires of the gauze catalyst, complex flow patterns can develop as a function of the Reynolds number. These flow patterns have a strong influence on the heat and mass-transfer rates. In order to account for this influence in the reactor model, the effective diffusion coefficients were calculated using a Sherwood-correlation for forced convection of gases to a cylinder in crossflow (Churchill and Bernstein, 1977) and the diffusion coefficient in the absence of convection. In the isothermal case this leads to:

$$Sh = 0.39 + \frac{0.66 \cdot Re^{1/2} \cdot Sc^{1/3}}{\left[1 + (0.4/Sc)^{2/3}\right]^{1/4}} \cdot \left[1 + \left(\frac{Re}{282000}\right)^{5/8}\right]^{4/5} \quad (5)$$

and:

$$D_{m,i}|_{eff} = \frac{p^2}{8} \cdot D_{m,i} \cdot \left(\frac{h}{D_{w-w}}\right) \cdot \frac{Sh^2}{Re \cdot Sc} \quad (6)$$

Equation (6) was derived by requiring identical conversions in case of a single row of parallel cylinders and a single row of parallel flat plates (see Figure 1) at total mass-transfer limited conditions.

The set of partial differential equations, together with the initial and boundary conditions, were solved numerically, using the method of lines and the method of Gear in the standard NAG-library routine D03PGF (NAG Fortran Library, 1991). The resulting radial mole fraction profiles at the reactor outlet were integrated, and used to calculate the conversions and selectivities corresponding to a given reactant space-time, inlet methane-to-oxygen ratio, and catalyst temperature. The complete derivation of the reactor model and the solution procedure can be found in de Smet et al. (1999).

5.3.2 Parameter estimation

Intrinsic kinetic parameters were estimated by means of non-linear regression, using a single-response Marquardt-Levenberg algorithm implemented in Odrpack (Boggs et al., 1992). As the observed methane and oxygen conversions are completely determined by mass-transport, the kinetic parameters are obtained from the least-squares criterion, applied to the observed and calculated CO selectivity. The parameter estimates were tested for significance by means of the approximate, individual t-values. The statistical significance of the global regression was expressed by means of the F-ratio, which is based on the ratio of the mean calculated sum of squares and the mean regression sum of squares. In order to avoid the correlation between the activation energy and the pre-exponential factor of the methane adsorption rate coefficient, reparametrisation of the Arrhenius equation was applied (Kitrell, 1970):

$$k = A \exp\left(\frac{-E_{\text{act}}}{RT_{\text{avg}}}\right) \exp\left(\frac{-E_{\text{act}}}{R} \left(\frac{1}{T_{\text{cat}}} - \frac{1}{T_{\text{avg}}}\right)\right) \quad (7)$$

in which T_{avg} is the average catalyst temperature of the experiments ($T_{\text{avg}} = 1115$ K). The total number of 40 experiments was used during the regression analysis.

5.4 Effects of reaction conditions

At the range of conditions investigated, CO, CO₂, and H₂O were the main products. H₂ was found only at catalyst temperatures above 1273 K. At these temperatures, however, the gauze catalyst did not exhibit stable performance with time-on-stream. Platinum deposits were found downstream of the gauze catalyst, as a result of the formation of volatile Pt-oxide species. In addition, a slow increase of the reactant conversions with time-on-stream was observed, which is generally ascribed to morphological changes of the Pt catalyst (Bergene et al., 1996). In order to perform experiments at constant catalyst activity, the catalyst

temperature was always kept below 1200 K. The influence of the catalyst temperature, the reactant space-time, $W/F_{\text{CH}_4,0}$, and the inlet CH_4/O_2 ratio on conversions and selectivities is shown in Figures 2 to 4.

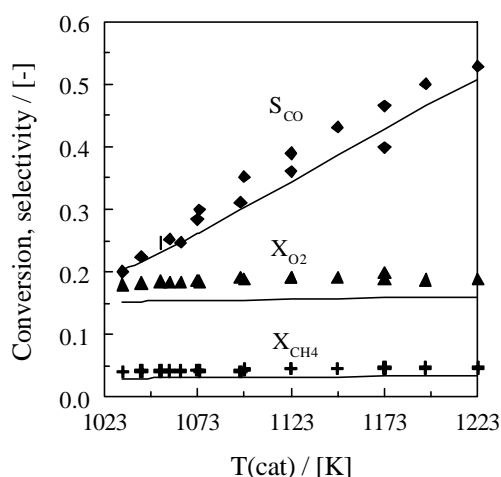


Figure 2. Conversions and selectivities vs catalyst temperature. Lines: calculated using the flat-plate reactor model (de Smet et al., 1999) and the kinetic model with corresponding kinetic parameters listed in Table 2. Points: experiments. Conditions: $P_{\text{tot}} = 130 \text{ kPa}$, $F_{\text{tot}} = 1 \times 10^{-2} \text{ mol s}^{-1}$, $W/F_{\text{CH}_4,0} = 39.9 \text{ g s mol}^{-1}$, $\text{CH}_4/\text{O}_2/\text{He}^{1/2}_0 = 14.3/5.7/80$.

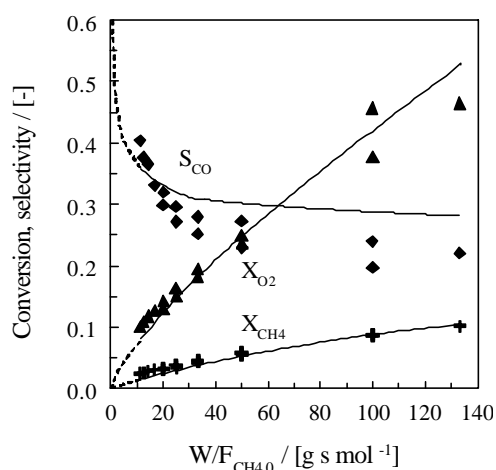


Figure 3. Conversions and selectivities vs space-time. Full lines: calculated using the flat-plate reactor model (de Smet et al., 1999) and the kinetic model with corresponding kinetic parameters listed in Table 2. Dashed lines: calculated at low space-times, outside the range listed in Table 1. Points: experiments. Conditions: $P_{\text{tot}} = 160 \text{ kPa}$, $T_{\text{cat}} = 1123 \text{ K}$, $\text{CH}_4/\text{O}_2/\text{He}^{1/2}_0 = 28.6/11.4/60$.

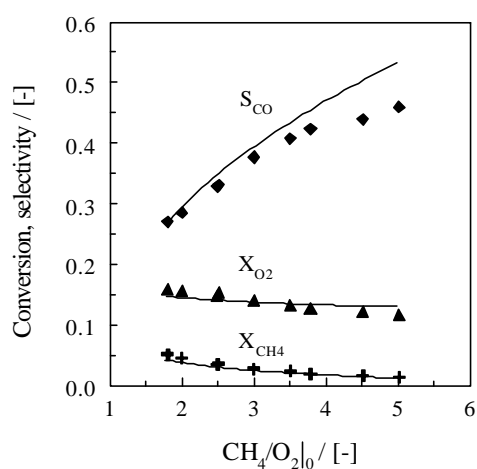


Figure 4. Conversions and selectivities vs inlet methane-to-oxygen ratio. Lines: calculated using the flat-plate reactor model (de Smet et al., 1999) and the kinetic model with corresponding kinetic parameters listed in Table 2. Points: experiments. Conditions: $P_{\text{tot}} = 130 \text{ kPa}$, $T_{\text{cat}} = 1123 \text{ K}$, $F_{\text{tot}} = 1 \times 10^{-2} \text{ mol s}^{-1}$, $y_{\text{O}_2}^{1/2}_0 = 0.114$.

Figure 2 demonstrates that the methane and oxygen conversions are hardly temperature dependent, indicating that the reaction rates are determined by transport phenomena. The selectivity to carbon monoxide, however, varies considerably with catalyst temperature. The CO production rate thus appears to be influenced significantly by the surface chemistry. The measured methane and oxygen conversions increase at increasing reactant space-times, see Figure 3. The selectivity to CO decreases at increasing space-time, which suggests that CO is a primary product of the oxidation reaction. Figure 4 shows that both the methane and oxygen conversions decrease at increasing CH₄/O₂ ratio. The selectivity to CO increases considerably at increasing methane-to-oxygen ratio. Similar trends were observed by Hickman and Schmidt (1992), Heitnes Hofstad et al. (1996) and Fahti et al. (1998) using both Pt and Pt-10%Rh gauzes.

5.5 Kinetic model development

5.5.1 Reaction network

The kinetic model used in this work, which will be referred to as the oxygen-assisted CPO mechanism, is shown in Table 2, together with the corresponding rate equations.

Table 2. *Oxygen-assisted CPO reaction mechanism with corresponding rate equations and kinetic parameters.*

No.	Reaction	Rate equation	A c.q. s ₀ ^a	E _{act} ^b	Reference
1	O _{2g} + 2* → 2O*	r ₁ = k ₁ p _{O2} q _*	0.023	0	Elg et al (1997)
2	CH _{4g} + 2O* → C* + 2H ₂ O _g + *	r ₂ = k ₂ p _{CH4} q _* q _O	2.39·10 ⁵	48.2	Present work
3	C* + O* → CO* + *	r ₃ = k ₃ q _C q _O	1·10 ¹³	62.8	Hickman and Schmidt (1993)
4	CO* + O* → CO _{2g} + 2*	r ₄ = k ₄ q _{CO} q _O	1·10 ¹³	100	Campbell et al (1980)
5	CO* → CO _g + *	r ₅ = k ₅ q _{CO}	1·10 ¹³	126	McCabe and Schmidt (1977)
6	CO _g + * → CO*	r ₆ = k ₆ p _{CO} q _*	0.84	0	Campbell et al (1981)

^a Units: Pa⁻¹ s⁻¹ (2), s⁻¹ (3,4,5). ^b Units: kJ mol⁻¹. t-values: t (A₂exp(-E_{act,2}/RT_{avg})) = 37.8, t (E_{act,2}) = 5.5.

The mechanism consists of six reaction steps; oxygen and methane adsorption, surface reactions towards CO and CO₂, desorption and adsorption of CO are taken into account. All reaction steps, with the exception of CO adsorption/desorption, are considered to be irreversible. This is justified since both the methane and oxygen conversions are considerably lower than 100%. Irreversible methane and oxygen adsorption may lead to a structurally unstable kinetic model, as a result of the occurrence of a transcritical bifurcation point (Nibbelke et al., 1998). Reactor simulations with the kinetic parameters obtained after regression show, however, that these structural instabilities do not occur. This is a result of the low surface coverages of both adsorbed carbon and oxygen species at the conditions investigated.

Oxygen adsorption. The first step in the reaction mechanism concerns the activation of oxygen through dissociative adsorption. The adsorption rate is assumed to be first order in the fraction of vacant surface sites 2^* (Williams et al., 1992), which implies that the rate-determining step in the adsorption involves the interaction of molecular oxygen with a single catalytic site. Oxygen adsorption is considered to be competitive, in contrast to the mechanism proposed by Hickman and Schmidt (1993). In the latter 19-step mechanism, oxygen is assumed to adsorb on specific catalytic sites, i.e. non-competitively with other species, in order to be able to simulate the experimentally observed O₂ adsorption-limited CO production rate.

Methane adsorption. Dissociative adsorption of methane, resulting in the formation of a surface carbon species and gaseous water, is taken into account in step 2. Methane adsorption is considered to be oxygen-assisted, directly resulting in adsorbed hydroxyl species that recombine instantaneously to gaseous water. Oxygen-assisted methane adsorption is included in the kinetic model to be consistent with the observed decrease of the CO selectivity at increasing space-times. This will be illustrated later, by examining analytical expressions for the intrinsic selectivity to CO. Also, oxygen-assisted methane adsorption is in line with the observation that H₂O is the only hydrogen-containing product at the conditions investigated.

Reaction 2 obviously is not an elementary step, but proceeds through a number of intermediates such as adsorbed CH_x (x=1,3) fragments and adsorbed OH species. A possible reaction sequence, accounting for the global methane adsorption step is shown in Table 3. Methane adsorption on the Pt surface is considered to be reversible and in quasi-equilibrium. The abstraction of the first hydrogen atom by adsorbed oxygen species is considered as the rate-determining step in methane decomposition. The subsequent abstraction of hydrogen atoms from adsorbed CH_x fragments, and the recombination of hydroxyl species to water are

potentially very fast. As a result, no CH_x species appear as surface intermediates in the kinetic model. The global rate coefficient for dissociative adsorption of methane, k_2 , is the product of the equilibrium coefficient for molecular adsorption of methane and the rate coefficient of the rate determining step $2b^I$, see Table 3.

Carbon monoxide and carbon dioxide production. Steps 3 to 6 concern the reaction paths towards carbon monoxide and carbon dioxide. Reaction 3 describes the formation of adsorbed CO species, which is generally considered to be very fast (Hickman and Schmidt, 1993). Adsorbed CO species are converted to CO_2 in step 4, which desorbs instantaneously. CO_2 adsorption is not taken into account in the kinetic model, since the heat of adsorption of CO_2 on Pt is very low (Shustorovich, 1990). Finally, CO desorption and adsorption are described in the kinetic model by steps 5 and 6.

Table 3. Possible reaction sequence for dissociative methane adsorption.

No.	Reaction	σ_i
2a	$\text{CH}_{4,g} + * \xrightleftharpoons[k_{2a,des}]{k_{2a,ads}} \text{CH}_4^*$	1
2b	$\text{CH}_4^* + \text{O}^* \xrightarrow{k_{2b}^I} \text{CH}_3^* + \text{OH}^*$	1
	$\text{CH}_3^* + \text{O}^* \xrightarrow{k_{2b}^{II}} \text{CH}_2^* + \text{OH}^*$	1
	$\text{CH}_2^* + \text{O}^* \xrightarrow{k_{2b}^{III}} \text{CH}^* + \text{OH}^*$	1
	$\text{CH}^* + \text{O}^* \xrightarrow{k_{2b}^{IV}} \text{C}^* + \text{OH}^*$	1
2c	$\text{OH}^* + \text{OH}^* \xrightarrow{k_{2c}} \text{H}_2\text{O}_g + \text{O}^* + *$	2
2	$\text{CH}_{4,g} + 2\text{O}^* \xrightarrow{k_2} \text{C}^* + 2\text{H}_2\text{O}_g + *$	

5.5.2 Surface species mass-balances

The kinetic model as shown in Table 2 involves five molecules and four surface species. The steady-state mass-balances for the surface species are written as:

$$\text{C-balance:} \quad k_2 p_{\text{CH}_4} q_* q_{\text{O}} - k_3 q_{\text{C}} q_{\text{O}} = 0 \quad (8)$$

$$\text{O-balance:} \quad 2k_1 p_{\text{O}_2} q_* - 2k_2 p_{\text{CH}_4} q_* q_{\text{O}} - k_3 q_{\text{C}} q_{\text{O}} - k_4 q_{\text{CO}} q_{\text{O}} = 0 \quad (9)$$

$$\text{CO-balance:} \quad k_3 q_{\text{C}} q_{\text{O}} - k_4 q_{\text{CO}} q_{\text{O}} - k_5 q_{\text{CO}} + k_6 p_{\text{CO}} q_* = 0 \quad (10)$$

$$\text{Vacant sites:} \quad q_{\text{C}} + q_{\text{O}} + q_{\text{CO}} + q_* = 1 \quad (11)$$

The terms in Equations (8) to (10) are in units s^{-1} . The mass-balances were solved numerically in the flat-plate reactor model, using a modified Newton-Raphson method in the NAG-library routine C05NBF (NAG Fortran Library, 1991). The turnover frequencies of the individual surface steps are used to determine the net areal production and consumption rates of all components. These rates are entered into the flat-plate reactor model, via the boundary condition at the catalyst surface, see Equation 4.

5.5.3 Consistency of the oxygen-assisted CPO mechanism with experimental results

In order to illustrate the qualitative consistency of the oxygen-assisted CPO mechanism with the observed decrease of the CO selectivity with increasing space-time (Figure 3), the intrinsic CO selectivity is considered at given axial reactor coordinate z :

$$S_{\text{CO}}|_z^{\text{intr}} = \frac{r_5 - r_6}{r_2} = 1 - \frac{r_4}{r_2} \quad (12)$$

The intrinsic selectivity to CO is thus defined as the ratio of the intrinsic CO production rate to the intrinsic methane disappearance rate. Substitution of the corresponding rate equations results in:

$$S_{\text{CO}}|_z^{\text{intr}} = 1 - \frac{k_4 q_{\text{CO}} q_{\text{O}}}{k_2 p_{\text{CH}_4} q_* q_{\text{O}}} = 1 - \frac{k_4 q_{\text{CO}}}{k_2 p_{\text{CH}_4} q_*} \quad (13)$$

Since both the methane adsorption rate and the CO_2 production rate are proportional to the oxygen surface coverage, the CO selectivity is independent of θ_{O} . The CO adsorption/desorption reaction is approximately in equilibrium at sufficiently high reactant space-times, as will be shown later. As a result, the CO adsorption equilibrium coefficient, equal to $K_{\text{CO,ads}} = k_6/k_5 = 2q_{\text{CO}}/(2q_* p_{\text{CO}})$, can then be substituted into Equation (13):

$$S_{\text{CO}}|_z^{\text{intr}} = 1 - \frac{k_4 K_{\text{CO,ads}} P_{\text{CO}}}{k_2 P_{\text{CH}_4}} \quad (14)$$

Hence, the intrinsic CO selectivity is determined by (i) the rate coefficients of the CH₄ adsorption and CO₂ production steps, (ii) the ratio of the rate coefficients for CO adsorption/desorption, as well as (iii) the partial pressures of CO and CH₄ at the catalyst surface. According to Equation (14), the intrinsic selectivity for CO will decrease at increasing space-times, when the ratio of the partial pressures of CO and CH₄ increases.

The measured gas-phase partial pressures of methane, oxygen, and carbon monoxide at the reactor outlet are shown in Figure 5a as a function of space-time. These observed partial pressures are bulk values, and therefore only provide an indication of the actual partial pressures at the catalyst surface. The influence of space-time on the intrinsic CO selectivity can nevertheless be understood qualitatively. As methane is present in excess during the experiments, the partial pressure decreases only slightly at increasing space-time. The partial pressure of CO increases considerably at increasing space-times. As a result, the ratio of the partial pressures of CO and CH₄ (see Figure 5b) increases at increasing space-time, and consequently, the intrinsic CO selectivity will decrease (Equation (14)).

In case of dissociative methane adsorption, resulting in adsorbed carbon and hydrogen species (Hickman and Schmidt, 1993, Bui et al., 1997, Deutschmann et al., 1998a, 1998b) without the involvement of O-adatoms, the CH₄ disappearance rate is given by:

$$r_2 = k_2 P_{\text{CH}_4} q_* \quad (15)$$

The intrinsic CO selectivity now becomes:

$$S_{\text{CO}}|_z^{\text{intr}} = 1 - \frac{k_4 q_{\text{CO}} q_{\text{O}}}{k_2 P_{\text{CH}_4} q_*} \quad (16)$$

and when the CO adsorption/desorption reaction is at quasi-equilibrium:

$$S_{\text{CO}}|_z^{\text{intr}} = 1 - \frac{k_4 K_{\text{CO,ads}} P_{\text{CO}} q_{\text{O}}}{k_2 P_{\text{CH}_4}} \quad (17)$$

In this case, the intrinsic CO selectivity is also governed by the surface coverage of oxygen. The oxygen surface coverage follows from the steady-state mass balances of adsorbed carbon and oxygen and can be written in this case as:

$$q_{\text{O}} = \frac{2k_1 P_{\text{O}_2} - 3k_2 P_{\text{CH}_4}}{k_4 K_{\text{CO,ads}} P_{\text{CO}}} \quad (18)$$

Substitution of Equation (18) into (17) results in:

$$S_{\text{CO}}|_z^{\text{intr}} = 4 - 2 \frac{k_1 p_{\text{O}_2}}{k_2 p_{\text{CH}_4}} \quad (19)$$

Because of the stoichiometric excess of methane, the decrease of the partial pressure of O_2 at increasing space-time is more pronounced than the decrease of the CH_4 partial pressure, see Figure 5a. The ratio of the partial pressures of oxygen and methane consequently decreases (Figure 5b), and the intrinsic selectivity to CO will *increase* at increasing space-times, which is not consistent with the experimental observations.

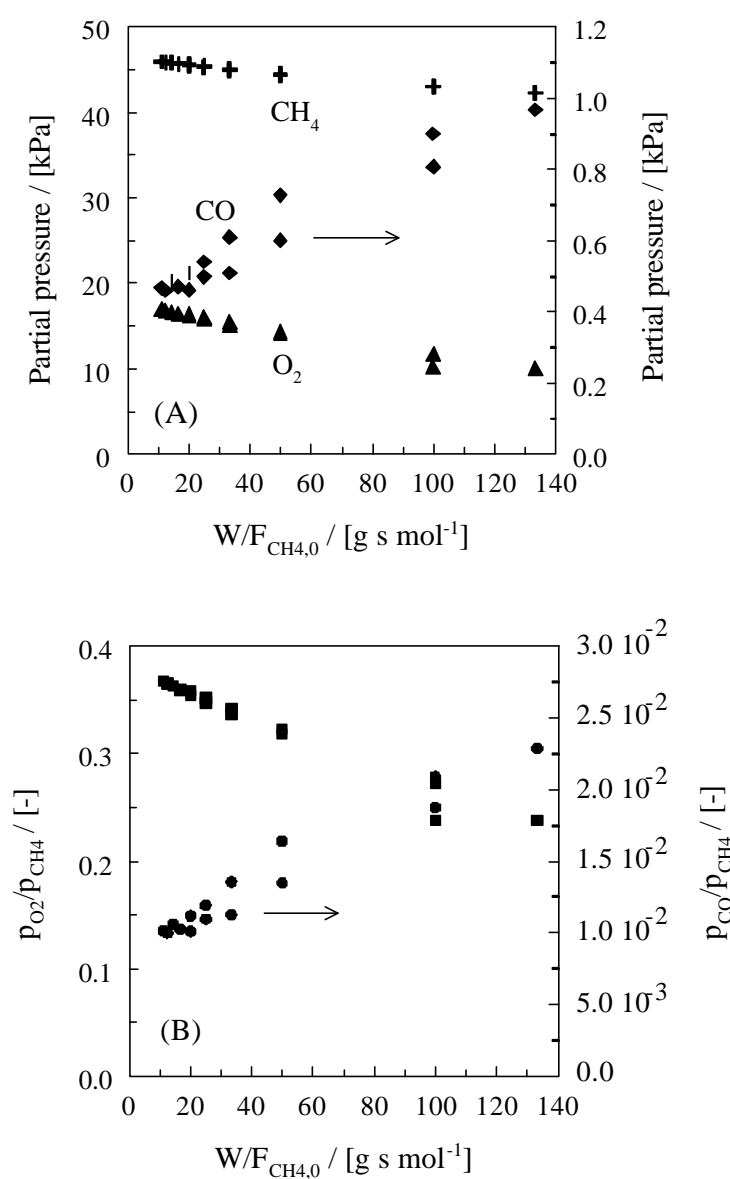


Figure 5. Measured bulk partial pressures (A), and partial pressure ratios (B) at the reactor outlet vs space-time. Conditions: see Figure 3.

The current analysis thus indicates that the influence of space-time on the intrinsic CO selectivity can only be accounted for when methane adsorption is considered to be oxygen-assisted. Dissociative methane adsorption into adsorbed carbon and hydrogen species will lead to increasing intrinsic CO selectivities with increasing space-time. In addition, simulations with the kinetic model of Hickman and Schmidt (1993) for CPO on Pt, in which dissociative methane adsorption is taken into account, showed that significant amounts of hydrogen are formed even in the presence of non-converted O₂. This observation is also not consistent with the experimental results.

5.5.4 Kinetic parameter determination

The adsorption rate coefficients of O₂ and CO were calculated from collision theory:

$$k_{\text{ads},i} = \frac{s_{i,0}}{L_t \sqrt{(2pM_i RT_{\text{cat}})}} \quad (20)$$

in which $s_{i,0}$ is the initial sticking coefficient, and L_t the total surface concentration of active sites, taken as $1.67 \cdot 10^{-5} \text{ mol m}_{\text{Pt}}^{-2}$. Campbell et al. (1981) investigated CO chemisorption on Pt(111) at 310 K, and reported an initial sticking coefficient of 0.84, which is used in this work. In case of oxygen adsorption on Pt, a wide range of sticking coefficients can be found in literature. Elg et al. (1997) investigated the temperature dependence of the initial sticking coefficient of oxygen on Pt(111). It was shown, that s_0 decreased exponentially from a value of 0.054 at 300 K to 0.023 at 670 K. Here, the high temperature value of 0.023 was used.

The pre-exponential factors of reactions 3, 4 and 5 were set at a typical value of 10^{13} s^{-1} , which approximately corresponds to the value predicted by the transition state theory (Zhdanov et al., 1988). The corresponding activation energies were taken from literature, see Table 2. Two kinetic parameters had to be estimated by regression: A and E_{act} of reaction 2. The estimated parameter values, together with the corresponding t -values are shown in Table 2. The t -values indicate that the estimates of the Arrhenius parameters of the methane adsorption are statistically significant. The F -value of the regression amounts to 1900; the binary correlation coefficient is 0.85. Figure 6 shows a parity plot of the experimental and calculated CO selectivities. The deviation between the observed and calculated values is usually within 15%.

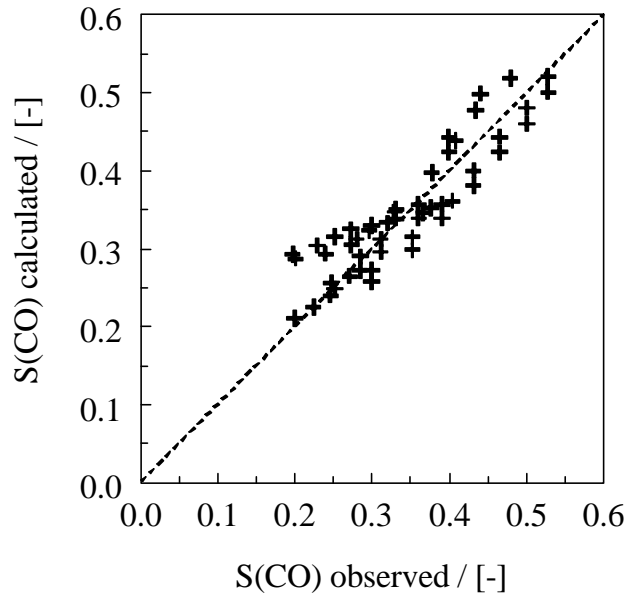


Figure 6. Calculated vs experimental CO selectivities. Calculated values obtained with the flat-plate reactor model (de Smet et al., 1999) and the kinetic model with corresponding kinetic parameters listed in Table 2. Experimental conditions: see Table 1.

5.5.5 Physico-chemical assessment of the parameter estimates

As mentioned earlier, the rate coefficient k_2 is given by the product of the equilibrium coefficient of molecular methane adsorption, and the rate coefficient of the rate determining step $2b^I$, see Table 3. The activation energy of the rate-determining step $2b^I$ thus follows from:

$$E_{\text{act},2b^I} = E_{\text{act}}^{\text{global}} - \mathbf{DH}_{\text{ads}}^0 \quad (21)$$

in which $E_{\text{act}}^{\text{global}}$ is the global activation energy of dissociative methane adsorption, and $\mathbf{DH}_{\text{ads}}^0$ the standard adsorption enthalpy of methane. Substitution of the estimated global activation energy, 48.2 kJ mol^{-1} , and the standard adsorption enthalpy of methane, $\mathbf{DH}_{\text{ads}}^0 = -25.1 \text{ kJ mol}^{-1}$ (Shustorovich, 1990), results in an activation energy of the rate-determining step $2b^I$ of 73.3 kJ mol^{-1} . In the literature, no data was found regarding the activation energy of oxygen-assisted methane adsorption. The calculated value, however, is higher than the reported activation energy of 43.1 kJ mol^{-1} (Anderson and Maloney, 1988) for dissociative methane adsorption into adsorbed carbon and hydrogen species.

The standard activation entropy of the oxygen-assisted methane adsorption reaction, can be calculated from the estimated pre-exponential factor, using:

$$A_2 = e \frac{k_b T_{\text{avg}}}{h_p} \exp\left(\frac{D^\# S_2^0}{R}\right) \quad (22)$$

in which A_2 is in units $\text{bar}^{-1} \text{s}^{-1}$, i.e. with 1 bar as standard pressure. Substitution of the estimated value of A_2 and the average catalyst temperature of the experiments, $T_{\text{avg}} = 1115 \text{ K}$, results in $D^\# S_2^0 = -65.6 \text{ J mol}^{-1} \text{ K}^{-1}$. The activation entropy corresponds to the total entropy change in the oxygen-assisted methane adsorption reaction, including both the entropy loss during methane adsorption, step 2a, and the rate-determining step 2b^I, see Table 3. The standard gas-phase entropy of methane at T_{avg} approximately amounts to $250 \text{ J mol}^{-1} \text{ K}^{-1}$. This indicates that the calculated activation entropy is physically realistic, since the methane molecule cannot lose more entropy than it possesses.

5.6 Simulation results and discussion

5.6.1 Influence of space-time

The experimental and simulated conversions and selectivities are shown in Figure 3 as a function of space-time. The dashed lines in Figure 3 represent the calculated conversions and selectivities at low $W/F_{\text{CH}_4,0}$ ratios, outside the experimental range shown in Table 1. Clearly, the measured methane and oxygen conversions are simulated accurately. As indicated before, the oxygen sticking coefficient was fixed at a value of $2.3 \cdot 10^{-2}$. An increase of $s_{\text{O}_2,0}$ did not result in significantly higher conversions as expected for the mass-transfer limited regime. The experimentally observed decrease in the CO selectivity with increasing space-time is well reproduced by the model. The calculated selectivities, however, are lower than the experimental values at low $W/F_{\text{CH}_4,0}$, and slightly higher at high $W/F_{\text{CH}_4,0}$ ratios.

The calculated surface coverages together with the CO and CO₂ production rates at the reactor outlet are shown in Figure 7. The surface coverage of carbon monoxide approximately amounts to 0.15, while the coverages of carbon and oxygen are in the order of 10^{-3} . At increasing space-times, the oxygen surface coverage decreases rapidly, as a result of the higher oxygen conversion. The carbon monoxide coverage increases first, and levels off at $W/F_{\text{CH}_4,0}$ ratios larger than 20 g s mol^{-1} . The CO and CO₂ production rates both decrease at increasing space-time. However, the decrease of R_{CO} is much more pronounced at low $W/F_{\text{CH}_4,0}$ ratios, which results in a lower value of the CO selectivity at increasing space-time. At $W/F_{\text{CH}_4,0}$ ratios greater than 20 g s mol^{-1} , the ratio between R_{CO} and R_{CO_2} remains approximately constant, and the initial decrease in the CO selectivity is levelled off significantly.

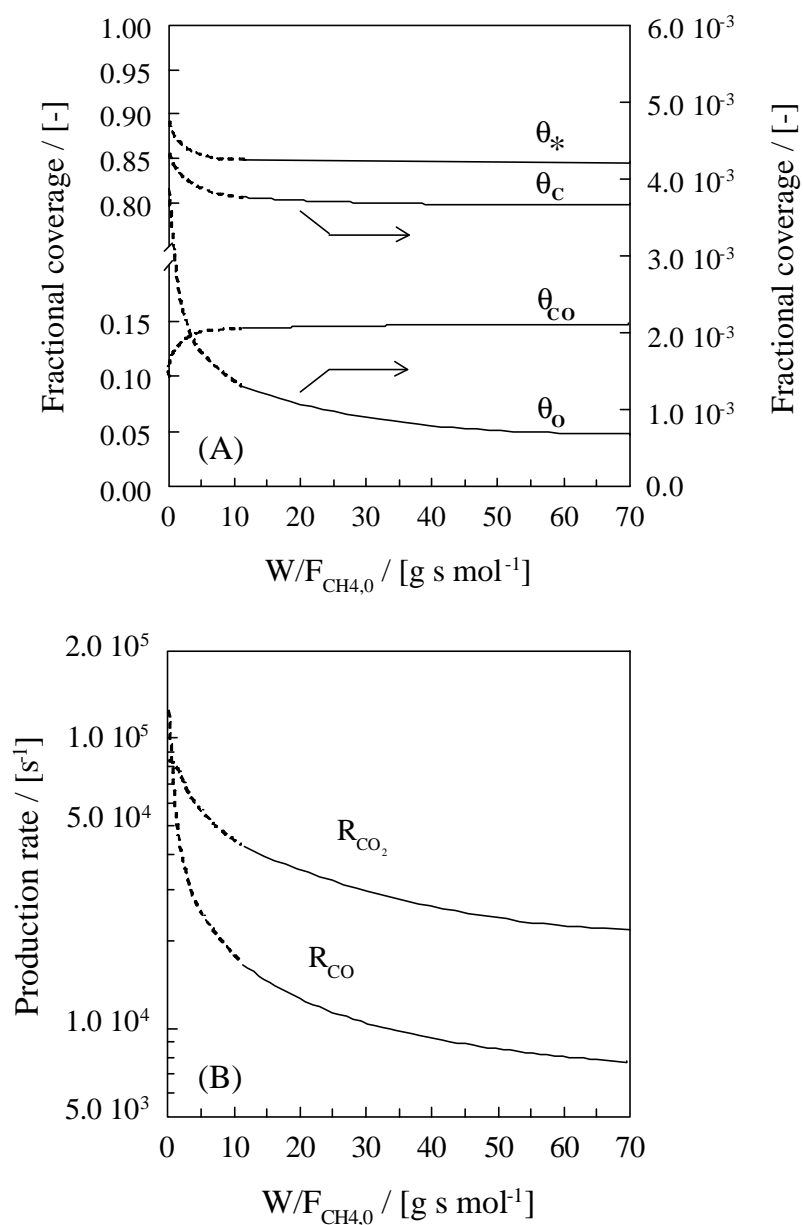


Figure 7. Calculated surface coverages (A), CO, and CO₂ production rates (B) vs space-time. Dashed lines: simulation results at low space times, outside the range in Table 1. Conditions: see Figure 3.

5.6.2 Primary formation of carbon monoxide

Figure 7 indicates, that the calculated CO and CO₂ production rates at the catalyst surface are very high and, hence, are certainly affected by mass-transport limitations. In order

to investigate the influence of the *intrinsic kinetics* on CO formation, calculations were performed at conditions where no transport limitations occur for the reactants and products. Intrinsic conversions and selectivities were obtained by increasing the molecular diffusion coefficients of all gas-phase species with a factor 10, using the kinetic parameters listed in Table 2. A further increase of the molecular diffusion coefficients did not result in significantly higher conversions and selectivities, which indicates that the calculated results indeed correspond to the intrinsic values. The intrinsic conversions and selectivities are shown in Figure 8 as a function of the reactant space-time, together with the conversions and selectivities obtained without adjusting the molecular diffusion coefficients.

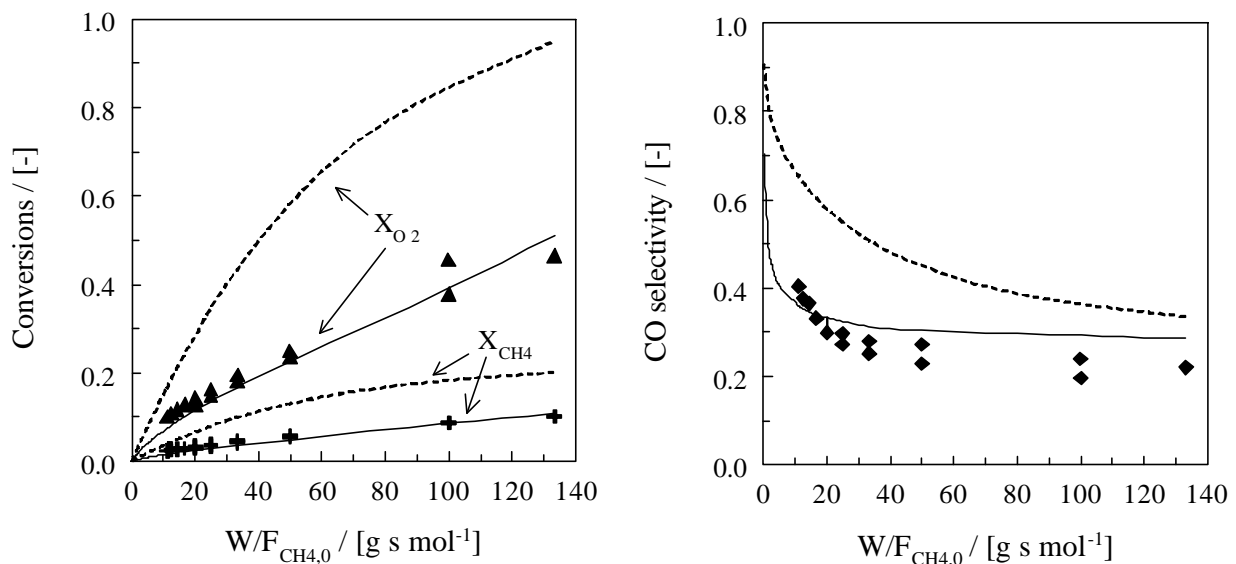
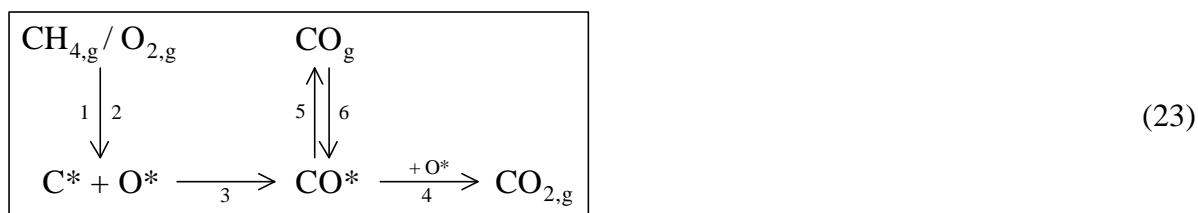


Figure 8. Conversions and selectivities vs space-time. Full lines: calculated with the flat-plate reactor model (de Smet et al., 1999) and the kinetic model with corresponding kinetic parameters listed in Table 2. Dashed lines: intrinsic values, calculated by increasing the molecular diffusion coefficients of all gas-phase species with a factor 10, using the same kinetic model. Points: experimental results. Conditions: see Figure 3.

It is clear, that the intrinsic methane and oxygen conversions are significantly higher than the corresponding values in case of the actual diffusion coefficients. The intrinsic selectivity to CO is also considerably higher than the value calculated without adjusting the diffusion coefficients, but is still decreasing with increasing space-times. The decrease of the CO selectivity with increasing space-time is evidently caused by the kinetics of the surface reactions. An explanation can be given using the schematic representation of the oxygen-assisted CPO reaction mechanism as shown in Equation (23):



At intrinsic conditions, in the absence of mass-transport limitations, the partial pressures of the reactants and products at the catalyst surface are identical to the values in the bulk of the gas phase. At low space-times, i.e. at low methane and oxygen conversions, the partial pressure of CO is relatively small, as well as the CO adsorption rate (step 6). At increasing $W/F_{\text{CH}_4,0}$ ratios, the CO partial pressure increases, thus enhancing the CO adsorption rate. This is also reflected in Figure 9, in which the dimensionless affinity of the CO adsorption/desorption reaction is plotted at intrinsic conditions as a function of space-time.

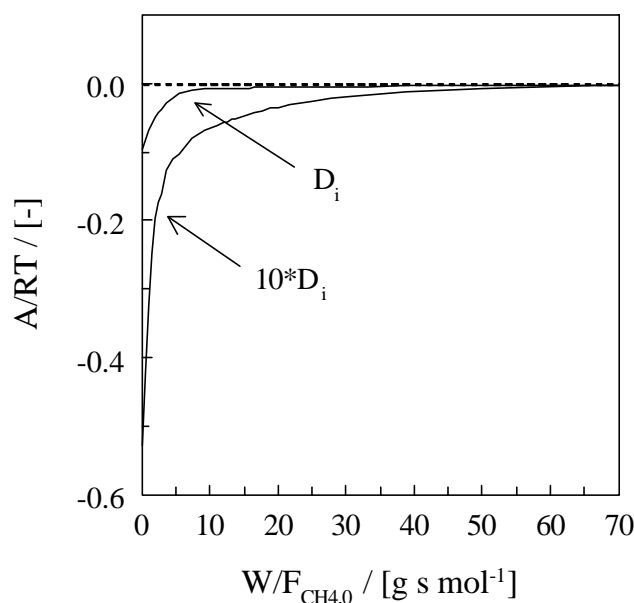


Figure 9. Calculated dimensionless affinity of the CO adsorption-desorption reaction vs space-time. Conditions: see Figure 3.

The dimensionless affinity is obtained from:

$$\frac{A}{RT_{\text{cat}}} = \ln\left(\frac{r_6}{r_5}\right) \quad (24)$$

and is a measure of the degree at which the CO adsorption/desorption equilibrium is approached. At low $W/F_{\text{CH}_4,0}$ ratios, the dimensionless affinity is relatively high, which indicates that the CO adsorption/desorption reaction is reversible, but not at equilibrium. At these conditions, the intrinsic selectivity to CO is given by Equation (13). At increasing

values of the reactant space-time, the dimensionless affinity decreases rapidly, as the CO adsorption/desorption equilibrium is approached. At $W/F_{CH_4,0}$ ratios larger than 25 g s mol^{-1} the CO adsorption reaction is within 2.5 % of its equilibrium. At these space-times, the intrinsic selectivity to CO is given by Equation (14). The observed decrease of the CO selectivity at increasing space-times is thus caused by the asymptotic approach of the CO adsorption/desorption reaction towards its equilibrium.

Figure 9 also indicates, that the dimensionless affinity in case of the actual diffusion coefficients is much smaller than the affinity corresponding to the intrinsic situation. This is evidently caused by mass-transport limitations for CO at these conditions. As a consequence of these transport limitations, the CO partial pressure at the catalyst surface is considerably higher than the bulk partial pressure. The CO adsorption rate is thus much higher than in case of the intrinsic regime, which results in lower selectivities to CO. In addition, Figure 9 indicates that the CO adsorption equilibrium is already reached at much lower space times. As a result, the decrease of the CO selectivity with increasing space-times is much more pronounced, and is levelled off significantly at high space-times.

5.6.3 Initial CO selectivity

Figure 8 indicates, that high CO selectivities are calculated at low values of the reactant space-time. At these conditions, the CO adsorption/desorption reaction is reversible, but not in equilibrium. The intrinsic CO selectivity can thus be represented by Equation (13). This equation can be used to calculate the value of the initial CO selectivity, i.e. the selectivity at $W/F_{CH_4,0} = 0$. At this $W/F_{CH_4,0}$ ratio, CO adsorption can be neglected. The ratio of the surface coverages of adsorbed CO and vacant sites, see Equation (13), can now be solved analytically, using the steady-state balances for adsorbed C, O, and CO species:

$$S_{CO}|_{ini}^{intr} = 1 - \frac{k_4}{k_2 p_{CH_4}} \frac{q_{CO}}{q_*} = \frac{5}{2} + a - \sqrt{\left\{ \left(\frac{3}{2} + a \right)^2 + 2a \right\}} \quad (25a)$$

in which:

$$a = \frac{k_1 k_4}{k_2 k_5} \frac{p_{O_2}}{p_{CH_4}} \quad (25b)$$

Substitution of the corresponding rate coefficients and inlet partial pressures of methane and oxygen results in an initial CO selectivity of 0.93 at the conditions applied during the $W/F_{CH_4,0}$ experiments. The minimum value of the initial CO selectivity is found at a catalyst

temperature of 1023 K, and corresponds to 0.86, while a maximum value of 0.96 is found at an inlet methane-to-oxygen ratio of 5. Obviously, CO_2 is produced over the entire range of $W/F_{\text{CH}_4,0}$ ratios. However, the analysis does show, that CO is the most important primary product.

5.6.4 Influence of catalyst temperature

The experimental and simulated conversions and selectivities as a function of the catalyst temperature are shown in Figure 2, at a $W/F_{\text{CH}_4,0}$ ratio of 40 g s mol^{-1} . As expected for a mass-transfer limited regime, the calculated conversions are hardly influenced by the catalyst temperature. The simulated conversions are slightly lower than the experimentally observed values. The observed increase in the CO selectivity at increasing catalyst temperature is predicted accurately. The latter observation clearly indicates, that the kinetics of the surface reactions are indeed crucial in determining the absolute value of the CO production rate.

The corresponding surface coverages together with the CO and CO_2 production rates as a function of the catalyst temperature are shown in Figure 10. At increasing temperature, the desorption rate of CO is considerably enhanced, resulting in a decrease of the surface coverages of carbon, oxygen and carbon monoxide. The CO_2 production rate decreases slightly at increasing catalyst temperatures. This is mainly caused by the large decrease of the oxygen surface coverage. At increasing temperature, R_{CO} increases rapidly: the decrease of the CO surface coverage with increasing temperature is obviously more than compensated by the large increase of the CO desorption rate coefficient. As a result of the increase of the CO production rate, and the decreasing CO_2 production rate, the selectivity to CO increases at increasing catalyst temperatures (Figure 2).

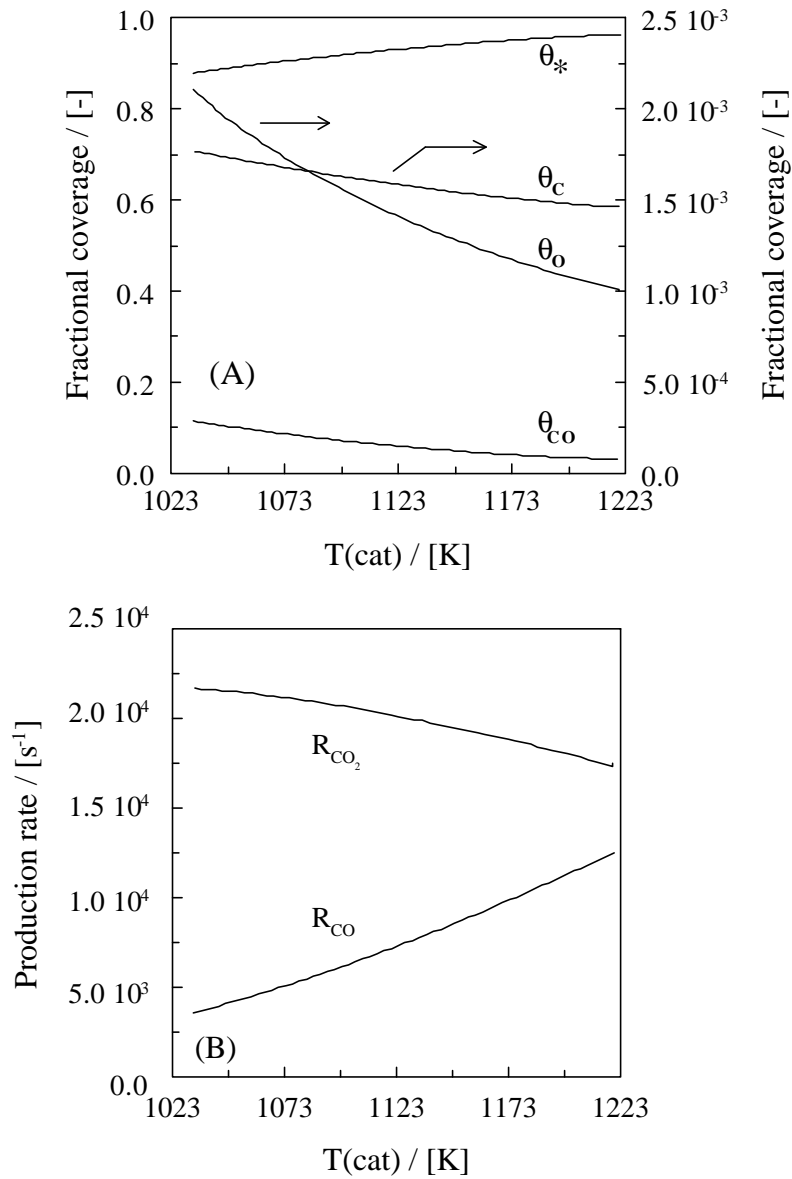


Figure 10. Calculated surface coverages, (A) and CO, and CO₂ production rates (B) vs catalyst temperature. Conditions: see Figure 2.

5.6.5 Influence of CH₄/O₂ ratio

Figure 4 demonstrates that the effect of the inlet methane-to-oxygen ratio on the conversions and selectivities is also accurately simulated. The corresponding calculated surface coverages, and the production rates of CO and CO₂ at the reactor outlet are shown in Figure 11 as a function of $\text{CH}_4/\text{O}_2|_0$. At increasing methane-to-oxygen ratios, the surface

coverages of adsorbed carbon and carbon monoxide increase, while the coverages of oxygen and vacant surface sites decrease. The increase of the surface coverage of adsorbed carbon is mainly caused by the increase of the CH_4 partial pressure at increasing methane-to-oxygen ratios. The decrease of the oxygen surface coverage, is more pronounced than the increase of the CO coverage, which results in decreasing CO_2 production rates at increasing CH_4/O_2 ratios. The CO production rate, however, increases at increasing CH_4/O_2 ratios, which results in the observed increase of the CO selectivity.

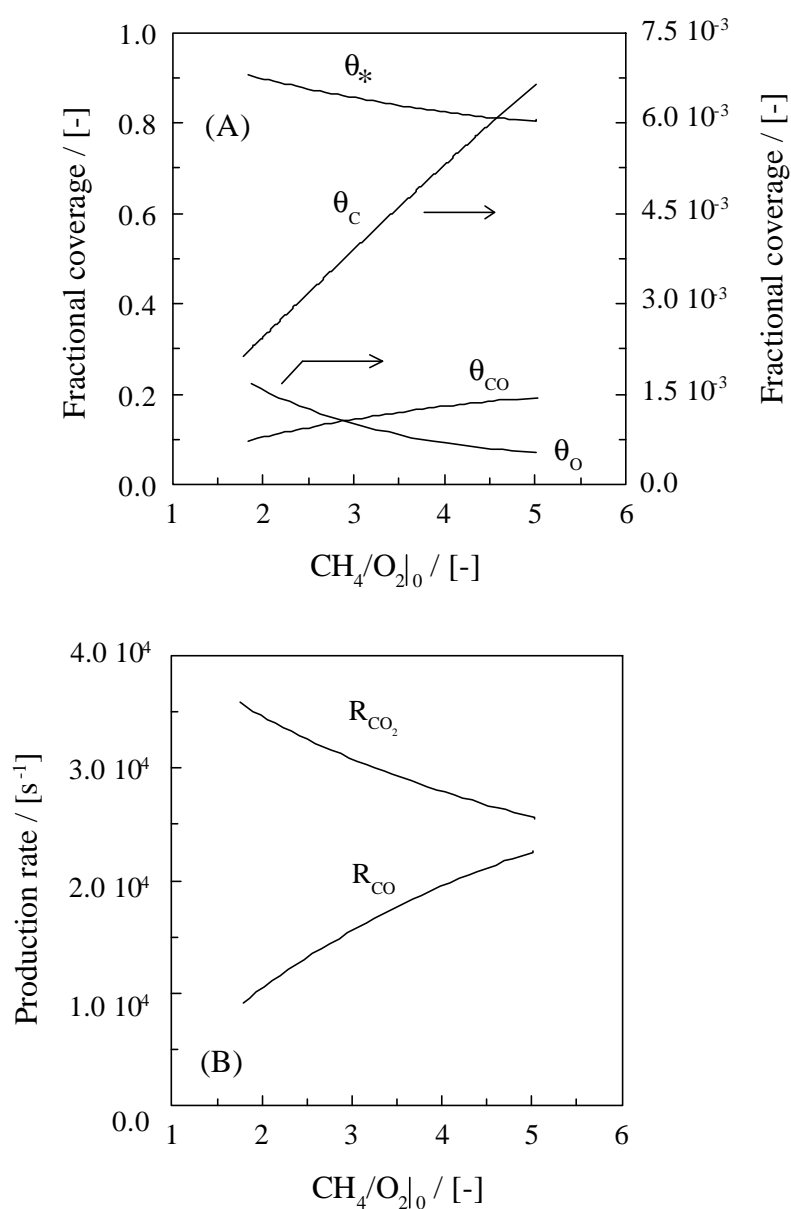


Figure 11. Calculated surface coverages (A), and CO, and CO_2 production rates (B) vs inlet methane-to-oxygen ratio. Conditions: see Figure 4.

5.7 Conclusions

The catalytic partial oxidation of methane was studied at atmospheric pressure on a single Pt gauze catalyst. The structured laboratory reactor proved to be a valuable experimental tool to determine the *intrinsic kinetics* of the CPO reaction, as the *catalyst temperature* was measured directly. It was shown that CO, CO₂, and H₂O were the main products at oxygen conversions lower than 100 %. Both the methane and oxygen conversion rates were determined by mass transport, whereas the selectivity to CO was also influenced significantly by the kinetics of the surface reactions.

A kinetic model consisting of 6 reactions among 5 molecules and 4 surface intermediates was developed to describe the experimental observations. Oxygen-assisted methane adsorption was shown to be consistent with the experimental results. In order to obtain the corresponding kinetic parameters, a reactor model without adjustable parameters was applied that takes into account the mass-transport phenomena in a quantitative way. Single-response regression, applied to the observed CO selectivity, resulted in statistically significant and physically meaningful estimates of the *intrinsic* kinetic rate parameters of the methane adsorption.

The effects of catalyst temperature, reactant space-time, and inlet methane-to-oxygen ratio on the conversions and selectivities could be simulated adequately by the model. The modelling results indicate initial CO selectivities between 0.86 and 0.96. In addition, the present work *quantitatively* illustrates the role of surface kinetics and mass-transfer in CO formation.

Acknowledgement

The financial support provided by the Commission of the European Union in the framework of the Copernicus project, No. 41GO4597, is gratefully acknowledged by the authors.

Notation

A	pre-exponential factor (s ⁻¹ , s ⁻¹ Pa ⁻¹), affinity (J mol ⁻¹)
A _{cat}	catalyst surface area (m ²)
C _{t,b}	total concentration at bulk conditions (mol m ⁻³)
d _w	wire diameter (m)

$D_{m,i}$	molecular diffusion coefficient in mixture ($\text{m}^2 \text{s}^{-1}$)
D_{w-w}	distance between the centres of two wires (m)
E_{act}	activation energy (kJ mol^{-1})
$F_{\text{CH}_4,0}$	inlet molar flow rate of CH_4 (mol s^{-1})
$F_{v,b}$	volumetric flow rate at bulk conditions ($\text{m}^3 \text{s}^{-1}$)
h	distance between two flat plates (m)
h_p	Planck constant ($= 6.6262 \cdot 10^{-34} \text{ J s}$)
ΔH_{ads}^0	methane adsorption enthalpy (kJ mol^{-1})
k_b	Boltzmann constant ($= 1.3807 \cdot 10^{-23} \text{ J K}^{-1}$)
k_i	reaction rate parameter (s^{-1} , $\text{s}^{-1} \text{ Pa}^{-1}$)
$K_{\text{CO,ads}}$	CO adsorption equilibrium coefficient (Pa^{-1})
L_t	total surface concentration (mol m^{-2})
M_i	molecular mass (kg mol^{-1})
p_i	partial pressure (Pa)
r	dimensionless radial reactor coordinate (-)
$r_{i,A}$	areal reaction rate ($\text{mol m}^{-2} \text{s}^{-1}$)
R	gas constant ($\text{J mol}^{-1} \text{K}^{-1}$)
R_i	net production rate (s^{-1})
Re	Reynolds number (-)
$\Delta^\#S^0$	standard activation entropy ($\text{J mol}^{-1} \text{K}^{-1}$)
S_{CO}	selectivity to carbon monoxide (-)
$s_{i,0}$	initial sticking coefficient (-)
Sc	Schmidt number (-)
Sh	Sherwood number (-)
t	t-value (-)
T_{avg}	average temperature of the experiments (K)
T_{cat}	catalyst temperature (K)
W_{cat}	catalyst mass (g)
X_{CH_4}	conversion of methane (-)

X_{O_2}	conversion of oxygen (-)
y_i	mole fraction (-)
z	dimensionless axial reactor coordinate (-)

Greek symbols

α	parameter (-)
θ_i	fractional surface coverage (* = vacant site)

Subscripts

0	Inlet
eff	Effective
ini	Initial
intr	Intrinsic
z	at dimensionless axial position z

References

- Anderson, A.B., & Maloney, J.J. (1988). Activation of methane on iron, nickel, and platinum surfaces. A molecular orbital study. *J. Phys. Chem.*, 92, 809-812.
- Berger, R.J., & Marin, G.B. (1999). Investigation of gas-phase reactions and ignition delay occurring at conditions typical for partial oxidation of methane to synthesis gas. *Ind. Eng. Chem. Res.*, 38, 2582-2592.
- Beretta, A., Baiardi, P., Prina, D., & Forzatti, P. (1999). Analysis of a catalytic annular reactor for very short contact times. *Chem. Eng. Sci.*, 54, 765-776.
- Bergene, E., Trondstad, O., & Holmen, A. (1996). Surface areas of Pt-Rh catalyst gauzes used for ammonia oxidation. *J. Catal.*, 160, 141-147.
- Boggs, P.T., Byrd, R.H., Rogers, J.E. & Schnabel, R.B. (1992). *Odrpack Version 2.01, Software for Weighted Orthogonal Distance Regression*. National Institute of Standards and Technology, Gaithersburg.
- Bui, P.A., Vlachos, D.G. & Westmoreland, P.R. (1997). Catalytic ignition of methane/oxygen mixtures over platinum surfaces: comparison of detailed simulations and experiments. *Surf. Sci.*, 385, L1029-L1034.
- Campbell, C.T., Ertl, G., Kuipers, H. & Segner, J. (1980). A molecular beam study of the catalytic oxidation of CO on a Pt(111) surface. *J. Phys. Chem.*, 73, 5862-5873.
- Campbell, C.T., Ertl, G., Kuipers, H. & Segner, J. (1981). A molecular beam investigation of the interactions of CO with a Pt(111) surface. *Surf. Sci.*, 107, 207-219.
- Christensen, T.S. & Primdahl, I.I. (1994). Improve syngas production using autothermal reforming. *Hydrocarbon processing*, 39, 39-46.

- De Smet, C.R.H., de Croon, M.H.J.M., Berger, R.J., Marin, G.B. & Schouten, J.C. (1999). An experimental reactor to study the intrinsic kinetics of the catalytic partial oxidation of methane in the presence of heat-transport limitations. *Appl. Cat. A.*, 187, 33-48.
- Deutschmann, O., Behrendt, F. & Warnatz, J. (1994). Modeling and simulation of heterogeneous oxidation of methane on a platinum foil. *Catal. Today*, 21, 461-470.
- Deutschmann, O., & Schmidt, L.D. (1998a). Modeling the partial oxidation of methane in a short-contact-time reactor. *AIChE J.*, 44, 2465-2477.
- Deutschmann, O., Behrendt, F. & Warnatz, J. (1998b). Formal treatment of catalytic combustion and catalytic conversion of methane. *Catal. Today*, 46, 155-163.
- Elg, A.-P., Eisert, F. & Rosén A. (1997). The temperature dependence of the initial sticking probability of oxygen on Pt(111) probed with second harmonic generation. *Surf. Sci.*, 382, 57-66.
- Fathi, M., Heitnes Hofstad, K., Sperle, T., Rokstad O.A., & Holmen A. (1998). Partial oxidation of methane to synthesis gas at very short contact times. *Catal. Today*, 42, 205-209.
- Heitnes Hofstad, K., Rokstad, O.A. & Holmen, A. (1996). Partial oxidation of methane over platinum metal gauze. *Catal. Lett.*, 36, 25-30.
- Hickman, D. A. & Schmidt, L.D. (1992). Synthesis gas formation by direct oxidation of methane over Pt monoliths. *J. Catal.*, 138, 267-282.
- Hickman, D.A., & Schmidt, L.D. (1993). Steps in CH₄ oxidation on Pt and Rh surfaces: High-temperature reactor simulations. *AIChE J.*, 39, 1164 -1177.
- Kitrell, J.R. (1970). Mathematical modelling of chemical reactions. *Adv. Chem. Eng.*, 8, 97-183.
- Mallens, E.P.J., Hoebink, J.H.J.B. & Marin, G.B. (1995). An investigation on the reaction mechanism for the partial oxidation of methane to synthesis gas over platinum. *Catal. Lett.*, 33, 291-304.
- NAG, Numerical Algorithm Group (1991). *Fortran Library Manual, Mark 15*. Wilkinson House, Oxford.
- Nibbelke, R.H., Hoebink, J.H.B.J., de Croon, M.H.J.M. & Marin, G.B. (1998). Structural stability of kinetic models: anomalies due to irreversible adsorption. *AIChE J.*, 44, 937-949.
- Prettre, M., Eichner, C. & Perrin, M. (1946). The catalytic oxidation of methane to carbon monoxide and hydrogen. *Trans. Farad. Soc.*, 43, 335-340.
- Shustorovich, E. (1990). The bond-order conservation approach to chemisorption and heterogeneous catalysis: applications and implications. *Adv. Catal.*, 37, 101-163.
- Treviño, C. (1999). Analysis for the catalytic ignition of methane in a stagnation point flow. *AIChE J.*, 45, 567-573.
- Vermeiren, W.J.M., Blomsma, E. & Jacobs, P.A. (1992). Catalytic and thermodynamic approach of the oxyreforming of methane. *Catal. Today*, 13, 427-436.
- Vernon, P.D.F., Green, M.L.H., Cheetham, A.K. & Ashcroft, A.T. (1990). Partial oxidation of methane to synthesis gas. *Catal. Lett.*, 13, 181-186.
- Williams, W.R., Marks, C.M. & Schmidt, L.D. (1992). Steps in the reaction $H_2 + O_2 \leftrightarrow H_2O$ on Pt: OH desorption at high temperatures. *J. Phys. Chem.*, 96, 5922-5931.
- Zhdanov, V.P., Pavlíček, J. & Knor Z. (1988). Pre-exponential factors for elementary surface processes. *Catal. Rev. -Sci. Eng.*, 30, 501-517.

6

Design of adiabatic fixed-bed reactors for the partial oxidation of methane to synthesis gas. Application to production of methanol and hydrogen-for-fuel-cells

This chapter will be published in Chem. Eng. Sci.

Abstract - Adiabatic fixed-bed reactors for the catalytic partial oxidation (CPO) of methane to synthesis gas were designed at conditions suitable for the production of methanol and hydrogen-for-fuel-cells. A steady-state, one-dimensional heterogeneous reactor model was applied in the simulations. Intraparticle concentration gradients were taken into account explicitly, by solving the continuity equations in the catalyst pellet at each position along the fixed-bed reactor coordinate. The reactor designs are based on supported Ni catalysts, which catalyse the indirect formation of synthesis gas via total oxidation followed by steam reforming and water-gas shift. Atmospheric, air-based fixed-bed CPO reactors for fuel-cell applications are feasible due to low catalyst temperatures. At high-pressure methanol conditions, however, catalyst deactivation will be very important as a result of the calculated high catalyst temperatures. The influence of the steam-reforming rate was investigated separately by performing simulations with the kinetic reforming models proposed by Numaguchi and Kikuchi (1988) and Xu and Froment (1989). The influence of the oxidation kinetics was studied as well. Application of different reforming models leads to significantly different maximum catalyst temperatures. Also, the possible occurrence of gas-phase reactions was investigated: homogeneous reactions will be very important at conditions suitable for methanol production.

Keywords: Partial oxidation; Adiabatic fixed-bed reactor; Reactor simulations; Methanol production; Fuel cell; Kinetics; Gas-phase reactions

6.1 Introduction

The potential of catalytic partial oxidation (CPO) as a novel route to convert methane into synthesis gas has been investigated intensively in the past decade. Many catalysts and reactor configurations have been studied on a laboratory scale. Transition metal catalysts, in particular Ni and Rh, are presently considered to be the most promising. The high-cost and limited availability of noble metals imply that Ni catalysts are preferred from an industrial standpoint. In spite of the intensive research efforts, however, industrial application of CPO has not been realized yet. The choice of suitable operating conditions and scale-up problems relating to catalyst stability and process safety still require considerable attention. At industrial conditions, i.e. at high temperatures and pressures, hot-spot formation due to exothermal oxidation reactions can lead to severe catalyst deactivation. This applies in particular to Ni catalysts, that promote synthesis gas production via indirect partial oxidation, i.e. via total combustion of part of the methane and subsequent reforming of the remaining methane. Process safety mainly concerns the possible occurrence of explosions and runaways at high operating pressures, due to homogeneous gas-phase reactions. In order to gain insight into these phenomena and to obtain suitable conditions for synthesis gas production via CPO on an industrial scale, detailed reactor modelling is required.

De Groote and Froment (1996a) have simulated adiabatic fixed-bed reactors for the catalytic partial oxidation of methane to synthesis gas at high temperatures and pressures ($P_{\text{tot}} = 25$ bar, $T_g = 808$ - 1785 K), using a supported Ni catalyst. A one-dimensional, heterogeneous reactor model was used in their calculations, taking into account the continuity, energy, and pressure drop equations. Intraparticle diffusion limitations were expressed in terms of uniform effectiveness factors, i.e. the corresponding values were considered to be constant along the reactor coordinate, independent of concentration and temperature. The intrinsic kinetics of the reforming, water-gas shift, and the oxidation reactions were taken from Xu and Froment (1989) and Trimm and Lamm (1980), respectively. Special attention was paid in the calculations to coke formation and the influence of the degree of reduction of the catalyst. The results indicated that CPO can be carried out on an industrial scale, i.e. at catalyst temperatures within acceptable limits ($T_s < 1473$ K), when air is used instead of oxygen or when steam or carbon dioxide are added to the feed.

Ostrowski et al. (1998) simulated the catalytic partial oxidation of methane to synthesis gas at industrial conditions ($P_{\text{tot}} = 5$ and 30 bar, $T_g = 1023$ - 1073 K) using both fixed-bed and fluidized-bed reactors. The kinetics proposed by De Groote en Froment (1996a) for Ni catalysts were used in the calculations. The simulation results indicated that low synthesis gas yields are obtained in case of fixed-bed reactors, as a result of the large influence of

intraparticle diffusion limitations. Equilibrium conditions were achieved in this case when the space time was increased by a factor of 6. In the fluidized-bed reactor, significantly higher yields are achieved at identical space-times. In the latter case, small catalyst particles were applied compared to the fixed-bed reactor, and the effect of pore diffusion on the reaction rates was negligible. It was shown that integrated product separation by means of membranes can improve the synthesis gas yields significantly.

Despite the industrial potential of CPO reactors, few additional studies have been reported in the field of reactor design and simulation. The objective of this work is therefore to obtain more detailed insight into fixed-bed CPO reactors for the production of methanol and hydrogen-for-fuel-cells, using supported Ni catalysts. In case of the 10 kW fuel-cell application considered, atmospheric operating conditions are applied, and air is used as oxygen source. The fixed-bed CPO reactor suitable for the production of 1000 metric tons per day (MTPD) methanol concerns high pressures (40 bar), and feed mixtures containing oxygen instead of air. Adiabatic conditions are assumed to obtain insight into the operational limits of the CPO reactors. Special attention will thus be paid in the simulations to hot-spot formation. The effect of the intrinsic reforming and oxidation kinetics on the hot-spot temperature will be investigated. In addition, the possible occurrence of gas-phase reactions will be studied.

6.2 Model description and solution procedure

6.2.1 Reactor model

Adiabatic fixed-bed CPO reactors were simulated using a steady-state 1-dimensional heterogeneous reactor model. Both external concentration and temperature gradients as well as intraparticle concentration gradients are taken into account. The catalyst particle is assumed to be isothermal: the main transport resistance inside the catalyst pellet is due to mass transfer, even in case of highly exothermic reactions (Froment and Bischoff, 1990). The gas-phase and solid-phase continuity and energy equations are presented in Table 1 together with the corresponding initial and boundary conditions.

The transport mechanism in the axial direction is considered to be of the plug-flow type. Axial dispersion of heat and mass is neglected. In addition, pressure drop was found to be negligible at the investigated conditions. Species concentrations are expressed in units $\text{mol}_i \text{ kg}_{\text{tot}}^{-1}$, which implies that the increase of the total number of moles due to reforming is accounted for implicitly in the reactor model (Bos and Westerterp, 1991). Intraparticle concentration gradients are often expressed in terms of constant effectiveness factors for the

reactions involved, to reduce the required computational time (De Groote and Froment, 1996a, De Groote et al., 1996b, Ostrowski et al., 1998). Gosiewski et al. (1999), however, showed that the calculated maximum catalyst temperatures in case of reverse-flow CPO reactors can be underestimated by more than 200 K when constant effectiveness factors are assumed. Hence, intraparticle concentration gradients are taken into account in this work by solving the pellet-scale continuity equations at each point along the adiabatic fixed-bed reactor coordinate.

Table 1. Reactor model equations with corresponding boundary conditions

Gas phase		$\varphi_m \frac{d}{dz} \left(\frac{C_i}{\rho_f} \right) + k_g a_v (C_i - C_{i,s}^s) = 0$	(1)
		$\varphi_m c_p \frac{dT_g}{dz} + h_f a_v (T_g - T_s) = 0$	(2)
Solid phase		$\rho_f \frac{1}{r_p^2} \frac{D_{e,i}}{\xi^2} \frac{d}{d\xi} \left(\xi^2 \frac{d}{d\xi} \left(\frac{C_{i,s}}{\rho_f} \right) \right) + R_{w,i} \rho_s = 0$	(3)
		$h_f a_v (T_g - T_s) + (1 - \epsilon_B) \sum_i (-\Delta_f H_i) \rho_s R_{w,i} = 0$	(4)
Gas-phase boundary conditions	$z = 0$	$C_i = C_i^0, T_g = T_g^0$	(5)
Solid-phase boundary conditions	$\xi = 0$	$\frac{d}{d\xi} \left(\frac{C_{i,s}}{\rho_f} \right) = 0$	(6)
	$\xi = 1$	$\rho_f \frac{D_{e,i}}{r_p} \frac{d}{d\xi} \left(\frac{C_{i,s}}{\rho_f} \right) \Big _{\xi=1} = k_g (C_i - C_{i,s}^s)$	(7)

In case of multi-component mixtures, molecular diffusion should be described by means of the Stefan-Maxwell theory. Preliminary reactor simulations were performed to investigate the effect of multi-component diffusion. The effective binary diffusion coefficients were calculated in this case according to the Wilke equation. Application of the Stefan-Maxwell equations, however, resulted in severe numerical problems. In order to reduce the computational complexity, Stefan-Maxwell calculations were performed in the absence of external concentration gradients. Only minor differences on the calculated concentration and temperature profiles were observed compared to those based on effective binary diffusion. At conditions suitable for methanol production, the difference between the calculated maximum catalyst temperatures was limited to 5 K. This is mainly caused by the small differences in diffusion coefficients of the different reactants and products. Consequently, diffusion in the catalyst pellet was described by Fick's law, assuming effective binary diffusion (see Eq. (3) in Table 1).

The corresponding effective diffusion coefficients are calculated from the Bosanquet equation, i.e. from the molecular and Knudsen diffusion coefficients, corrected for the pellet porosity and tortuosity (0.53 and 4.0, respectively). The physical constants ρ_f and c_p are considered to be a function of composition and temperature. The mass (k_g) and heat-transfer (h_f) coefficients are calculated from Chilton-Colburn j-factors (Yoshida et al., 1962).

6.2.2 Reaction kinetics

As the reactor simulations concern the indirect partial oxidation of methane to synthesis gas on supported Ni catalysts, rate equations for the total combustion, steam reforming, and water-gas shift reactions have to be combined in the calculations. Many kinetic models for steam reforming are available in the literature. In order to investigate the influence of the reforming kinetics on the simulation results, two intrinsic reforming models were considered: (i) the reforming model proposed by Xu and Froment (1989), and (ii) the kinetic model derived by Numaguchi and Kikuchi (1988). These models will be referred to as the XF and NK models, respectively. The kinetics of methane combustion were taken from Trimm and Lamm (1980). Since this kinetic model was derived for supported Pt catalysts, the corresponding adsorption parameters were adjusted for Ni. The Ni catalyst was assumed to be in the reduced state, which implies that total combustion and reforming occur in parallel, c.f. Blanks et al. (1990), Ostrowski et al. (1998), and Gosiewski et al. (1999).

Intrinsic reforming and water-gas shift kinetics

Xu and Froment (1989) investigated the intrinsic kinetics of methane steam reforming using a Ni/MgO-Al₂O₃ catalyst. The kinetic experiments were conducted with hydrogen in the feed ($H_2/CH_4 = 1.25$) to avoid reoxidation of the Ni catalyst by steam. An elementary step kinetic model was proposed, and used to construct Langmuir-Hinshelwood rate equations for steam reforming towards CO and CO₂, as well as for the water-gas shift reaction, see Table 2. Note that the different rate equations display a negative order in the partial pressure of hydrogen. The reaction rates consequently become infinite when the partial pressure of hydrogen is zero. Xu and Froment (1989) indicate, however, that simulation of an industrial reformer will not suffer from this problem, since the feed generally contains some hydrogen. In the present work, infinite reaction rates were avoided in case of simulations with the XF reforming model, by adding some hydrogen to the feed mixture. The corresponding values of the kinetic and adsorption parameters are listed in Tables 4 and 5. The XF reforming model was obtained using relatively low temperatures, $773 < T_s < 848$ K, and pressures between 3

and 15 bar. During the indirect partial oxidation of methane to synthesis gas, however, high catalyst temperatures can occur due to the exothermal total combustion reaction. In addition, high operating pressures will be required in case of CPO reactors for methanol production.

Table 2. Reaction rate equations for methane oxidation, reforming, and water-gas shift reactions used to simulate the adiabatic fixed-bed reactors: reforming kinetics of Xu and Froment (1989)

Reaction	Rate equation
1 $\text{CH}_4 + 2\text{O}_2 \rightarrow \text{CO}_2 + 2\text{H}_2\text{O}$	$r_1 = \frac{k_{1a}p_{\text{CH}_4}p_{\text{O}_2}}{(1 + K_{\text{CH}_4}^{\text{ox}}p_{\text{CH}_4} + K_{\text{O}_2}^{\text{ox}}p_{\text{O}_2})^2} + \frac{k_{1b}p_{\text{CH}_4}p_{\text{O}_2}}{(1 + K_{\text{CH}_4}^{\text{ox}}p_{\text{CH}_4} + K_{\text{O}_2}^{\text{ox}}p_{\text{O}_2})}$
2 $\text{CH}_4 + \text{H}_2\text{O} \leftrightarrow \text{CO} + 3\text{H}_2$	$r_2 = \frac{k_2^{\text{Xu}} / p_{\text{H}_2}^{2.5}(p_{\text{CH}_4}p_{\text{H}_2\text{O}} - p_{\text{H}_2}^3p_{\text{CO}} / K_{\text{eq}2})}{(1 + K_{\text{CO}}p_{\text{CO}} + K_{\text{H}_2}p_{\text{H}_2} + K_{\text{CH}_4}p_{\text{CH}_4} + K_{\text{H}_2\text{O}}p_{\text{H}_2\text{O}} / p_{\text{H}_2})^2}$
3 $\text{CO} + \text{H}_2\text{O} \leftrightarrow \text{CO}_2 + \text{H}_2$	$r_3 = \frac{k_3^{\text{Xu}} / p_{\text{H}_2}(p_{\text{CO}}p_{\text{H}_2\text{O}} - p_{\text{H}_2}p_{\text{CO}_2} / K_{\text{eq}3})}{(1 + K_{\text{CO}}p_{\text{CO}} + K_{\text{H}_2}p_{\text{H}_2} + K_{\text{CH}_4}p_{\text{CH}_4} + K_{\text{H}_2\text{O}}p_{\text{H}_2\text{O}} / p_{\text{H}_2})^2}$
4 $\text{CH}_4 + 2\text{H}_2\text{O} \leftrightarrow \text{CO}_2 + 4\text{H}_2$	$r_4 = \frac{k_4^{\text{Xu}} / p_{\text{H}_2}^{3.5}(p_{\text{CH}_4}p_{\text{H}_2\text{O}}^2 - p_{\text{H}_2}^4p_{\text{CO}_2} / K_{\text{eq}4})}{(1 + K_{\text{CO}}p_{\text{CO}} + K_{\text{H}_2}p_{\text{H}_2} + K_{\text{CH}_4}p_{\text{CH}_4} + K_{\text{H}_2\text{O}}p_{\text{H}_2\text{O}} / p_{\text{H}_2})^2}$

Table 3. Reaction rate equations for total oxidation, reforming, and water-gas shift reactions used to simulate adiabatic fixed-bed reactors: reforming kinetics of Numaguchi and Kikuchi (1988)

Reaction	Rate equation
1 $\text{CH}_4 + 2\text{O}_2 \rightarrow \text{CO}_2 + 2\text{H}_2\text{O}$	$r_1 = \frac{k_{1a}p_{\text{CH}_4}p_{\text{O}_2}}{(1 + K_{\text{CH}_4}^{\text{ox}}p_{\text{CH}_4} + K_{\text{O}_2}^{\text{ox}}p_{\text{O}_2})^2} + \frac{k_{1b}p_{\text{CH}_4}p_{\text{O}_2}}{(1 + K_{\text{CH}_4}^{\text{ox}}p_{\text{CH}_4} + K_{\text{O}_2}^{\text{ox}}p_{\text{O}_2})}$
2 $\text{CH}_4 + \text{H}_2\text{O} \leftrightarrow \text{CO} + 3\text{H}_2$	$r_2 = \frac{k_2^{\text{Num}}(p_{\text{CH}_4} - p_{\text{H}_2}^3p_{\text{CO}} / K_{\text{eq}2})}{p_{\text{CH}_4}^{\alpha_2}p_{\text{H}_2\text{O}}^{\beta_2}} (*)$
3 $\text{CO} + \text{H}_2\text{O} \leftrightarrow \text{CO}_2 + \text{H}_2$	$r_3 = \frac{k_3^{\text{Num}}(p_{\text{CO}} - p_{\text{H}_2}p_{\text{CO}_2} / K_{\text{eq}3})}{p_{\text{CH}_4}^{\alpha_3}p_{\text{H}_2\text{O}}^{\beta_3}} (*)$

(*) Coefficients α_i and β_i obtained by Numaguchi and Kikuchi (1998) by fitting the gas-phase composition at the outlet of the fixed-bed reactor: $\alpha_2 = 0.0$, $\beta_2 = 0.596$, $\alpha_3 = 0.0$, $\beta_3 = 0.0$

Table 4. Arrhenius parameter values for combustion, reforming, and water-gas shift reactions

Reaction	Kinetic model	A_i^*	E_{act} (kJ mol ⁻¹)
1a	Trimm and Lam	$8.11 \cdot 10^5$	86.0
1b	Trimm and Lam	$6.82 \cdot 10^5$	86.0
2	Xu and Froment	$1.17 \cdot 10^{15}$	240.1
	Numaguchi and Kikuchi	$2.62 \cdot 10^5$	106.9
3	Xu and Froment	$5.43 \cdot 10^5$	67.1
	Numaguchi and Kikuchi	$2.45 \cdot 10^2$	54.5
4	Xu and Froment	$2.83 \cdot 10^{14}$	243.9

* Units: (1a), (1b): mol bar⁻² kg_{cat}⁻¹ s⁻¹; (2): Xu and Froment: mol bar^{0.5} kg_{cat}⁻¹ s⁻¹, Numaguchi and Kikuchi : mol bar^{-0.404} kg_{cat}⁻¹ s⁻¹, (3): mol bar⁻¹ kg_{cat}⁻¹ s⁻¹, (4): mol bar^{0.5} kg_{cat}⁻¹ s⁻¹

Table 5. Van 't Hoff parameter values for the adsorption reactions

Component	$A(K_i)^*$	ΔH_i^0 (kJ mol ⁻¹)
CH ₄ (combustion)	$1.26 \cdot 10^{-1}$	-27.3
O ₂ (combustion)	$7.87 \cdot 10^{-7}$	-92.8
CH ₄	$6.65 \cdot 10^{-4}$	-38.3
CO	$8.23 \cdot 10^{-5}$	-70.7
H ₂	$6.12 \cdot 10^{-9}$	-82.9
H ₂ O	$1.77 \cdot 10^5$	+88.7

* Units: CH₄(combustion), O₂(combustion), CH₄, CO, H₂: bar⁻¹, H₂O: -

Hence, the kinetic model proposed by Numaguchi and Kikuchi (1988), derived at higher catalyst temperatures (up to 1160 K), and higher pressures (up to 25 bar), was also used to simulate adiabatic fixed-bed CPO reactors. Langmuir-Hinshelwood rate equations for steam reforming towards CO and for the water-gas shift reaction were proposed by the authors, see Table 3, based on a rate-determining surface reaction step. The corresponding values of the kinetic rate parameters are shown in Table 4. The catalyst properties and applied reaction conditions are presented in Table 6. The Ni-content of the NK catalyst evidently is lower than the catalyst used by Xu and Froment. The Ni-surface areas, however, are more or less identical and allow a reasonable comparison of both kinetic models.

Table 6. Catalyst specifications

	Trimm and Lam (1980)	Xu and Froment (1989)	Numaguchi and Kikuchi (1988)
Catalyst	Pt/Al ₂ O ₃	Ni/MgAl ₂ O ₄	Ni/Al ₂ O ₃
Metal content (wt%)	0.4	15.2	8.7
Metal surface area (m ² /g)	4.9	4.1	3.6
Density, ρ_s (kg m _p ⁻³)	2130	1870	1970

In order to examine the apparent differences between the applied rate equations for methane steam reforming, the corresponding reforming rates were calculated as a function of operating pressure, see Figure 1.

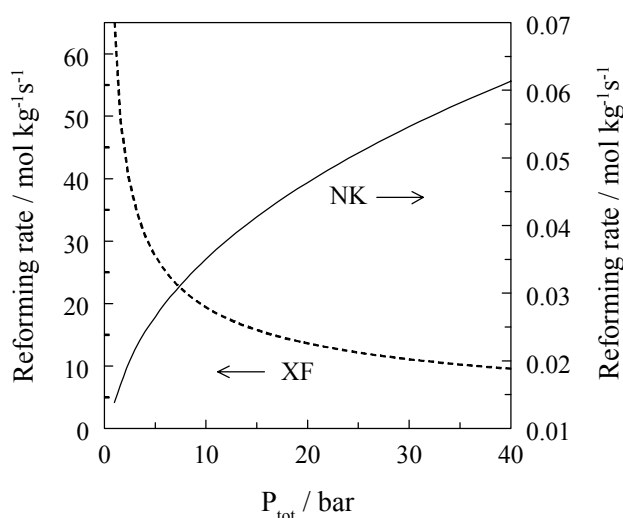


Figure 1. Methane steam-reforming rates in case of the XF and NK reforming models vs total pressure. Conditions: $CH_4/O_2/H_2O/H_2 = 33.3/16.7/49.9/0.1$, $T_S = 800$ K.

Figure 1 clearly indicates that the reforming rate *decreases* considerably at increasing total pressure in case of the XF model, whereas the reforming rate *increases* in case of the rate equation proposed by Numaguchi and Kikuchi. These trends were also observed at various other feed compositions and catalyst temperatures. The large difference between the calculated reforming rates in case of the NK and XF models (note the different y-axis in Figure 1) is mainly caused by the negative partial reaction order with respect to hydrogen in the latter model. During the reactor simulations, i.e. in the presence of significant amounts of hydrogen, the difference between the calculated reforming rates is less pronounced. Application of the proposed rate equations at different operating pressures can thus lead to

significantly different temperature and concentration profiles at the scale of the reactor. This will be illustrated in more detail when discussing the simulation results in case of the low-pressure reactor for fuel-cell applications, and the high-pressure reactor for methanol production.

Intrinsic kinetics of methane oxidation

The intrinsic kinetics of methane oxidation have been studied extensively in the literature on noble metal catalysts (Pt, Rh, Pd, Ir), at low catalyst temperatures ($T_s < 1000$ K), and at fuel-lean conditions, i.e. at O_2/CH_4 ratios > 1 . Relatively few studies were carried out using Ni catalysts. Aryafar and Zaera (1997) investigated methane oxidation on Ni foils at catalyst temperatures up to 973 K, using fuel-lean conditions and low reactant partial pressures. The reaction rate was found to be first order with respect to the methane concentration and zeroth order with respect to oxygen. Power-law rate equations are generally limited to a narrow range of operating conditions. In addition, fuel-lean conditions and low reactant partial pressures bear little relation to partial oxidation, in which O_2/CH_4 ratios < 0.5 and high operating pressures are applied.

Hence, the Langmuir-Hinshelwood rate equation proposed by Trimm and Lamm (1980) for methane oxidation on supported Pt catalysts, valid at temperatures above 830 K, and at O_2/CH_4 ratios between 0.3 and 5, was used in this work. The corresponding rate equation is shown in Tables 2 and 3. The first term of the rate equation accounts for the reaction between molecularly adsorbed methane and oxygen, while the second term describes the Eley-Rideal reaction between molecularly adsorbed methane and gaseous oxygen. It should be noted that Trimm and Lamm (1980) accounted for the latter reaction using $p_{O_2}^{1/2}$, which evidently is not correct. Consequently, the Eley-Rideal reaction is described using p_{O_2} in the numerator of the second term in the corresponding rate equation.

Trimm and Lamm (1980) used a non-linear regression method to estimate the rate coefficients and adsorption constants at a fixed temperature of 830 K. In this work, the corresponding adsorption constants for methane and oxygen on Pt were adjusted for Ni catalysts. The adsorption constant is written as:

$$K_i^{ox} = \exp\left(\frac{\Delta S_i^0}{R} - \frac{\Delta H_i^0}{RT}\right) = A(K_i) \exp\left(-\frac{\Delta H_i^0}{RT}\right) \quad (8)$$

The standard CH_4 and O_2 adsorption enthalpies in case of Pt and Ni were taken from Shustorovich (1990). The standard adsorption entropies on *platinum* were calculated next, using the reported values of $K(CH_4)$ and $K(O_2)$ at 830 K, together with the corresponding

adsorption enthalpies for Pt. The standard adsorption entropies in case of Ni, are assumed to be identical to the values obtained for Pt. The adsorption enthalpies and entropies for Ni were used accordingly to calculate the adsorption constants, see Table 5.

The rate coefficients k_{1a} and k_{1b} , listed in Tables 2 and 3, are considered to be dependent on temperature according to an Arrhenius type equation. The values of k_{1a} , k_{1b} , and the high-temperature global activation energy (86 kJ mol^{-1}) reported by Trimm and Lamm (1980), were used to calculate the corresponding pre-exponential factors, see Table 4. The activation energies of the surface and Eley-Rideal reactions are considered to be identical. The calculated values of the pre-exponential factors were not adjusted for Ni. The influence of the oxidation kinetics on the simulation results, however, will be investigated separately in this paper.

6.2.3 Solution procedure

The model equations (1)–(4) form a set of differential and algebraic equations. Integration along the reactor coordinate was carried out using the NAG-library routine D02NGF (NAG Fortran Library, 1991). This routine integrates a set of ordinary differential equations coupled with algebraic equations using the Backward Differentiation Formulae (BDF). The solid-phase continuity equations were solved at each increment of the axial direction by means of the method of orthogonal spline collocation (Finlayson, 1972). In this method, the differential equations are approximated by trial functions, consisting of a set of orthogonal polynomials. The species concentrations inside the catalyst particle are calculated at the collocation points, i.e. at the roots of the orthogonal polynomials, from a set of algebraic equations. Two collocation intervals are applied in this work, since the concentration gradients are expected to be limited to a thin layer near the catalyst surface. The corresponding spline-point was positioned at a dimensionless pellet coordinate of 0.95. Both in the first and second collocation interval, 10 collocation points were defined. The resulting algebraic equations were solved at each increment of the axial reactor coordinate using the NAG-library routine C05NBF (NAG, 1991), in which a modified Newton-Raphson method is applied. Rapid convergence is obtained when sufficiently accurate initial estimates of the concentration profiles are applied.

In case of a heterogeneous reactor model accounting for external concentration and temperature gradients, both the catalyst temperature as well as the surface concentrations are unknown. In order to obtain the *initial* guess of the latter variables, i.e. the value at the first point in the fixed-bed reactor, both the heat production rate in the catalyst (Q_G), and the heat removal rate in the film surrounding the catalyst particle (Q_R) were calculated as a function of the catalyst

temperature, see Figure 2. In this figure, the NK reforming model was applied, and the operating conditions correspond to the high-pressure methanol case. The Q_G and Q_R curves were obtained by integration of the solid-phase continuity equations together with the corresponding boundary conditions, using a step-wise increase of the catalyst temperature. The calculations were always started at a low value of the catalyst temperature, to avoid numerical difficulties due to large intraparticle concentration gradients. The intersection point of the heat production and heat removal curves gives the initial steady-state temperature and corresponding surface concentrations for the catalyst particle. At this intersection point, the condition implied by the solid-phase energy equation, see Eq. (4) in Table 1, is thus satisfied.

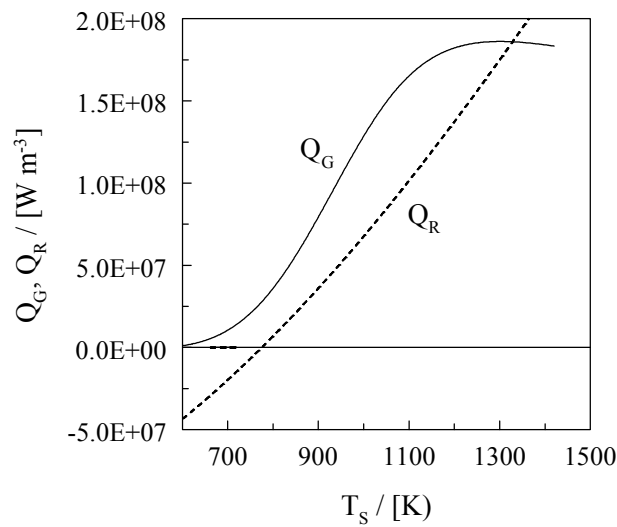


Figure 2. Heat production rate in the catalyst particle (Q_G), and heat removal rate in the film surrounding the catalyst particle (Q_R) vs catalyst temperature. Conditions: methanol case, see Table 7. Kinetic model: see Table 3; Parameter values: see Tables 4 and 5.

Figure 2 clearly indicates that the initial catalyst temperature can be significantly higher than the actual gas-phase temperature. Possible transient behavior of the fixed-bed reactor due to the difference between the initial gas-phase and the catalyst temperature (Froment and Bischoff, 1990) is neglected in this work. The procedure for the calculation of the initial catalyst temperature and intraparticle concentration profiles was always applied prior to the integration in the axial direction. In each reactor increment, the intraparticle concentration gradients of the previous step were used to solve the solid-phase continuity equations in the next step. This procedure resulted in rapid convergence of the model equations: the average computational times on a Silicon Graphics Cray Origin2000 computer did not exceed 300 s.

6.3 Model simulation results

6.3.1 Reactor dimensions and operating conditions

The reactor and catalyst dimensions, as well as the operating and equilibrium conditions used to design CPO reactors for methanol and hydrogen-for-fuel-cells production, are shown in Table 7. In case of the fuel-cell application, the fixed-bed CPO reactor is operated at atmospheric pressure. The applied mass-flux and pellet diameter resulted in negligible pressure drop. The reactor diameter was calculated from the mass-flux and the required hydrogen capacity to operate a 10 kW fuel cell. At 50% fuel-cell efficiency, the latter capacity approximately corresponds to $2.5 \cdot 10^{-2}$ mol/s H_2 . The applied inlet CH_4/O_2 and H_2O/CH_4 ratios resulted in maximum equilibrium methane conversion and hydrogen yield. Air was used as oxygen source because operation of an oxygen separation unit is not economic at the scale applied.

Table 7. Reactor dimensions, catalyst dimensions, and operating conditions

Simulation case	Fuel cell	Methanol
<i>Reactor and catalyst</i>		
Capacity	10 kW	1000 MTPD
d_r (m _r)	0.1	1.6
l_r (m _r)	0.5	3.0
ϵ_b (m ³ _g m ⁻³ _r)	0.43	0.43
r_p (m _p)	$2.5 \cdot 10^{-3}$	$7.5 \cdot 10^{-3}$
<i>Operating conditions</i>		
P_{tot} (bar)	1	40
T_g^0 (K)	773	773
ϕ_m (kg m _r ⁻² s ⁻¹)	0.15	10
<i>Feed composition</i>		
$CH_4/O_2 _0$	2.0	1.8
$H_2O/CH_4 _0$	1.5	1.0
Oxygen source	air	O ₂
<i>Equilibrium conditions</i>		
T_g^{eq} (K)	971.7	1286.6
$X_{CH_4,eq}$ (%)	98.5	94.6
$H_2/CO _{eq}$	4.23	2.64

The fixed-bed CPO reactor suitable for 1000 MTPD methanol production is operated at high pressure, to reduce downstream compression costs. The reactor length required to obtain equilibrium conditions amounted to 3 m. As in case of the fuel-cell application, the applied mass flux and pellet diameter resulted in negligible pressure drop. The reactor diameter was calculated from the required methanol capacity and the equilibrium methane conversion rate. The applied CH_4/O_2 and $\text{H}_2\text{O}/\text{CH}_4$ ratios of the feed resulted in maximum methane conversion and a H_2/CO ratio suitable for methanol production. Oxygen was used instead of air in the methanol case to avoid downstream nitrogen separation. In both cases, an inlet gas-phase temperature of 773 K was selected.

6.3.2 Fuel-cell case

A fixed-bed reactor suitable for the operation of the 10 kW fuel cell was investigated first, using the reactor and kinetic models discussed in section 6.2.1 and 6.2.2, and the solution procedure presented in section 6.2.3. The calculated catalyst temperature profiles along the reactor coordinate are shown in Figure 3 for both the XF and NK reforming models. In case of the NK reforming model, the catalyst temperature first increases due to the large amount of heat produced in the methane oxidation reaction. The catalyst temperature then reaches a maximum value of 1003 K, and decreases consecutively as a result of the prevailing endothermic reforming reaction. Note that the simulation results indicate a local minimum of the catalyst temperature of 948 K. This minimum value is caused by the complex interplay between the heat consumed in the reforming reaction, and the heat produced in the water-gas shift and oxidation reactions. Finally, the catalyst temperature increases to the equilibrium temperature of 972 K. The pronounced temperature increase, and subsequent decrease towards equilibrium is characteristic of indirect CPO catalysts (Prettre et al., 1946, Vermeiren et al., 1992). The relatively low value of the maximum catalyst temperature indicates that catalyst deactivation will not be important in this case. The catalyst temperature at the reactor inlet is approximately 40 K higher than the inlet gas-phase temperature. This temperature difference decreases rapidly at increasing axial reactor coordinate: at the position of $T_{s,\text{max}}$, the gas-phase temperature amounts to 1001 K. Beyond the temperature maximum, the gas-phase and catalyst temperatures are approximately equal within 3 K.

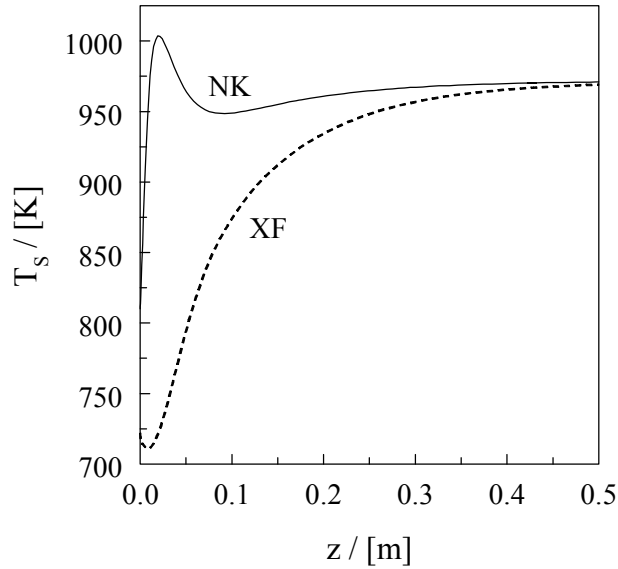


Figure 3. Catalyst temperatures vs axial reactor coordinate in case of the NK and XF reforming models. Simulation conditions: fuel-cell case, see Table 7. Kinetic model: see Tables 2 and 3; Parameter values: see Tables 4 and 5.

The simulation results in case of the XF reforming model show that the catalyst temperature initially *decreases* due to the prevailing endothermic reforming reactions. The catalyst temperature then reaches a minimum value: at this position, the gas-phase and catalyst temperatures are identical. The catalyst temperature consecutively increases to the equilibrium temperature: a hot spot is clearly not observed. This marked difference between the calculated temperature profiles is caused by the significantly higher reforming rates in case of the XF model at the applied conditions. The reforming rate at the reactor inlet is considerably higher than the methane oxidation rate. As a result, the initial catalyst temperature first decreases. Beyond the minimum value of T_s , the heat produced in the methane oxidation reaction is sufficiently high to cause an increase of the catalyst temperature. However, the net heat of reaction remains relatively low throughout the reactor, and a hot spot is therefore not observed. The gas-phase and catalyst temperatures are approximately equal beyond the observed minimum, indicating that external heat-transport limitations are insignificant.

The calculated axial mole-fraction profiles, obtained in case of the NK reforming model, are shown in Figure 4. The reactant and product mole fractions were calculated according to: $y_i = (C_i/p_f) / (\sum_i C_i/p_f)$. Figure 4 indicates that both the methane and oxygen mole fractions decrease rapidly. At $z = 0.1$ m, approximately 95% of methane and oxygen has been converted. Since the Ni catalyst was assumed to be in the reduced state during the simulations, the reforming and oxidation reactions occur in parallel. As a result, significant

amounts of H_2 and CO are observed in the first part of the reactor. In the second part of the reactor, the calculated mole fractions become approximately constant as the equilibrium conditions are approached. In case of the simulations with the XF model, the decrease of the reactant mole fractions and increase of the product mole fractions is much less pronounced (not shown in Figure 4). This is obviously caused by the low catalyst temperatures throughout the fixed-bed reactor. However, the calculated mole fractions at the reactor outlet are equal to the equilibrium values for both models.

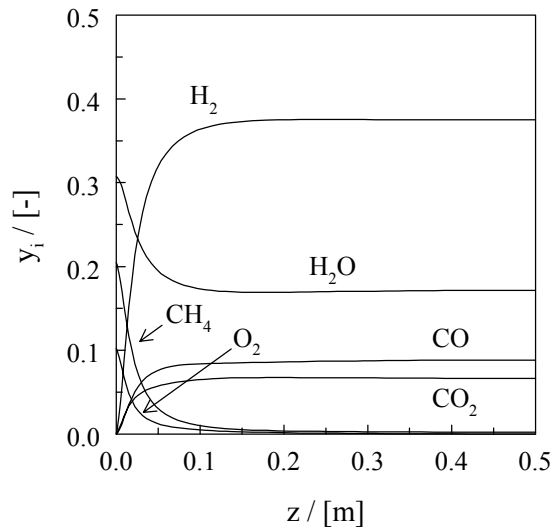


Figure 4. Reactant and product mole fractions vs axial reactor coordinate in case of the NK reforming model. Simulation conditions: fuel-cell case, see Table 7. Kinetic model: see Table 3; Parameter values: see Tables 4 and 5.

Typical intraparticle mole-fraction profiles are shown in Figure 5 in case of the simulations with the NK reforming model. The calculated mole fractions are plotted as a function of the axial reactor coordinate and the dimensionless pellet coordinate. Significant intraparticle mole-fraction gradients occur for both the reactants and products. These gradients become less pronounced at increasing values of the axial reactor coordinate.

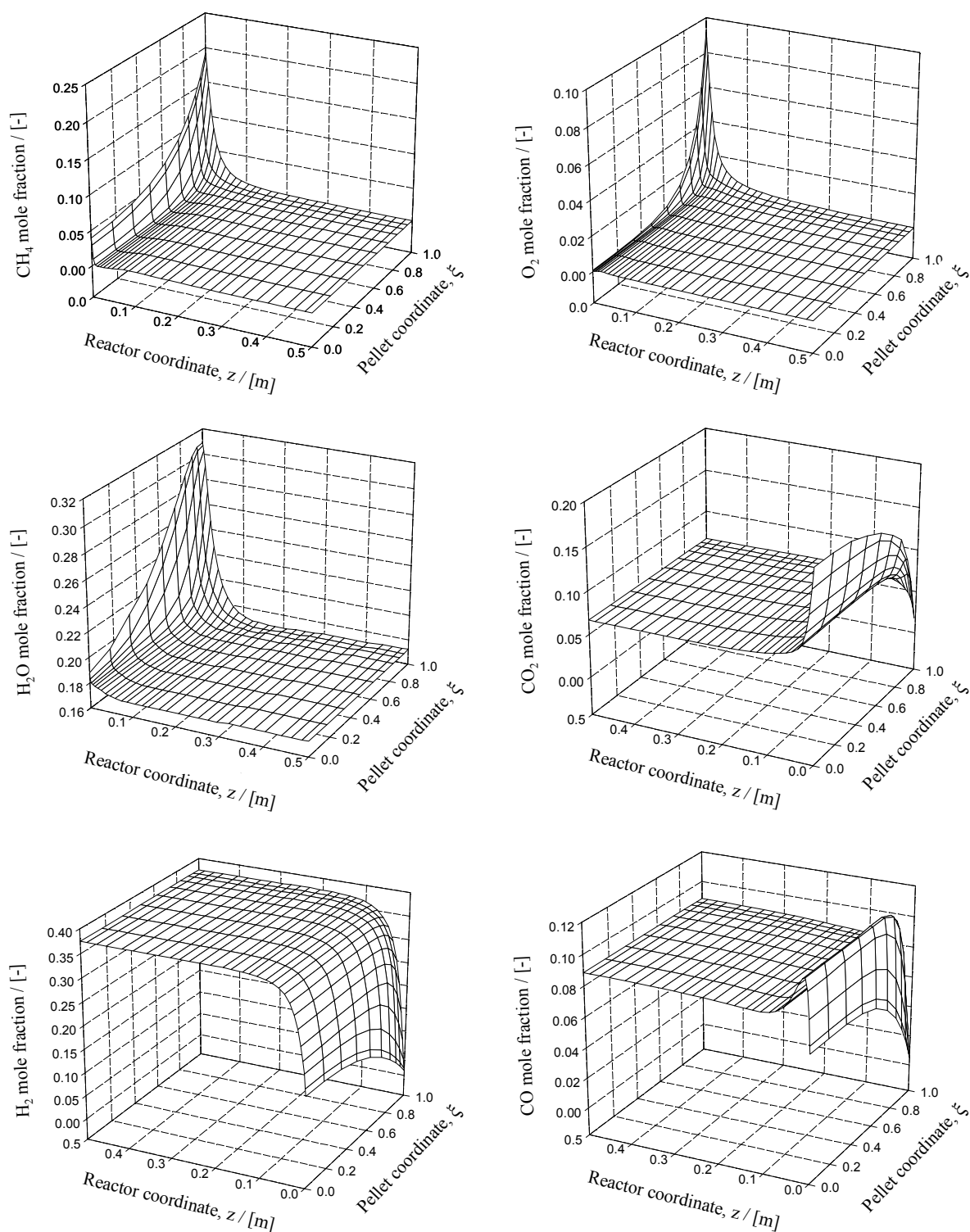


Figure 5. Intraparticle reactant and product mole fractions vs axial reactor coordinate and dimensionless pellet coordinate in case of the NK reforming model. Simulation conditions: fuel-cell case, see Table 7. Note that the reactor-coordinate axis has been inverted in case of the CO_2 , CO , and H_2 mole fractions.

The mole fractions of CH₄, O₂, H₂O, and CO₂ decrease gradually in the first part of the reactor. In case of carbon monoxide, a maximum is observed in the mole-fraction profile. Near the reactor inlet, significant amounts of CO are produced by the reforming reaction. At increasing values of the axial reactor coordinate, however, the rate of the water-gas shift reaction increases significantly, thereby decreasing the intraparticle CO mole fractions.

As indicated previously, intraparticle concentration gradients are generally taken into account in the literature by means of constant effectiveness factors for the reactions involved (De Groote and Froment, 1996a, Ostrowski et al., 1998). In case of the simulations with the NK reforming model, however, the calculated average and surface reaction rates revealed that the effectiveness factors varied considerably along the axial reactor coordinate, e.g. $0.06 < \eta(\text{ref}) < 0.61$, and $0.08 < \eta(\text{ox}) < 0.48$. This indicates that the intraparticle concentration gradients indeed have to be accounted for by solving the solid-phase continuity equations at each position in the fixed bed reactor. Constant effectiveness factors inevitably will lead to different concentration and temperature profiles.

6.3.3 Methanol case

The catalyst temperature profiles in case of the fixed-bed CPO reactor suitable for methanol production are shown in Figure 6. Here, the NK and XF reforming models both result in a temperature maximum in the first part of the reactor. In case of the NK model, the maximum catalyst temperature amounts to 1455 K, while the XF model results in a maximum catalyst temperature of 1512 K. The latter observation clearly contrasts with the results presented in the previous section for the low-pressure fuel-cell case. As indicated in Figure 1, total pressure exerts a strong negative influence on the reforming rate in case of the XF model, whereas the reforming rate increases with total pressure in case of the NK model. At the high pressure applied in the methanol case, the latter trends effectively result in lower reforming rates in case of the XF model compared to the NK reforming model, which is reflected in the observed difference between the maximum catalyst temperatures.

The catalyst temperatures at the reactor inlet (approximately 1330 K) are considerably higher than the inlet gas-phase temperature, see also Figure 2. At the position of the temperature maximum, the temperature difference between the gas-phase and the catalyst is significantly lower, and approximately amounts to 40 K for both the XF model and NK model. The calculated maximum catalyst temperatures clearly indicate that adiabatic fixed-bed CPO reactors in case of methanol production are expected to suffer from severe catalyst deactivation.

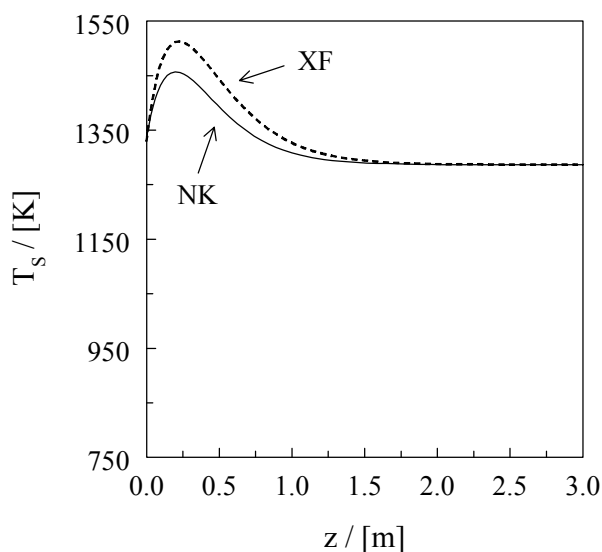


Figure 6. Catalyst temperatures vs axial reactor coordinate in case of the NK and XF reforming models. Simulation conditions: methanol case, see Table 7. Kinetic model: see Tables 2 and 3; Parameter values: see Tables 4 and 5.

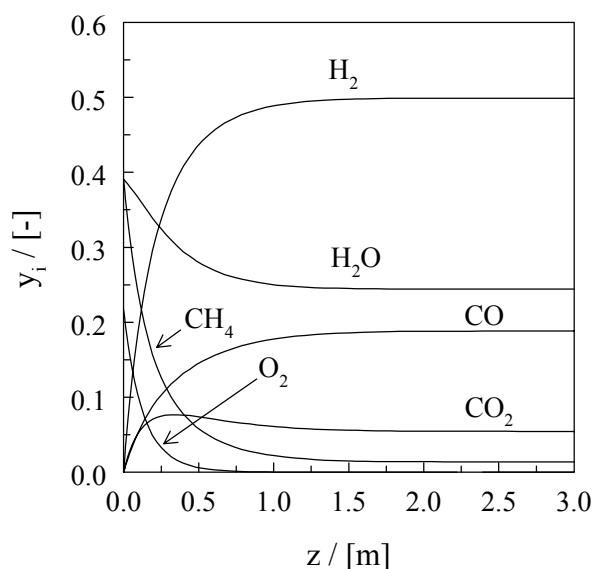


Figure 7. Reactant and product mole fractions vs axial reactor coordinate in case of the NK reforming model. Simulation conditions: methanol case, see Table 7. Kinetic model: see Table 3; Parameter values: see Tables 4 and 5.

Typical axial mole-fraction profiles are shown in Figure 7 in case of the simulations with the NK reforming model. The oxygen conversion is complete at $z = 0.75$ m. The methane mole fraction decreases gradually along the axial reactor coordinate, and reaches its equilibrium value at the reactor outlet. The equilibrium values of the H_2 , CO , CO_2 , and H_2O

mole fractions are approached at approximately 2 m reactor length. The observed trends in the intraparticle mole-fraction profiles are more or less similar to the profiles shown in Figure 5 for the fuel-cell case. The mole-fraction gradients, however, are much more pronounced at the applied reaction conditions. The calculated effectiveness factors were approximately constant in this case along the axial reactor coordinate: $\eta(\text{ref}) \approx 10^{-2}$, $\eta(\text{WGS}) \approx 10^{-2}$, $\eta(\text{ox}) \approx 10^{-3}$.

6.4 Model sensitivity analysis

6.4.1 Influence of the oxidation state of the Ni catalyst

The simulation results presented in this work were obtained using the assumption that the Ni catalyst is in the reduced state. According to Dissanayake et al. (1991), however, the oxidation state of supported Ni catalysts can vary considerably throughout a fixed-bed CPO reactor. It is suggested additionally that different oxidation states, such as NiAl_2O_4 and NiO , correspond with different combustion and reforming activities. De Groote and Froment (1996a) incorporated the effect of the variable Ni oxidation state in the simulation of fixed-bed CPO reactors, by multiplying the rates of the steam reforming and water-gas shift reactions with a so-called reduction factor. This reduction factor is assumed to depend on the fractional oxygen conversion according to $(X_{\text{O}_2})^{12}$. The power in this reduction factor was determined by trial and error with respect to the calculated maximum catalyst temperature, using a CH_4/O_2 feed.

Reactor simulations were performed by De Groote and Froment (1996a) using this reduction factor (VDR-model), and the corresponding results were compared to simulations in which the catalyst was assumed to be in the reduced state (BV-model). In both cases, the reforming kinetics proposed by Xu and Froment (1989) and the oxidation kinetics from Trimm and Lamm (1980) were used. At the applied conditions ($p_{\text{tot}} = 25$ bar, $\text{CH}_4/\text{O}_2|_0 = 1.67$, $\text{H}_2\text{O}/\text{CH}_4 = 1.4$), a maximum in the catalyst temperature profile was only observed in case of the VDR-model. The BV-model resulted in a gradual increase of the catalyst temperature to the equilibrium value. Note that the latter observation was also found in case of the simulation results obtained with the XF model at fuel-cell conditions, see Figure 3.

The results presented in this work in case of the NK model, and the XF model at high pressure, show that a maximum in the catalyst temperature profile is also observed when the Ni catalyst is assumed to be in the reduced state. A priori assumptions with respect to the oxidation state of the Ni catalyst are clearly not required in the latter cases. Nevertheless, additional simulations were performed to investigate the effect of the oxidation state of the Ni

catalyst. The reduction factor proposed by De Groote and Froment (1996a) was used in the calculations.

At conditions suitable for methanol production, the calculated maximum catalyst temperatures are slightly higher (approximately 10 K) when the reduction factor is incorporated in the reactor model. In case of the fixed-bed reactor for fuel-cell application, using the NK reforming model, the maximum catalyst temperature was only 65 K higher. Hence, catalyst deactivation due to high temperatures will not be important in this case either. The catalyst temperature profile in case of the XF model at fuel-cell conditions was hardly influenced by the applied reduction factor: the catalyst temperature still increased gradually towards the equilibrium value.

6.4.2 Influence of the oxidation kinetics

The kinetic rate constants for methane oxidation on Pt, obtained by Trimm and Lamm (1980) at a fixed catalyst temperature of 830 K, were converted in this work to an Arrhenius type expression, see section 6.2.2. The corresponding pre-exponential factors, however, were not adjusted for the Ni catalyst. In general, Ni catalysts are considered to be less active compared to Pt in promoting methane oxidation (Ma et al., 1996). Hence, the influence of the methane oxidation rate on the simulation results was investigated separately by performing calculations at reduced intrinsic total oxidation activity, i.e. at reduced values of the pre-exponential factors of the oxidation rate constants. The reforming kinetics and operating conditions were taken identical to the previous simulations.

Table 8 shows the calculated initial, maximum, and outlet catalyst temperatures obtained with the NK reforming model at different values of the rate constants for methane oxidation. At fuel-cell conditions, decreasing values of the rate constants k_{1a} and k_{1b} result in lower values of the different catalyst temperatures. This observation clearly illustrates that the methane oxidation rate is not completely determined by mass-transport phenomena at the conditions applied. The influence of the decreasing oxidation rate constants is particularly reflected in case of the maximum catalyst temperatures. A 2-fold decrease of k_{1a} and k_{1b} results in a reduction of the maximum temperature by 82 K. At 10 and 25% of the original oxidation activity, a maximum value of the catalyst temperature is not observed. In this case, the catalyst temperature increases gradually towards the reactor outlet. The outlet catalyst temperatures indicate that equilibrium is not achieved at the reactor outlet at decreasing values of the rate constants. In order to obtain the required methane conversion and hydrogen yield, the reactor length has to be increased in these cases.

Table 8. Influence of the oxidation kinetics on the calculated initial, maximum, and outlet catalyst temperatures in case of simulations with the reforming model of Numaguchi and Kikuchi (1988).

k_{1a}, k_{1b}	Fuel-cell case			Methanol case ⁽¹⁾	
	$T_{s,initial}$ (K)	$T_{s,max}$ (K)	$T_{s,outlet}$ (K)	$T_{s,initial}$ (K)	$T_{s,max}$ (K)
* 1.00	818	1003	972	1338	1455
* 0.75	801	970	971	1332	1452
* 0.50	792	921	967	1318	1447
* 0.25	779	⁽²⁾	954	1270	1433
* 0.10	772	⁽²⁾	885	848	1409

⁽¹⁾ Catalyst temperatures at the reactor outlet correspond to the equilibrium temperature

⁽²⁾ A maximum value of the catalyst temperature was not observed in this case

At conditions suitable for methanol production, the calculated maximum catalyst temperatures decrease only slightly at lower values of the oxidation rate constants. This is caused by the large influence of mass-transport limitations on the oxidation rate. High catalyst temperatures are thus calculated, even at low values of the methane oxidation rate constants, indicating that catalyst deactivation remains inevitable. At decreasing values of the oxidation rate constants, the heat production curve (Q_G , see Figure 2) is shifted progressively to lower catalyst temperatures. As a result, the initial catalyst temperatures decrease. A 10-fold decrease of the oxidation rate constants, however, results in a more than proportional decrease of the initial catalyst temperature. In this case, the initial steady-state catalyst temperature corresponds to the intersection point of the heat-removal curve (Q_R) and the *low-activity* branch of the heat-production curve.

In case of the simulations with the XF reforming model, identical trends were observed. At fuel-cell conditions, the catalyst temperature at the reactor outlet decreased progressively at lower values of the oxidation rate constants. In case of methanol production, the initial and maximum catalyst temperatures decreased slightly at reduced oxidation activity.

6.5 Influence of gas-phase reactions

At the conditions applied during the reactor simulations, i.e. at high temperatures and pressures, homogeneous gas-phase reactions can become important. In order to investigate the influence of gas-phase reactions on reactor operation, simulations have to be performed taking into account the homogeneous and heterogeneous reactions simultaneously. In the literature, a few homogeneous gas-phase kinetic models are available. These models

generally consist of a large number of reactions, involving many molecules and radical species. To avoid the complexity and large computational times associated with the combination of these models with heterogeneous reactions, the possible occurrence of gas-phase reactions was investigated separately in this work by means of off-line reactor simulations. In these simulations, only gas-phase reactions are considered: heterogeneous reactions are not taken into account.

Calculations were performed with the gas-phase kinetic model proposed by Berger and Marin (1999), using an adiabatic, one-dimensional plug-flow reactor model. The kinetic model is based on data obtained at typical CPO conditions, i.e. at pressures up to 8 bar, temperatures up to 1300 K, and inlet methane-to-oxygen ratios between 2.1 and 3.1. At the most severe conditions in the fixed-bed CPO reactors, i.e. at the maximum catalyst temperatures obtained in the fuel-cell and methanol cases, residence times required to achieve complete *homogeneous* oxygen conversion were calculated. The calculations are based on the local gas-phase composition corresponding to the calculated maximum catalyst temperature, i.e. on feed mixtures containing both the reactants and products. The calculated residence times were then compared to the corresponding residence times in the fixed-bed reactor required for complete *heterogeneous* oxygen conversion.

In case of the fuel-cell simulations using the NK reforming model, the residence time required for complete heterogeneous oxygen conversion amounts to 0.21 s. The residence time for complete homogeneous conversion equals 0.57 s. This indicates that gas-phase reactions are not likely to play a significant role at these conditions. In case of the CPO reactor for methanol production, the required residence times amount to 0.15 s and $1.5 \cdot 10^{-4}$ s, respectively. At these conditions, gas-phase reactions will be inevitable.

6.6 Conclusions

A steady-state, one-dimensional heterogeneous reactor model was used to design adiabatic fixed-bed CPO reactors for methanol and hydrogen-for-fuel-cells production. Intraparticle concentration gradients were taken into account explicitly, by solving the corresponding continuity equations at each position along the reactor coordinate. The initial guess of the catalyst temperature was obtained from the intersection point of the calculated heat-removal (Q_R) and heat-production (Q_G) curves. The required computational times generally did not exceed 300 s. The simulation results indicated that adiabatic fixed-bed CPO reactors for fuel-cell applications are feasible due to low catalyst temperatures, typically below 1000 K. In case of CPO reactors for methanol production, however, high catalyst temperatures (> 1450 K) were observed, which implies that catalyst deactivation will be very important.

Application of the reforming models proposed by Xu and Froment (1989) and Numaguchi and Kikuchi (1988) resulted in significantly different catalyst temperature profiles at the low-pressure fuel-cell conditions. The NK model resulted in a temperature maximum of 1003 K in the first part of the reactor. In case of the XF model, the catalyst temperatures were significantly lower, and increased gradually to the equilibrium temperature of 972 K. A maximum in the catalyst temperature profile was not observed. In case of the fixed-bed reactors for methanol production, both the XF and NK models resulted in a temperature maximum in the first part of the reactor. Here, the highest catalyst temperature (1512 K) was observed with the XF model.

In the methanol case, the oxidation kinetics hardly affect the observed temperature profiles as a result of mass-transport limitations. At fuel-cell conditions, reduced total oxidation activity resulted in significantly lower catalyst temperatures. The influence of both the reforming and oxidation kinetics thus indicates that bench-scale testing and determination of the intrinsic kinetics of novel catalysts remains essential for reliable reactor design and operation. In case of the low-pressure fuel-cell case, gas-phase reactions are not likely to ignite, which implies safe and stable reactor operation. At conditions suitable for methanol production, however, gas-phase reactions will be very important.

Acknowledgement

The financial support by the Commission of the European Union in the framework of the Joule program, Contract No. JOU2-CT92-0073 and No. JOU3-CT95-0026 is gratefully acknowledged by the authors.

Notation

a_v	external pellet surface area per unit reactor volume, $m_i^2 m_r^{-3}$
A_i	pre-exponential factor, reaction dependent
c_p	specific heat at constant pressure, $J kg^{-1} K^{-1}$
C_i	molar concentration of species i , $mol m_g^{-3}$
$C_{i,s}$	intraparticle molar concentration of species i , $mol m_g^{-3}$
$C_{i,s}^S$	molar concentration of species i , at the external pellet surface, $mol m_g^{-3}$
d_r	reactor diameter, m_r
$D_{e,i}$	effective diffusion coefficient of species A in catalyst, $m_g^{-3} m_p^{-1} s^{-1}$
h_f	gas-to-solid heat transfer coefficient, $W m_i^{-2} K^{-1}$
ΔH_i^0	standard adsorption enthalpy, $J mol^{-1}$
$-\Delta_f H_i$	heat of formation of species i , $J mol^{-1}$

k_g	gas-to-solid mass transfer coefficient, $m_g^3 m_i^{-2} s^{-1}$
k_i	reaction rate constant of reaction i , reaction dependent
$K_{eq,i}$	equilibrium constant of reaction i , reaction dependent
K_i	adsorption constant for component i in reforming and water-gas shift reactions, bar^{-1}
K_i^{ox}	adsorption constant for component i in combustion reaction, bar^{-1}
l_r	reactor length, m_r
NK	reforming model of Numaguchi and Kikuchi (1988)
p_i	partial pressure of component i , bar
P_{tot}	total pressure, bar
Q_G	heat production rate in the catalyst, $W m_r^{-3}$
Q_R	heat removal rate in the film surrounding the catalyst particle, $W m_r^{-3}$
r_i	rate of reaction i , $mol kg_{cat}^{-1} s^{-1}$
r_p	pellet radius, m
$R_{w,i}$	net catalytic production rate of species i per unit catalyst mass, $mol kg_{cat}^{-1} s^{-1}$
ΔS_i^0	standard adsorption entropy, $J mol^{-1} K^1$
T_g	gas-phase temperature, K
T_g^{eq}	gas-phase temperature at equilibrium conditions, K
T_s	solid temperature, K
$T_{s,max}$	maximum solid temperature, K
$T_{s,outlet}$	solid temperature at the reactor outlet, K
$X_{CH_4,eq}$	conversion of methane at equilibrium conditions, -
X_{O_2}	fractional oxygen conversion, -
XF	reforming model of Xu and Froment (1989)
y_i	mole fraction of species i , $mol_i mol_{tot}^{-1}$
z	axial reactor coordinate, m_r

Greek symbols

ϵ_B	void fraction of packing, $m_g^3 m_r^{-3}$
ρ_s	catalyst density, $kg m_p^{-3}$
ρ_f	fluid density, $kg m_g^{-3}$
ξ	dimensionless pellet coordinate, -
ϕ_m	superficial mass flow velocity, $kg m_r^{-2} s^{-1}$

References

- Aryafar, M., & Zaera, F., (1997). Kinetic study of the catalytic oxidation of alkanes over nickel, palladium, and platinum foils. *Catal. Lett.*, *48*, 173-183.
- Berger, R.J., & Marin, G.B., (1999). Investigation of gas-phase reactions and ignition delay occurring at conditions typical for partial oxidation of methane to synthesis gas. *Ind. Eng. Chem. Res.*, *38*, 2582-2592.
- Blanks, R.F., Wittrig, T.S., & Peterson, D.A., (1990). Bidirectional adiabatic synthesis gas generator. *Chem. Eng. Sci.*, *45*, 2407-2413.
- Bos, A.N.R., & Westerterp, K.R. (1991). The mass balance for gas-phase reactions in tubular reactors. *Chem. Eng. Commun.*, *99*, 139-153.
- De Groote, A.M., & Froment, G.F., (1996a). Simulation of the catalytic partial oxidation of methane to synthesis gas. *Appl. Catal. A*, *138*, 245-264.
- De Groote, A.M., Froment, G.F., & Kobylinski, Th., (1996b). Synthesis gas production from natural gas in a fixed bed reactor with reversed flow. *Can. J. Chem. Eng.*, *74*, 735-742.
- Dissanayake, D., Rosynek, M.P., Kharas, K.C.C., & Lunsford, J.H., (1991). Partial oxidation of methane to CO and H₂ over a Ni/Al₂O₃ catalyst. *J. Catal.*, *132*, 117-127.
- Finlayson, B.A. (1972). The method of weighted residuals and variational principles, with application in fluid mechanics, heat and mass transfer. In *Mathematics in Science and Engineering*, *87*, ed. R. Bellman, Academic Press, New York.
- Froment, G.F., & Bischoff, K.B., (1990). *Chemical reactor analysis and design*, pp. 467-471 and 477-478, Wiley, London.
- Gosiewski, K., Bartmann, U., Moszczynski, M., & Mleczko, L., (1999). Effect of intraparticle transport limitations on temperature profiles and catalytic performance of the reverse-flow reactor for the partial oxidation of methane to synthesis gas. *Chem. Eng. Sci.*, *54*, 4589-4602.
- Ma, L., Trimm, D.L., & Jiang, C., (1996). The design and testing of an autothermal reactor for the conversion of light hydrocarbons to hydrogen. I. The kinetics of the catalytic oxidation of light hydrocarbons. *Appl. Catal. A*, *138*, 275-283.
- NAG, Numerical Algorithm Group, 1991, Fortran Library Manual, Mark 15, Wilkinson House, Oxford.
- Numaguchi, T., & Kikuchi, K., (1988). Intrinsic kinetics and design simulation in a complex reaction network: steam-methane reforming. *Chem. Eng. Sci.*, *43*, 2295-2301.
- Ostrowski, T., Giroir-Fendler, A., Mirodatos, C., & Mleczko, L., (1998). Comparative study of the catalytic partial oxidation of methane to synthesis gas in fixed-bed and fluidized-bed membrane reactors. *Catal. Today*, *40*, 181-190.
- Prettre, M., Eichner, C., & Perrin, M., (1946). The catalytic oxidation of methane to carbon monoxide and hydrogen. *Trans. Farad. Soc.*, *43*, 335-340.
- Shustorovich, E., (1990). The bond-order conservation approach to chemisorption and heterogeneous catalysis: applications and implications. *Adv. Catal.*, *37*, 101-130.
- Trimm, D.L., & Lam, C-W., (1980). The combustion of methane on platinum-alumina fibre catalysts - I. Kinetics and mechanism. *Chem. Eng. Sci.*, *35*, 1405-1413.
- Vermeiren, W.J.M., Blomsma, E., & Jacobs, P.A., (1992). Catalytic and thermodynamic approach of the oxyreforming of methane. *Catal. Today*, *13*, 427-436.
- Xu, J., & Froment, G.F., (1989). Methane steam reforming, methanation and water-gas shift: I. Intrinsic kinetics. *AIChE J.*, *35*, 88-96.
- Yoshida, F., Ramaswami, D., & Hougen O.A., (1962). Temperatures and partial pressures at the surfaces of catalyst particles.



General conclusions & Outlook

The research described in this thesis focused at the *reaction kinetics* of the catalytic partial oxidation (CPO) of methane and at *reactor modelling* of synthesis gas production via CPO at industrially relevant conditions. The kinetic investigations were carried out at low conversions to obtain insight into the primary reaction products. Reactor modelling was aimed at the design of fixed-bed reactors for methanol and hydrogen-for-fuel-cells production.

The literature review indicated that group VIII metal catalysts, in particular Ni and Rh, are the most active and selective for the CPO reaction. Kinetic studies using these catalysts remain essential, however, considering the ongoing debate with respect to the reaction mechanism. Monolith reactors were found to be the most suitable configuration for synthesis gas production. Nevertheless, practical difficulties, e.g. the influence of homogeneous gas-phase reactions and transport limitations, still require considerable attention.

Homogeneous gas-phase reactions were found to be very important at the conditions of high temperature and pressure as applied in case of the 0.3 wt% Rh/ α -Al₂O₃ catalyst. This was concluded from simulations with a gas-phase kinetic model, which was derived from homogeneous gas-phase experiments. At 1345 K, the heterogeneous catalytic reactions on the Rh catalyst resulted in production of the total oxidation products. Direct catalytic partial oxidation of methane to synthesis gas was found to occur at 1273 K.

The gauze reactor proved to be a valuable tool to study the intrinsic kinetics of the catalytic partial oxidation of methane in the presence of heat-transport limitations. The experimental results at low oxygen conversions showed that CO was a primary product. The intrinsic kinetics of CO formation were obtained using a kinetic model, together with a reactor model accounting for the transport limitations in a quantitative way. Oxygen-assisted methane adsorption had to be incorporated into the kinetic model to describe primary CO formation.

Single-response regression resulted in statistically significant and physically meaningful estimates of the *intrinsic* kinetic rate parameters of methane adsorption. The effects of catalyst temperature, reactant space-time, and inlet methane-to-oxygen ratio on the conversions and selectivities were simulated adequately. The role of surface kinetics and mass-transfer in CO formation was illustrated quantitatively.

A one-dimensional heterogeneous reactor model was used to study the CPO reaction at conditions which cannot be realised safely in a laboratory reactor. Low catalyst temperatures were simulated in case of the 10 kW fuel-cell application, whereas fixed-bed reactors for 1000 MTPD methanol production involved high catalyst temperatures. Different reforming models resulted in significantly different catalyst temperature profiles at low-pressure fuel-cell conditions. A temperature maximum was always observed in the first part of the reactor at methanol conditions, independent of the applied reforming model. Homogeneous gas-phase reactions are not likely to ignite in case of the fuel-cell application, which implies safe and stable operation. At methanol conditions, however, gas-phase reactions will be very important.

The experimental data at low conversions clearly allowed to investigate the primary products of the CPO reaction in detail. Incomplete oxygen conversions in case of the Rh/ α -Al₂O₃ catalyst, however, corresponded to low catalyst activity. Homogeneous gas-phase reactions consequently occurred to a significant extent at the applied conditions of high temperature and pressure. A quantitative description of the observed conversions and selectivities thus requires the simultaneous consideration of both homogeneous and heterogeneous reactions. The gauze reactor allowed to study the intrinsic kinetics of the CPO reaction in the presence of transport limitations. Due to the relatively low temperatures and the presence of significant amounts of unreacted oxygen, hydrogen was not observed. Nevertheless, detailed quantitative insights into primary CO formation could be obtained for the first time. The reactor simulations clearly showed that fixed-bed reactors for hydrogen-for-fuel-cells production hold great promise. Indeed, industry is currently involved in commercialising CPO technology for hydrogen-powered vehicles. Also, microchannel CPO reactors are attracting widespread attention. In such microreactors, the throughput level of conventional reactors can be maintained, while dramatically reducing the reactor size. Microchannel CPO reactors combined with fuel cells could become the future standard for portable power generation, e.g. in laptop computers and cellular phones.

Dankwoord

Het spreekt voor zich dat in een periode van ruim vier jaar een groot aantal mensen op al dan niet actieve wijze hebben bijgedragen tot dit proefschrift en mijn verblijf binnen de Capaciteitsgroep voor Chemische Reactortechnologie. Als laatste der Mohicanen kan ik stellen dat ik een complete generatie promovendi en hoogleraren de revue heb zien passeren. In het methaan oxidatie project alleen al hebben 2 professoren, 1 universitair docent, 2 post-docs, 2 AIO-4 studenten, 3 AIO-2 studenten, 3 OBP'ers en 12 afstudeerders samengewerkt. Bedankt allemaal ! Om de verblijftijd in dit proefschrift enigszins te beperken wil ik mij nu richten tot de personen waarmee ik in de afgelopen jaren het meest intensief heb samengewerkt.

Guy, toen ik na mijn afstuderen bij jou begon met mijn promotie dacht ik alle benodigde kennis wel op zak te hebben. Na al die jaren denk ik daar nu wel anders over. Jouw kennis en inzicht zijn voor mij altijd enorm stimulerend en waardevol geweest. Zelfs op afstand sinds je vertrek naar Gent ben je altijd actief betrokken gebleven bij mijn werk. Tevens heb ik veel waardering voor je vertrouwen, zoals gebleken uit mijn tijdelijke aanstelling binnen jouw groep in Gent na afloop van mijn contract.

Jaap, grote waardering heb ik voor de manier waarop je mijn project, dat al drie jaar bezig was voor jouw komst, hebt opgepakt en samen met mij hebt afgerond. Jouw kritische kijk op mijn werk en artikelen heeft geleid tot een mooi proefschrift en bijbehorende publicaties. Goede herinneringen zal ik bewaren aan ons bezoek aan Oslo en het weekend in de Ardennen.

Mart, je hebt heel wat borden vol moeten schrijven om dit proefschrift tot stand te kunnen laten komen. Zelfs toen je nog niet actief aan het project verbonden was, werden door jou de meest prachtige modellen ontwikkeld. Altijd stond je klaar, zelfs als je een vergelijking voor de twintigste keer moest afleiden. Bij deze een tip voor toekomstige AIO's: begin er niet aan om een differentiaal vergelijking zelf op te lossen, Mart doet het toch sneller.

Rob, als ontwerper van Symetha heb je mijn project op de rails gezet. Ondanks enkele tegenslagen heb je mij vaak weten op te beuren en te motiveren. Altijd was je bereid om mijn vragen te beantwoorden, zelfs op afstand in Delft. Ons gezamenlijk bezoek aan de congressen en bijeenkomsten in Villeurbanne, Florence, Thessaloniki en Oslo waren geweldige belevenissen. Hopelijk kunnen we onze fietstochten in Delft en Eindhoven in de toekomst voortzetten in het mooie Zeeuws-Vlaanderen.

Dirk, Dick en Marlies, dankzij jullie gouden handjes zijn de methaan oxidatie opstellingen grote successen geworden. Gezelligheid kent bij jullie geen grenzen.

Heren afstudeerders, David, Edwin, Roy, Jan en Ludwijn, bedankt voor het noeste werk dat jullie voor mij hebben verricht. Na enige correcties op plastisch taalgebruik, hebben jullie stuk voor stuk mooie afstudeerverslagen afgeleverd. De vele sessies in de socio-corner, en de lunch breaks onder het genot van Hans Teeuwen blijven hoogtepunten van mijn promotietijd. Hopelijk kunnen we de meetings in Den Haag nog vaak meemaken.

Alle collega AIO's, vaste medewerkers en afstudeerders wil ik tevens bedanken voor de leuke tijd. In het bijzonder moet ik hierbij de dart-, biljart- en filmavonden en verhuissessies met Jeroen vermelden. Mede onder het genot van een broodje bakpao hebben we samen een goede tijd gehad. Laten we zo doorgaan !

Onmisbaar in al die jaren is natuurlijk ook het thuisfront geweest. Esther, door dik en dun heb je me gesteund. Samen hebben we veel vrienden gemaakt in tien jaar Eindhoven, nu hopelijk ook in Terneuzen. Als wetenschapper heb ik altijd genoten van onze knip-, plak- en tekenactiviteiten voor je opleiding en werk op diverse scholen. Pa en ma, zonder jullie had ik nooit kunnen bereiken waar ik nu sta. Op loopafstand binnen Terneuzen zullen we samen nog prachtige jaren doormaken. De telefoonrekening zal in ieder geval aanzienlijk lager uitvallen.

Curriculum Vitae

Carlo Rudy Harold de Smet werd geboren op 9 november 1971 te Terneuzen. Na het behalen van het VWO diploma aan het Zeldenrust College begon hij in september 1990 met de studie Scheikundige Technologie aan de Technische Universiteit Eindhoven. In augustus 1994 studeerde hij af bij prof.dr.ir. G.B. Marin in het Laboratorium voor Chemische Technologie. De titel van het afstudeerwerk was: "Kinetics of silicon deposition at low pressure". Na afronding van de bedrijfsstage in de Verenigde Staten begon hij in april 1995 bij het Laboratorium voor Chemische Technologie met zijn promotieonderzoek dat leidde tot dit proefschrift. Het onderzoek werd verricht onder leiding van prof.dr.ir. J.C. Schouten en prof.dr.ir. G.B. Marin. Vanaf 1 december 1999 is hij werkzaam als research engineer bij DOW Benelux te Terneuzen binnen "Hydrocarbons and Energy R&D".

Stellingen

behorende bij het proefschrift

Partial Oxidation of Methane to Synthesis Gas: Reaction Kinetics and Reactor Modelling

van Carlo R.H. de Smet

1. Bij onvolledige zuurstofconversie en hoge temperaturen tijdens de katalytische partiële oxidatie van methaan over $\alpha\text{-Al}_2\text{O}_3$ en $\text{Rh}/\alpha\text{-Al}_2\text{O}_3$, wordt de productie van ethaan en etheen volledig bepaald door homogene gasfasereacties (*Hoofdstuk 3 van dit proefschrift*).
2. Voor betrouwbare kinetische studies omtrent de katalytische partiële oxidatie van methaan, is in-situ meting van de katalysator temperatuur noodzakelijk (*Hoofdstuk 2 en 4 van dit proefschrift*).
3. Het 19-staps mechanisme van Hickman en Schmidt (AIChE. J., **44**, 1164-1177, 1993) is niet in staat om de toename van de CO-selectiviteit bij lage ruimtetijden te beschrijven.
4. Primaire vorming van CO tijdens methaanoxidatie over een Pt-gaas, kan alleen worden verklaard wanneer de methaanadsorptie als zuurstof-geassisteerd wordt verondersteld (*Hoofdstuk 5 van dit proefschrift*).
5. Katalytische partiële oxidatie van methaan voor de productie van waterstof-voorbrandstofcellen zal, gezien de gunstige bedrijfscondities, in de nabije toekomst commerciële toepassing vinden (*Hoofdstuk 6 van dit proefschrift*).
6. In het bedrijfsleven is de scheidingslijn tussen afkortingen en zelfstandige naamwoorden afwezig.

7. De 'feel-good' factor van wonen en werken in Zeeland is zeer groot.
8. De toekenningen van de Zilveren Harp en de Gouden Harp aan producenten van House-muziek geven aan dat kwaliteit altijd boven komt.
9. Als 'groene chemie' daadwerkelijk kleur zou bekennen, zou de wereld een stuk schoner worden.
10. De huidige daling van de werkloosheid leidt tot banenverlies.
11. Reality-tv nivelleert het begrip 'bekende Nederlander'.
12. De begrippen 'massatoerisme' en 'ecotoerisme' dienen opnieuw te worden gedefinieerd wanneer de groei van het aantal Chinese vakantiegangers doorzet (Volkskrant, 8 januari 2000).